ISSN 0038-531X

Russian Original Vol. 57, No. 6, December, 1984

June, 1985

SATEAZ 56(6) 803–880 (1984)

SOVIET ATOMIC ENERGY

АТОМНАЯ ЭНЕРГИЯ
(ATOMNAYA ÉNERGIYA)

TRANSLATED FROM RUSSIAN

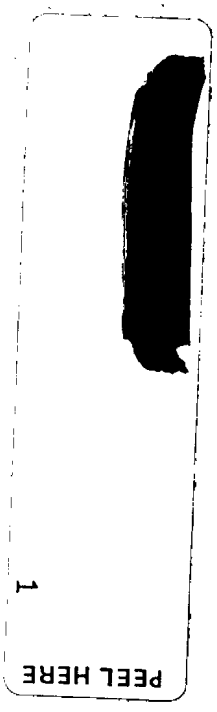

CONSULTANTS BUREAU, NEW YORK

SOVIET ATOMIC ENERGY

Soviet Atomic Energy is abstracted or indexed in *Chemical Abstracts, Chemical Titles, Pollution Abstracts, Science Research Abstracts, Parts A and B, Safety Science Abstracts Journal, Current Contents, Energy Research Abstracts,* and *Engineering Index.*

Mailed in the USA by Publications Expediting, Inc., 200 Meacham Avenue, Elmont, NY 11003.

POSTMASTER: Send address changes to *Soviet Atomic Energy,* Plenum Publishing Corporation, 233 Spring Street, New York, NY 10013.

Soviet Atomic Energy is a translation of *Atomnaya Énergiya,* a publication of the Academy of Sciences of the USSR.

An agreement with the Copyright Agency of the USSR (VAAP) makes available both advance copies of the Russian journal and original glossy photographs and artwork. This serves to decrease the necessary time lag between publication of the original and publication of the translation and helps to improve the quality of the latter. The translation began with the first issue of the Russian journal.

Consultants Bureau journals appear about six months after the publication of the original Russian issue. For bibliographic accuracy, the English issue published by Consultants Bureau carries the same number and date as the original Russian from which it was translated. For example, a Russian issue published in December will appear in a Consultants Bureau English translation about the following June, but the translation issue will carry the December date. When ordering any volume or particular issue of a Consultants Bureau journal, please specify the date and, where applicable, the volume and issue numbers of the original Russian. The material you will receive will be a translation of that Russian volume or issue.

Subscription (2 volumes per year)
Vols. 56 & 57: $560 (domestic), $621 (foreign)
Vols. 58 & 59: $645 (domestic), $715 (foreign)
Single Issue: $100
Single Article: $8.50

CONSULTANTS BUREAU, NEW YORK AND LONDON

c/b
233 Spring Street
New York, New York 10013

Published monthly. Second-class postage paid at Jamaica, New York 11431.

SOVIET ATOMIC ENERGY

A translation of *Atomnaya Énergiya*

June, 1985

Volume 57, Number 6 December, 1984

CONTENTS

CONTENTS

(continued)

Engl./Russ.

The Russian press date (podpisano k pechati) of this issue was 11/28/1984. Publication therefore did not occur prior to this date, but must be assumed to have taken place reasonably soon thereafter.

ARTICLES

MAJOR SAFETY PROVISIONS IN NUCLEAR-POWERED SHIPS

N. S. Khlopkin, O. B. Samoilov, V. M. Belyaev, A. M Dubrovin, É. M Mel'nikov, and B. G. Pologikh

UDC 621.039.68

Considerable experience has been accumulated in this country on the design, construction, and operation of nuclear-powered civilian ships: the icebreakers Lenin, Leonid Brezhnev, and Sibir'. The nuclear steam plants (NSP) used on these as the main energy source have been found to be highly reliable and safe, and it is desirable to use them in the future not only in icebreakers but also in transport ships for use in ice fields.

The Soviet program for building and developing nuclear-powered ships has involved careful attention to safety in ships containing NSP. The experience with the design and operation of nuclear icebreakers in recent years has led to the revision of safety standards for the nuclear ships and correspondingly ship NSP [1, 2] and international guidelines have been developed. If one meets the requirements of these documents, one has a safe basis for future Soviet nuclear-powered ships.

Basic Safety Principles. Basic safety problems implied by the features of NSP are related to screening the radiation sources and preventing the escape of radioactive substances, in addition to reliable core cooling preventing hazardous situations by transferring the reactor to a subcritical state, and maintaining it in that state for an appropriate time. The execution of these functions is delegated to independent safety systems. The composition, structure, and mode of operation in these systems are chosen in accordance with the following basic principles:

1) high fault-free operation parameters for all units;

2) the safety system should perform its functions when there is a single failure in any component;

3) a reliable and fast emergency reactor protection system;

4) the conditions should rule out damage to the fuel pins in all modes of operation;

5) prevention of coolant loss from the core in emergencies related to loss of coolant from the first loop;

6) fission products should not be allowed to pass beyond set barriers; and

7) preventing the pressure in the first loop from rising above a permissible level set by the strength in any design emergency.

To provide reliable NSP safety, one combines the deterministic method of meeting the standard safety requirements with a probability method, in which one considers not only the consequences of emergencies but also the possibilities of their occurrence; quantitative criteria from this method are currently being formulated. Two methods are to be considered as complementary in researching and providing safety. We note that a probability analysis is obligatory in designing nuclear power stations [3].

Basic Technical Specifications in Safety Provision in Future Nuclear-Powered Ships. The NSP in nuclear ships under design or construction usually employ well-tested designs and units, which have been thoroughly checked out on nuclear icebreakers and which have shown excellent safety and working life. During the manufacture, installation, and testing of NSP equipment, one uses well-evaluated technology and quality-control methods. Changes and improvements are made in the design of the equipment, particularly to increase the reliability and the monitoring performance and completeness. Provision is made for ongoing automatic monitoring of all technological parameters during operation, including the radiation environment in spaces within the ship, as well as periodic examination and checking of equipment, pipelines, and systems as a whole. These measures together ensure reliable and safe operation.

Translated from Atomnaya Énergiya, Vol. 57, No. 6, pp. 379-382, December, 1984. Original article submitted August 27, 1984.

0038-531X/84/5706-0803$08.50

One of the major means of attaining high reliability parameters in NSP is the provision of equipment backup.

The reactor core has a negative temperature coefficient of reactivity in the working temperature range, which provides self-regulation and dynamic stability. This self-regulation is a factor that restricts the increase in reactor power and thus tends to alleviate the consequences of emergencies associated with the power production rate exceeding the rate of core cooling.

The control and protection system provides for multichannel parameter monitoring under working conditions. The emergency-protection circuits are galvanically decoupled from the measurement channels. The discrete signals that operate the protective equipment are produced independently in each channel and pass to the effectors along duplicated circuits. The links between systems via the protection signals are also duplicated in the control system. Built-in monitoring devices at various levels enable one to detect and localize faults in individual units, which can be promptly replaced. The response rates of the electrical and mechanical emergency-protection components provide for shutting down the reactor in any emergency while maintaining permissible temperatures in the fuel pins.

Under normal working conditions, with the circulation pumps running, the heat from the core is carried off by the coolant in the first loop passing through the steam generators and onward to contact with the coolant in the second loop. When the reactor is shut down, the residual heat is removed from the core by two independent cooling channels, which are activated automatically or remotely from the emergency protection signal. The first is the cooling channel for the water in the second loop passing through the steam generators when the circulation pumps in the first loop are working together with the pumps in the second loop. The second is the cooling channel with water in the third loop, which operates when it is impossible to supply feedwater to the steam generator.

The emergency feed pumps in the second loop with their pipes and equipment form an independent cooling system, which is not dependent on the main condensate–feed system, and this provides ways of cooling the reactor in any design emergency situation.

The users of the NSP have reliable uninterrupted power supplies under all normal and emergency conditions, in accordance with the requirements of [1]. Experience with the power plants in nuclear icebreakers indicates that complete current failure in the NSP needs to be envisaged only for the time required for the emergency power supplies to be activated. On the other hand, calculations show that the systems remain viable with much longer current failures, in spite of the severe working conditions assumed for emergencies. It is to be considered only as a purely hypothetical situation that the NSP fails to provide power for a prolonged period (i.e., loss of the main power supply and failure to obtain a supply from the backup and emergency sources), as there is multiple backup in the electrical power system. Nevertheless, this is considered in designing NSP. The main task in that case is to provide ongoing reactor cooling by means of facilities independent of the state of the ship's electrical power supply.

Foreign standardization documents dealing with safety in nuclear ships envisage installing safety valves in the first loop as a passive means of preventing overpressure. However, this is not an obvious solution, because of features of the first loop: It is a powerful source of radioactivity, and there is the potential hazard that the core will be deprived of coolant and thereby damaged, with its serious radiation consequences, while in addition there is the low reliability of such safety devices. The available experience with them confirms this viewpoint. One possible reason for pressure rise in the first loop is that the coolant acquires excess heat, and this makes it the most effective approach to provide high reliability in the facilities for shutting down the reactor and cooling the NSP, which should radically prevent impermissible pressure increase and eliminate the need to fit safety valves [4]. This is shown to be correct by prolonged experience in the accident-free operation of NSP in nuclear icebreakers.

New designs envisage automatic connection of an independent system to the steam generator, which consists of tanks containing water, a gas cylinder, pipelines, and other equipment designed to supply feedwater to the steam generator and to discharge the steam to the atmosphere without resort to external power supplies, in order to provide emergency cooling in the first loop when there is complete power failure (or failure of all the cooling plant). The heat is removed from the core by the natural circulation of the coolant in the first loop.

These cooling provisions restrict the pressure increase in the first loop under all normal and emergency conditions and ensure that it retains its integrity.

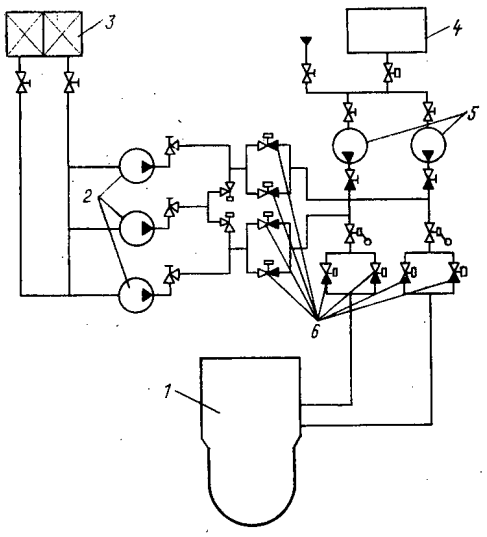

Fig. 1. Scheme for supplying the first loop and for providing emergency flushing to the core in a container transport ship: 1) reactor; 2) flushing pumps; 3) reserve tank; 4, 5) feedwater tank and pumps, correspondingly; 6) emergency flushing valves.

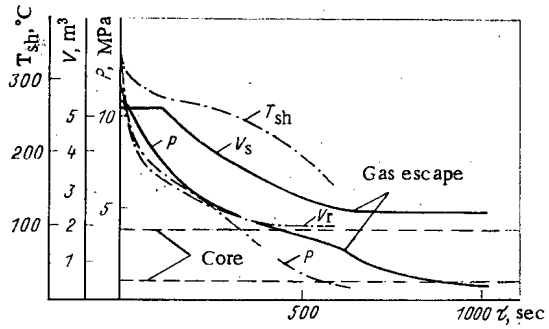

Fig. 2. Change in coolant parameters when the first loop fails; solid line and dot–dash line) pipeline failure in the feed and compensation systems, correspondingly; P) pressure in reactor; V_r) coolant volume in reactor; T_{sh}) maximum temperature of fuel-pin sheaths.

One of the most serious emergencies is a leak in the first loop. To reduce the probability of this occurring and to restrict the consequences, there are special design measures such as minimal length in the pipeline in the first loop and the pipelines connected to the reactor above the core. In new reactor systems such as for transport ships, there is provision for constriction nozzles in the reactor pipes. The systems adjoining the first loop are also fitted with a double pressurizing system. All the equipment and pipes in the first loop are located in a hermetic container. In accordance with the standardization documentation, it is conservatively assumed in considering emergencies involving leakage in the first loop that there is instantaneous failure in some pipe connecting the body of the reactor to the first-loop equipment. It should be noted that the estimate of the probability is less than 10^{-6} event/reactor · yr for an emergency involving failure in the structures within the containment (reactor, steam generator, and power pipes in the reactor), which represents a practical impossibility, and the consequences are not examined.

The following are the major operational measures to be taken when the coolant escapes from the first loop: Shutting down the reactor, identifying and localizing the leak, feeding the loop and flushing the core, and emergency cooling.

The signal indicating pressure drop in the first loop below the permissible value leads to the reactor being shut down automatically, and at the same time the purification system is shut off along with the working

groups of cylinders in the pressure-compensating system, and the backup pumps are started up along with the backup and emergency feed pumps, and the equipment in the flushing system is activated. When the pressure in the first loop falls to the pressure provided by the flushing pumps, controlled nonreturn valves on the flushing pipes open, and water begins to enter the reactor through two channels (Fig. 1). All these automatically executed operations can be duplicated remotely from the control panel. The flushing water is supplied via two independent branches, while the backup in the pumps and other equipment enables one to meet the above failure principles in the safety system. If the pipe fails in a part that cannot be shut off, one cannot localize the leak, and the main task in that case is to ensure that the core is supplied with coolant in order to provide acceptable temperature conditions in the fuel pins. The output of the flushing pumps is chosen accordingly.

As one provides temperatures such that the fuel pins remain viable, this prevents failure in the sheaths, which represent the first barrier to the escape of fission products, while the cooled core geometry is maintained, and thus any change in the state of the fuel-pin cores is ruled out such that the radionuclides contained in them are rapidly released.

If there is a leak in the first loop, which is the second barrier to the fission products, the protective containment comes into action (third barrier). To prevent the pressure in the containment rising to the permissible limit, provision is made for passing the steam–air mixture into a special ballast volume through a bubble tank or into a tank within the shielding.

A study of the consequences of leaks shows that the core remains flushed with water if there is a failure in any pipe in the first loop if the above protection facilities are fitted, and the fuel pins do not attain a critical state, while the pressure in the containment remains below the design value (Fig. 2).

This conception of nuclear ship safety is based on experience accumulated in the construction of power plants for nuclear icebreakers and the operating experience with these of total extent about 80 reactor-years. This experience has been utilized in drawing up standardization documents and in designing new nuclear ships.

LITERATURE CITED

1. Rules for Classifying and Constructing Nuclear Ships [in Russian], Leningrad (1982).
2. Nuclear Safety Rules for Ship-Borne Nuclear Power Systems (PBYa-08-81) [in Russian], Atomizdat, Moscow (1981).
3. General Safety Provisions for Nuclear Power Stations during Design, Construction, and Operation (OPB-82) [in Russian], Moscow (1982).
4. F. M. Mitenkov, L. A. Zvereva, B. I. Motorov, É. M. Mel'nikov, and O. B. Samoilov, "The use of a safety valve in the first loop of a nuclear power system containing a VVÉR reactor," At. Energ., 50, No. 5, 308-310 (1981).

TESTS ON IMPROVED STEAM SEPARATORS IN THE THIRD UNIT AT THE CHERNOBYL NUCLEAR POWER STATION

O. Yu. Novosel'skii, V. B. Karasev,
E. V. Sakovich, M. A. Lyutov,
and V. I. An'kov

UDC 621.039.577

Improved separator drums (Fig. 1) have been tested at the Chernobyl nuclear power station with its RBMK-1000 reactors, these differing from those used at Leningrad power station and the first units at Kursk and Chernobyl power stations [1] in having a larger internal diameter (2600 instead of 2300 mm) and a different design for the internal devices (ID). Features of the new ID design include the drainage diffusors 1 and the base of the compartments 2, the inclined perforated sheets 3, and the breather tubes 4 for taking off the steam from the space 5 between the compartments into the steam volume 6. Also, the separator characteristics have been improved by increasing the distance between the immersed perforated sheet 7 and the upper perforated shield 8. The increased diameter has reduced the mean speed at the evaporation surface by about 7.5%. The drainage diffusors enable one to use the water in the segments in emergency and transitional states. The inclined perforated sheet of section 12.5% equalizes the velocity pattern at the tapoff from the segments into the spaces between them, which tends to increase the water retained in the separator.

The design of the drainage channel in the immersed perforated sheet (unit A in Fig. 1) incorporates the advantage from modifying the ID in the 2300-mm-diameter separator [2]: The side piece 9 has a height of 170 mm, while the height of the drainage slot is not more than 55 mm. At the surface of the sheet there are stiffening ribs 10 with holes of height 100 mm and working section 18%.

The immersed perforated sheet in the improved separator is fitted with the end pieces 11 of height 485 mm. The brackets 12 in the segments have windows allowing the steam–water mixture to flow along the drum and which thus equalize the load along the length. These modifications were incorporated into the design when the separator drum of diameter 2300 mm constituted the bottleneck in the forced circulation loop in the RBMK-1000. The improved drum has four rows of steam–water tubes 13, whose diameter has been increased to 100 mm.

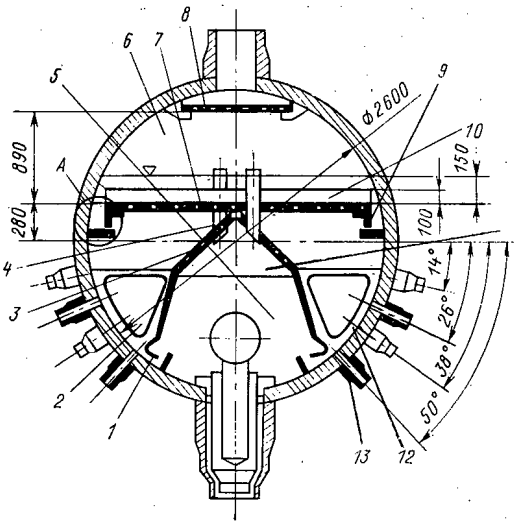

Fig. 1. Cross section of the separator drum in the third unit at Chernobyl nuclear power station.

Translated from Atomnaya Énergiya, Vol. 57, No. 6, pp. 382-385, December, 1984. Original article submitted March 26, 1984.

0038-531X/84/5706-0807$08.50

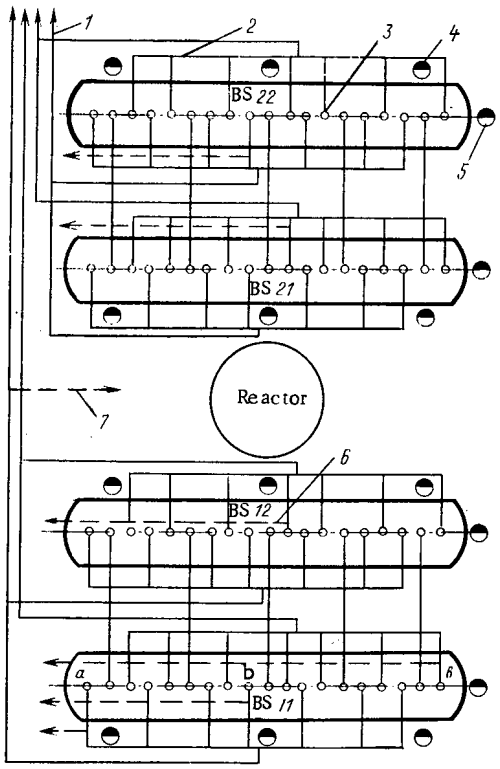

Fig. 2. Location of separator drums, steam pipes, balancing vessles, and steam sampling points: 1) pipes supplying steam to the machine hall; 2) steam collectors; 3) steam tapoff pipes in separator drum; 4) level gauges with balancing-vessel baseline of 630 mm to measure water level above immersed perforated sheet; 5) end level gauges with 1600-mm baseline of balancing vessels; 6) steam sampling lines in steam-collecting tubes; 7) steam sampling from steam pipe of diameter 600 mm; and a, c, and b) end and central steam-collecting tubes, correspondingly.

This third unit also employs a new assembly for the main equipment. In particular, the separator drums are turned through 90° and are set parallel to the machine bay (Fig. 2). The steam-pipe layout has also been altered. In the new layout, two collectors of diameter 400 mm from adjacent separator drums are combined in one steam pipe of diameter 600 mm, which goes to the turbine. The steam from the collectors is taken from the middle of the separator drum, which produces a more uniform distribution of the steam flow over the steam tubes. A new system is also used to measure the water level. All the balancing vessels are set up in the staffed (cold) location, and use is made of vessels with partially heated central chambers as devised by the Dzerzhinskii All-Union Thermal Engineering Institute. In each separator drum, one measures the water level above the immersed perforated sheet in three sections along the length in vessels with a baseline of 630 mm and the general level at the end in vessels with a baseline of 1600 mm.

During the installation and the runup to the nominal power, we commissioned and checked the level-measuring system, which involved checking that the balancing vessels had been correctly manufactured and installed, that the connecting and pulse lines had been correctly installed, checking the blowers, and checking the readings of the level gauges with a pressure difference $\Delta P = 0$. The readings of the gauges were checked before commissioning the unit with a water temperature of 20°C with the level in the separator drum varying in the range from −350 to +400 mm. In the period of runup to the nominal power, the scales of the secondary instruments ranging from −100 to +315 mm in the 630-mm-baseline gauges were replaced by scales of from −200 to +315 mm. The 0 level on a secondary instrument in that case corresponds to a mass level on the immersed perforated sheet of 150 mm.

To test the separators, steam samples were taken from the steam pipes and tapoffs in accordance with the scheme shown in Fig. 2. The water samples were taken from the body of the drum, while the steam was taken from the central tubes in each separator drum, and also from the two tubes in the BS 11 separator drum. There were also steam sampling points in the machine hall before the turbines, from which one could determine the average water content. However, the cooling system envisaged in the design did not provide isokinetic sampling ahead of the turbine with a thermal power of more than 80% of nominal. To determine the average water content of the steam at the exit from all the separator drums at power levels of over 80%, the samples were taken after the turbine condenser. The water content was determined from the ratio of the ^{24}Na concentrations in the condensate and in the circuit water by the method given in [3].

The tests were performed at a pressure of 7 MPa and thermal power levels of 65, 83, 93, and 100% of nominal. The purpose of these was to determine the dependence of the water content at the exit from the sepa-

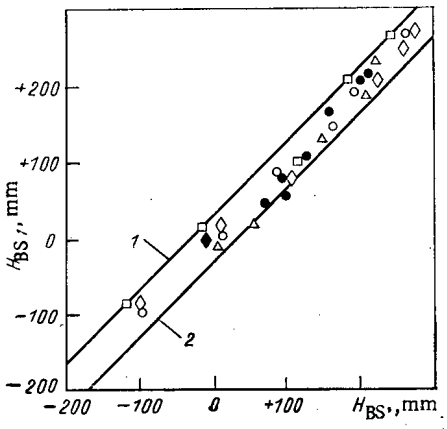

Fig. 3

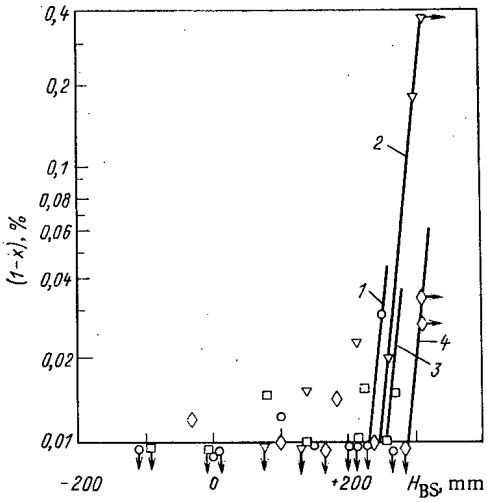

Fig. 4

Fig. 3. Comparison of readings for gauges measuring the mass water level above the immersed perforated sheet at various reactor thermal powers in MW: ○) 2100; □) 2660; Δ) 2960; ◇) 3200; ◆) 3350; ●) 3200.

Fig. 4. Dependence of the steam wetness 1 − x in the central steam-tapoff tubes in the separator drums on the mass water level above the immersed perforated sheet (from the middle gauge) at the nominal thermal power: 1) ○ BS 11; 2) ▽ BS 21; 3) □ BS 22; 4) ◇ BS 12; → central level gauge off scale; ↓ water content less than 0.01%.

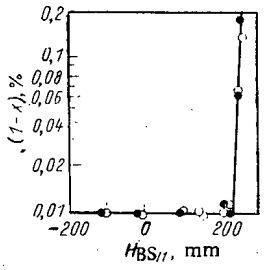

Fig. 5. Dependence of the average steam wetness after the separator drums on the mass water level above the immersed perforated sheet (from readings of middle gauge in BS 11) as indicated by taking samples in the turbine condensers at the nominal reactor thermal power; ● and ○) condensers K 5 and K6, correspondingly.

rator on the mass level at a given thermal power (steam production). The tests began at the nominal level, and then the level was raised in steps of 50 mm until the water content of the steam at the exit exceeded 0.1% or the upper limit was reached for the level gauges with scales of −200 to +315 mm. The limiting height of the mass level of water above the zero mark at which the upper sampling point was reached for the gauges with scales of −200 to +315 mm was determined by calculation from the formulas of [3], and it was 285 mm for the nominal unit power. We also made tests with a level of −100 mm indicated by the instruments with scales of −200 to +315 mm, i.e., +50 mm above the immersed perforated sheet.

When the steady state had been reached (constant power, level in the separator drum, pressure, and flow rate), we established isokinetic flow rates for the steam samples, which were calculated from the measured steam flow rates in the pipes. These conditions were maintained for 30 min, and during this time we recorded the basic working parameters. The levels in both pairs of separator drums were raised simultaneously in order to measure the average water content after all four. In the pair of drums 11 and 12, the level was maintained from the gauge installed at the middle of drum 11, while in the other pair 21 and 22 it was maintained from the gauge installed at the end of drum 21 remote from the steam pipes. During the commissioning period, the readings of these gauges were found to be the most reliable. Comparison of the readings (Fig. 3) showed that they agreed well (remained within the accuracy class) before and after commissioning the sets of level gauges in August 1982. Straight lines 1 and 2 in Fig. 3 define the boundaries within which the set of gauges with baseline 630 mm remained within the class. The deviations in the readings of the gauges with 630- and 1600-mm balancing-vessel baselines did not exceed the absolute error indicated by the accuracy class of various reactor power levels.

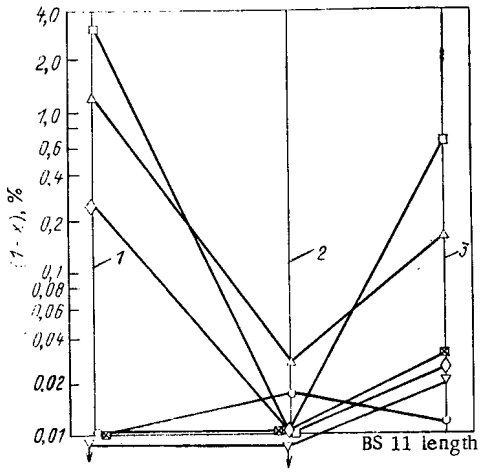

Fig. 6. Steam wetness distribution in steam tapoff tubes along the length of separator 11 for various values of the thermal power N_t in MW and various mass water levels H_m in mm above the immersed perforated sheet (as indicated by the middle gauge); ⊠) H_M = 0, N_t = 2960; ○) 10, 3350; ▽) 140, 3200; ◇) 200, 3200; △) 250, 3200; □) 260, 3200; ↓ wetness less than 0.01%; 1-3) sections of separator 11 at steam tapoff tubes a, b, and c, correspondingly.

Figure 4 shows that the wetness of the steam in the central tubes in all the separator drums did not exceed 0.02% up to levels of 200 mm above the nominal, but there was a sharp increase at 250-270 mm. An exception was represented by the separator 12 (curve 4 in Fig. 4), which was evidently due to overestimated readings from the middle gauge in this separator. Similar results were obtained at power levels of 83 and 93% of nominal. However, as the power level decreased, the sharp increase in the water content began at higher levels in the separators. With a thermal power of about 65% of nominal, we measured the steam wetness in front of the turbines. The measurements agreed with those on the central tubes in the separators.

The wetness data obtained at the nominal power by measuring the ^{24}Na activity in samples from the turbine condensers (K 5 and K 6) are given in Fig. 5 by reference to the readings of the middle gauge in separator 11. With mass levels above the immersed perforated sheet of from −100 to +200 mm, the wetness was less than 0.02%. When the mass level rose above +200 mm, the average wetness began to increase, and it attained 0.1% at +255 mm.

Comparison of Figs. 4 and 5 indicates that the limiting level corresponding to a wetness of 0.1% on measurements in the central tubes is higher than that from the determination of the average wetness, which is explained by the measurements on the three tubes in separator 11, which illustrates the wetness distribution over the length (Fig. 6). For a level less than 200 mm, the wetness in the central or end tubes does not exceed 0.02-0.03%, although there is a tendency for the wetness to be higher in tube *a*. With levels over +200 mm, the wetness in the end tubes is higher than that in the central one, and the difference is by two orders of magnitude with levels between +250 and +260 mm. The reason for the elevated wetness at the ends of the separator when the water level exceeds +200 mm is not due to the nonuniformity in the steam and water loads along the length, since the maximum occurs in the central part of the drum. With the working mass level in the separator, the wetness near the ends does not exceed 0.02%, and consequently this does not make an appreciable contribution to the average wetness ahead of the turbine. An average exit wetness of 0.1% is attained with the level lower than the wetness in the central tube on account of the elevated wetness at the ends of the separator drum when the level is more than +200 mm as indicated by the instruments with scales from −200 to +315 mm.

The test results led us to increase the nominal mass level in the separator by 100 mm (to the +100 mm mark as indicated by the gauges from −200 to +315 mm), which increased the water stock by 7 m^3 while keeping the steam wetness below 0.1%.

Therefore, the separators of diameter 2600 mm have a working margin as regards limiting permissible wetness. By maintaining the level over the immersed perforated sheet 100 mm higher than the design value,

one can increase the water stock in the forced circulation loop by 28 m^3 without interfering with increasing the steam output.

LITERATURE CITED

1. V. B. Karasev, Yu. M. Nikitin, O. Yu. Novosel'skii, and E. V. Sakovich, "The performance of steam separators at power units containing RBMK reactors," At. Energ., 53, No. 2, 70-74 (1982).
2. O. Yu. Novosel'skii, V. B. Karasev, E. V. Sakovich, et al., "Experience with operating and modifying separator drums in the first unit at Kursk nuclear power station," in: Nuclear Power Stations [in Russian], Issue 3, Énergiya, Moscow (1980), pp. 101-105.
3. A. G. Ageev, V. B. Karasev, I. T. Serov, and V. F. Titov, Separation Devices at Nuclear Power Stations [in Russian], Énergoizdat, Moscow (1982).

PECULIARITIES OF THE DISTRIBUTION OF PHASES IN THE UPDRAFT SECTION OF A HOUSED BOILING REACTOR

V. N. Fedulin, G. G. Bartolomei, V. A. Solodkii, and V. E. Shmelev

UDC 621.039.536.2

In order to increase the driving pressure head of the coolant natural circulation loop, one can mount a large-diameter updraft section above the active zone of a boiling reactor. The motion of a steam–water mixture in such a section is characterized by a complicated distribution of phases, and consequently the steam content. Nonuniformity of the energy liberation in the active zone and the velocity field of the phases at the entrance to the updraft section exerts a decisive influence on the structure of the two-phase flow.

At present there are no reliable recommendations on the calculation of the true volume steam content in a large-diameter channel, which is what the updraft section of a boiling reactor is. The value of the average steam content in the updraft section of a VK-50 reactor calculated by the VTI procedure [1] is 40% higher than the experimental values obtained on the basis of the measurement of the hydrostatic pressure differential. The main cause for this discrepancy consists, in our opinion, of the fact that the existing procedures for calculation of the steam content are based on the data of experimental investigations obtained in channels of small cross section and at a rather large distance from the entrance to the channel ($l/d > 20$), i.e., upon the motion of a hydrodynamically stabilized two-phase flow in which no significant transformation of the phase velocities and the steam content occurs from cross section to cross section in the channel.

The updraft section of boiling reactors is characterized by commensurable height and diameter dimensions ($H/D \approx 1$). This specifies incompleteness of hydrodynamic stabilization of the flow and makes inadmissible the use for calculation of the true volume steam content in them of the same relationships as for hydrodynamically stabilized flows. It is necessary for the improvement of the methods for calculation of the volume steam content in large-diameter channels to use data on the structure of hydrodynamically unstabilized two-phase flows. This is explained by the fact that one-dimensional computational models cannot take account of all the peculiarities of the spatial distribution of the phases.

An investigation of the structure of a two-phase flow in a large-diameter updraft section (D = 2 m, H = 3 m) using the electroprobing method was carried out on a VK-50 boiling reactor. The structure of the reactor, its operating regimes, and the layout of the placement of local steam content sensors have been described in [2, 3], and the procedure for analysis of the experimental results is discussed in [4].

The following peculiarities in the structure of a two-phase flow and in the hydrodynamics of the updraft section have been revealed in the analysis of the results:

1. The radial distribution of the steam content φ at the entrance to the updraft section is determined by the complex influence of the energy liberation q and the coolant flow rate W across the radius of the active zone

Translated from Atomnaya Énergiya, Vol. 57, No. 6, pp. 385-388, December, 1984. Original article submitted March 11, 1984.

0038-531X/84/5706-0811$08.50

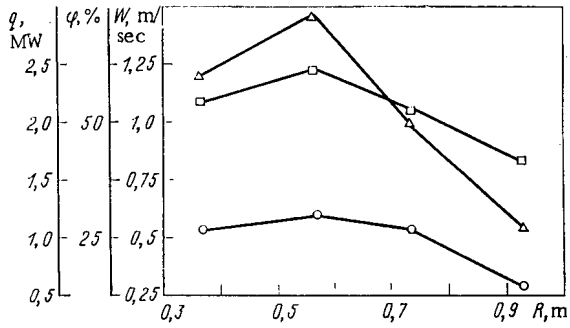

Fig. 1. Distribution of the energy liberation (○), steam content (△), and coolant velocity (□) across the radius of the active zone for a pressure of 2.0 MPa in the reactor and a thermal power of 80 MW.

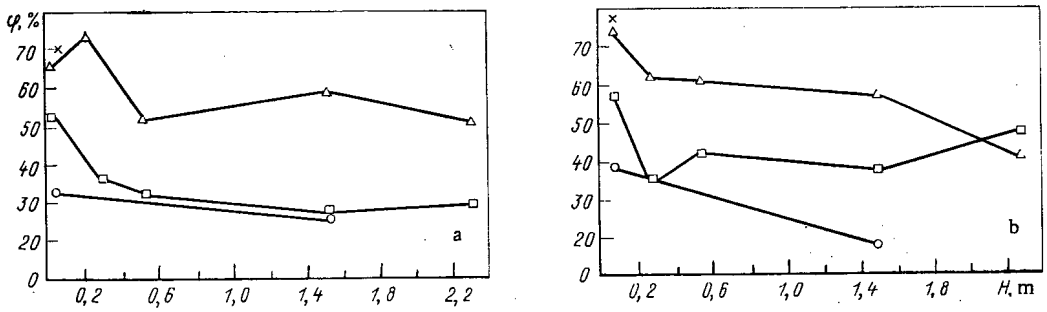

Fig. 2. Peculiarities of the steam content distribution with height of the updraft section for (a) p = 6.0 MPa and N = 170 MW and (b) p = 3.2 MPa and N = 150 MW: ○, ×, □, and △) R = 0.92, 0.74, 0.56, and 0.37 m, respectively.

R and, in connection with this, is of a sharply expressed nonuniform nature (Fig. 1). In particular, the steam content at the exit of the heat-generating assemblies (HGA) depends significantly on the position of the compensating rods (CR) in the active zone. Upon a rise in the reactor power, when the peripheral CR are essentially extracted, an increased steam content is noted above the HGA of the peripheral part of the active zone. The maximum of the steam content is shifted towards the center upon the subsequent extraction of the central CR.

2. The structure of the two-phase flow in the lower part of the updraft section, which is adjacent to the active zone, is determined to an appreciable extent by the jet nature of the coolant outflow from the HGA heads. To a large extent the jet nature of the outflow appears above the central HGA, and to a lesser extent above the peripheral HGA. The height of the jets depends on the velocity of the exiting two-phase flow, the working pressure p, and the hydrodynamics of the updraft section. For the VK-50 reactor the height of the jets does not exceed 0.4 m.

The jet nature of the outflow of the two-phase flow is exhibited in a corresponding variation of the steam content above the HGA heads. A maximum steam content is noted on axial lines of the jets. In power regimes (p = 6.0 MPa) with a supply of feed water to the "cold" drop section (i.e., under the central part of the active zone) the following effect of jet outflow of coolant from the central HGA has been noted: The steam content in the jet is higher at a distance of 280 mm from the HGA heads than at a distance of 80 mm (Fig. 2a). This effect is evidently explained by a "pressing down" of the steam–water flow, an increase in the rate of its movement, and a migration of the steam of its periphery to the jet axis. The jet effect disappears at a large height, which indicates a local equalization of the steam content.

At a low reactor power (< 100 MW), a lowered working pressure, and a change in the scheme of the feedwater supply the steam content in the jet at a distance of 280 mm from the HGA does not increase (Fig. 2b). This can be explained by a decrease in the velocity of the steam–water flow at the exit from the HGA and a breakdown of the jets at a lower level. This effect has not been detected in all regimes in the peripheral part of the updraft section, which may be caused by a deflection of the steam–water jets toward the center due to recirculation flows.

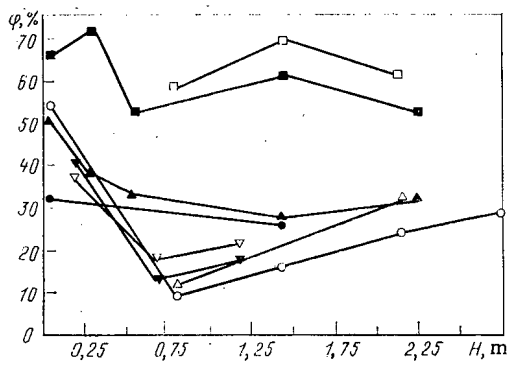

Fig. 3. Distribution of the steam content with height in the updraft section: ○, △, □) p = 6.5 MPa and N = 180 MW; ▽) p = 6.4 MPa and N = 181 MW; ▲) p = 6.4 MPa and N = 180 MW; ●, ▲, ■) p = 6.0 MPa and N = 170 MW; △, ▲) R = 0.74 m; □, ■) R = 0.37 m; and ○, ●, ▽, ▼) R = 0.92 m. m.

3. On the whole, the steam content distribution over the volume of the updraft section appears as follows. Near the axial line of the updraft section a coolant flow saturated with steam is formed with the maximum steam content at a distance of about 1-1.5 m from the active zone. The steam content decreases towards the output cross section of the updraft section. The steam content on the periphery of the updraft section first decreases sharply with height, reaching a minimum value at a height of 0.8 m, and then it gradually increases (Fig. 3). Complete equalization of the steam content in the output cross section of the updraft section is not attained [4].

4. It has been established on the basis of hydrodynamic measurements that the pressure differential on the periphery of the updraft section is higher than in its central region. In particular, the following values of the pressure differentials are obtained at a power of 168 MW with a pressure of 6.0 MPa: on the periphery, 12.8 kPa, and in the center, 11.22 kPa. Consequently, a definite radial pressure gradient exists in the updraft section which acts on the corresponding radial flows of the coolant.

Taking into account that in the output cross section of the updraft section equalization of the steam content (although incomplete) has been noted, one can assume in the first approximation that the static pressure on this cross section is constant. Then one can conclude that the maximum radial pressure gradient is observed in the lower part of the updraft section. An intensive migration of steam from the periphery of the updraft section to its central part has been noted precisely in this zone.

5. The values of the steam content averaged over the height of the updraft section which are calculated on the basis of the measured pressure differentials are related to each other and the calculated value as follows:

$$\varphi_c = \varphi_{calc} = (0.6)^{-1}\varphi_p,$$

where φ_c and φ_p are the experimental values of the steam content in the central and peripheral regions of the updraft section and φ_{calc} is the average value of the steam content calculated by the procedure of [1]. This result shows that the volume steam content in the updraft section above the central HGA is close to the calculated value and decreases significantly towards the periphery.

6. The nonuniformity of the steam content distribution in the updraft section determines the effectiveness of the individual updraft tubes mounted on the HGA heads. The isolated individual updraft tubes on the VK-50 reactor (height, 1.5 m, diameter, 150 mm) are mounted above different rows of HGA of the active zone. The investigations have shown that such mounting increases the coolant circulation velocity in the fifth (the periphery) row of HGA by 0.2 m/sec and in the fourth row by 0.1 m/sec. No increase has been noted in the coolant circulation velocity in the third row of HGA, which is determined by the rather high steam content above the HGA in question without installation of an individual updraft tube.

The experimental data obtained permit suggesting the following qualitative physical model of two-phase flow in the updraft section (Fig. 4). A jet outflow of a steam–water mixture exists at the exit from the HGA of the active zone. Due to the enhanced output of steam from the central HGA and the existence of a radial pressure gradient the steam–water mixture from the periphery of the updraft section is directed into its central region. In this connection an accelerated steam–water flow with an enhanced steam content is formed in this

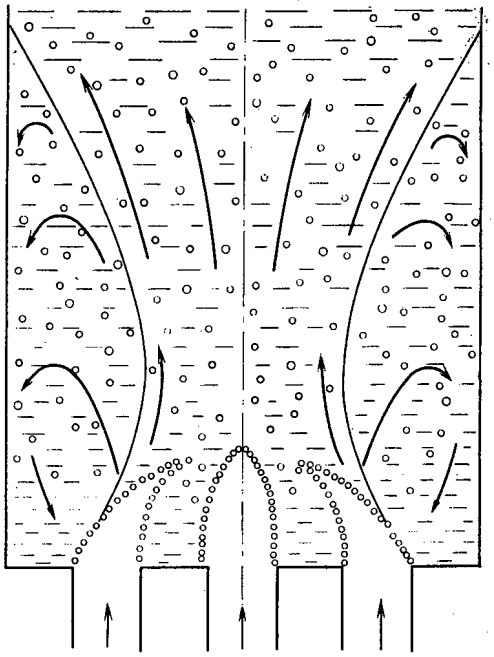

Fig. 4. Scheme of the flow of the steam–water mixture in the updraft section of the VK-50 reactor.

region. Upon the attainment of a specified height a gradual widening of the steam–water flow begins, which leads to equalization of the steam content over the cross section of the updraft section. A recirculation flow of coolant which deflects the steam–water jets from the peripheral HGA to the center is formed on the periphery of the updraft section in the zone of low steam contents.

The proposed physical model of the flow of a steam–water mixture and the experimental data obtained on the distribution of the steam content permit calculating more accurately the hydrodynamics of the updraft section of boiling reactors.

LITERATURE CITED

1. A. Ya. Kramerov and Ya. V. Shevelev, Engineering Calculations of Nuclear Reactors [in Russian], Atomizdat, Moscow (1964), pp. 320-322.
2. G. G. Bartolomei, V. A. Solodkii, V. N. Fedulin, et al., "Determination of the steam content in boiling reactors by the electroprobe method," Teploenergetika, No. 10, 15 (1980).
3. V. A. Solodkii, G. G. Bartolomei, V. N. Fedulin, et al., "An investigation of the hydrodynamics of an adiabatic two-phase flow in the updraft section of a VK-50 reactor," Teploenergetika, No. 6, 73 (1981).
4. V. N. Fedulin, V. E. Shmelev, V. A. Solodkii, and G. G. Bartolomei, "The steam content of a two-phase flow in the updraft section of a VK-50 boiling reactor," Preprint NIIAR-33 (598), Dmitrovgrad (1983).

EFFECTS OF STEAM GENERATOR SECTIONING ON THE RELIABILITY OF A NUCLEAR POWER STATION CONTAINING A FAST REACTOR

A. I. Klemin, O. B. Samoilov, and É. V. Frolov

UDC 621.039.526

One must provide adequate reliability in the individual units and in the station as a whole in order to meet current specifications for the economic performance and safety in nuclear power stations. In the case of sodium-cooled fast reactors, a current problem is to improve the reliability in the steam generators (SG) of sodium–water type. Various Soviet and foreign designs for such reactors use sectional SG, which raise the reliability and safety of the station because they localize possible faults caused by leaks in the SG heat-exchanger tubes to a single steam-generating section [1]. The SG sectioning makes it necessary to incorporate factors into the reliability model such as the SG repair strategy, the number of steam-generating sections in one cooling loop, and the working constraints on the available* unit power. We give below a model that has been used to examine the effects of these factors on the reliability of a fast-reactor system.

Model for the Structural Reliability of a Nuclear Power Station Unit Containing a Sectional SG. We consider a simplified structural scheme for the unit with one turbine and a fast reactor having m cooling loops, each of which includes pumps in the first and second loops, an intermediate heat exchanger, and a sectional SG (Fig. 1). The latter consists of a large number of components, including tube bundles, module bodies, steam–water chambers, sodium, steam, and water pipes, and cutoff equipment for the sodium and water (steam). The reliability calculations are based on two types of enlarged element in the sectional SG (Fig. 1): the element 5, which includes components whose failure makes it necessary to disconnect the entire SG and run down the corresponding cooling loop (for example, the sodium-handling gear), and element 6 (steam-generating section), which combines components whose failure leads to the disconnection of a separate section and corresponding reduction in the power of the given SG (tube bundle, module body, and seals on the covers on the steam–water chambers). Clearly, each of the elements 5 and 6 consists of corresponding SG components in series connection in the sense of reliability.

The reliability of the unit is most fully characterized by the power availability factor φ, which is calculated from the following formula for the basic mode of operation:

$$\varphi = \frac{1}{t_w} \int_0^{t_w} \overline{N}_a(\tau)\, d\tau, \tag{1}$$

where $\overline{N}_a(\tau)$ is the mean available power from the unit (as a fraction of the nominal power) at times $\tau \in t_w$, while t_w is the relevant working period.

A basic stage in constructing a model for power station reliability is to determine the dependence of N_a on the state y, which in turn is dependent on the states of various items. The basic principles have been considered in [2], according to which $N_a(y)$ is defined by means of special characteristics that are functions of the states of the individual units or sets of equipment (for example, cooling loop), which are subsequently called component parts. The state function for a component part characterizes the contribution to the station power (as a fraction of the nominal power) in a given state of the component part when the rest of the power station unit is completely free from faults. The state of element l (equipment unit) is defined by means of the binary variable x_l, which takes the value 0 in fault-free operation and 1 when the element fails.

The state functions $q_l(x_l)$, $l = \overline{1,7}$ for the equipment in this station are defined as follows:

*The maximum power that the unit can provide with all items fully viable.

Translated from Atomnaya Énergiya, Vol. 57, No. 6, pp. 388-393, December, 1984. Original article submitted August 9, 1982; revision submitted November 15, 1983.

0038-531X/84/5706- 0815$08.50

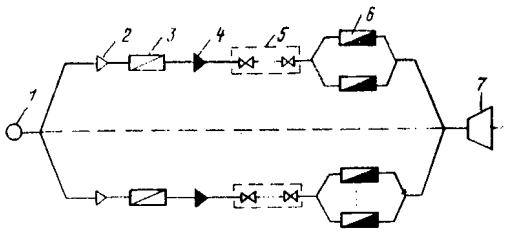

Fig. 1. Simplified structural scheme for a unit in a nuclear power station containing a fast reactor; 1) core; 2) first-circuit pump; 3) intermediate heat exchanger; 4) second-circuit pump; 5) enlarged element including the SG sodium equipment; 6) SG section; 7) turbine generator.

$$q_l(x_l)=\begin{cases}1-x_l & \text{for } l=1;\ 7;\\ \frac{1}{m}(1-x_l) & \text{for } l=\overline{2,5};\\ \frac{1}{m}\left(1-\frac{x_l}{n_s}\right) & \text{for } l=6,\end{cases} \tag{2}$$

where n_S is the number of steam-generator sections in a cooling loop. The values of the subscript l of 1 and 7 correspond to the core and the turbine generator, while the values of l of 2-6 correspond to the pump in the first circuit, the intermediate heat exchanger, the pump in the second circuit, and the enlarged elements of the SG, correspondingly.

As the sections are indistinguishable from the viewpoint of reliability (the elements 6), the state function $q_6(j)$ for a sectional SG and a separate cooling loop are defined by

$$q_6(j)=\begin{cases}\frac{1}{m}\left(1-\frac{j}{n_s}\right), & \text{if } j=\overline{0,\ j_{cr}-1},\\ 0, & \text{if } j=\overline{j_{cr},\ n_s},\end{cases} \tag{3}$$

where j is the number of failed sections in the SG for a cooling loop and j_{cr} is the critical number of SG sections whose failure causes the operation of the corresponding loop to be halted.

The state function for cooling loop j ($i = \overline{1, m}$) takes the following form because of the serial structure:

$$\psi_i=\min\{q_2(x_2^i),\ q_3(x_3^i),\ \ q_4(x_4^i),\ q_5(x_5^i),\ q_6(j_i)\}. \tag{4}$$

We use the state functions for the equipment in the cooling loop to represent the state vector for a unit in enlarged form:

$$y=\{q_1(x_1),\ q_7(x_7),\ \psi_1,\ \ldots,\ \psi_m\}. \tag{5}$$

If the reactor is operated with SG sections switched out (for overhaul), there may be differences in sodium temperature in the first circuit at the entry to the core resulting from the loops with different numbers of fault-free (or failed) SG sections. When certain limiting values of the temperature differences are reached, one usually has to impose constraints on the available power. To characterize such working constraints, we introduce the parameter $\Delta(y)$ for the state vector y, which is equal to the maximum difference between the power values (in relative units) for any two cooling loops:

$$\Delta(y)=m\{\max_{i=\overline{1,m}}[\psi_i]-\min_{i=\overline{1,m}}[\psi_i]\},\quad \psi_i>0. \tag{6}$$

We note that in (6) we envisage loops for which the values of ψ_i are different from zero, since otherwise the corresponding loop is taken out of service.

The constraints on the available power are determined by the limiting permissible value Δ_0 of $\Delta(y)$, which can be estimated as follows:

$$\Delta_0=\frac{d_0}{n_s}, \tag{7}$$

where d_0 is the maximum permissible difference in the numbers of fault-free (failed) SG sections in any two operating loops. The value of d_0 is defined from heat-engineering and strength calculations.

In accordance with (5), the desired $N_a(y)$ for the unit is

$$N_a(y) = \min\{q_1(x_1),\ q_7(x_7),\ Q\}, \tag{8}$$

where Q is the state function for the system of m cooling loops:

$$Q = \begin{cases} \sum_{i=1}^{m} \psi_i, & \text{if } \Delta(y) \leqslant \Delta_0; \\ \sum_{i=1}^{m} a_i, & \text{if } \Delta(y) > \Delta_0; \\ a_i = \min\left\{\psi_i,\ \left(b + \frac{\Delta_0}{m}\right)\right\}; \\ b = \min[\psi_i];\quad i = \overline{1,\ m},\ \psi_i \geqslant 0. \end{cases} \tag{9}$$

Expression (9) has been derived on the assumption that if there is a difference in sodium temperatures in the first circuit between any two cooling loops that exceeds the limiting permissible value, that difference is reduced to the permissible value by switching out the necessary number of sections in the loop with the higher power in order to provide the maximum unit power.

We now calculate the probabilities of realizing various states in the unit. We assume that planned preventative measures applied to the equipment are combined with reloading the reactor and form a periodic sequence, where the instants at which they are performed are points at which the equipment viability is completely restored. Also, we restrict consideration to the integral (tank) style for the equipment in the first circuit, which is very characteristic of fast reactors [1], where unplanned (emergency) repairs to the first-circuit pump and the intermediate heat exchanger make it essential to shut down the reactor. We subsequently assume that the equipment in the first circuit (pumps and intermediate heat exchanger) is not repairable in the interval [0, T] between planned preventative repairs, while unplanned repairs are combined with the next planned ones. Parts of the equipment that are repairable in the interval between planned preventative repairs include the core, the pumps in the second circuit, the SG elements, and the turbine generator. The probability that element l (Fig. 1) is fault-free at time τ is given by the standard formula in the case of exponential distributions for the time to failure and the recovery time:

$$P_l(\tau) = \frac{1}{\mu_l + \lambda_l}\{\mu_l + \lambda_l e^{-(\lambda_l + \mu_l)\tau}\},\quad \tau \in [0,\ T],\qquad (l = \overline{1,\ 7}) \tag{10}$$

where λ_l and μ_l are the rates of failure and recovery for element l, correspondingly. We note that (10) applies also when the equipment is not repairable, when $\mu_l = 0$.

On the basis of the above assumptions about the repairs, (1) becomes

$$\varphi \approx \left[\frac{1}{T}\int_0^T \overline{N}_a(\tau)\,d\tau\right](1-\delta), \tag{11}$$

where T is the interval between planned preventative repairs and δ is the mean proportion of station shutdowns related to planned preventative repairs and unplanned repairs combined with them for equipment in the first circuit not repairable in the interval [0, T] (pumps and intermediate heat exchanger).

We consider two types of repair strategy for a sectional SG in an individual loop:

1) strategy C_1, in which an SG section that fails is disconnected and repaired while the other sections operate; and

2) strategy C_2, where when a certain (critical) number of sections fail one switches out the corresponding cooling loop in order to repair the SG.

Within the framework of strategies C_1 and C_2 there is also the particular case where the repair of failed SG sections is combined with the next planned preventative repair to the unit.

Let $g_j(\tau)$ be the probability that at time $\tau \in [0, T]$ the sectional SG in a loop has j failed sections. For repair strategy C_1, the probability $g_j(\tau)$ is

$$g_j(\tau) = C_{n_s}^{j} P_6^{n_s - j}(\tau)\,|1 - P_6(\tau)|^j,\quad \tau \in [0,\ T], \tag{12}$$

where $C_{n_s}^{j}$ is a binomial coefficient and $P_6(\tau)$ is the probability of a viable state in the steam-generator section at time τ, which is calculated from (10).

For strategy C_2, the operation of the sectional SG is described by a Markov random process, and $g_j(\tau)$ is determined as the solution of a system of differential equations:

$$\begin{cases} \frac{dg_0(\tau)}{d\tau} = -\alpha_0 g_0(\tau) + \mu g_{j_{cr}}(\tau); \\ \frac{dg_j(\tau)}{d\tau} = \alpha_{j-1} g_{j-1}(\tau) - \alpha_j g_j(\tau), \quad j = \overline{1, j_{cr}-1}; \\ g_{j_{cr}}(\tau) = \sum_{j=0}^{j_{cr}-1} g_j(\tau), \end{cases} \tag{13}$$

where μ is the rate of SG recovery as a whole (with allowance for the time consumed in preparatory operations in disconnecting and connecting the loop), $\alpha_j = (n_S - j)\lambda_6$, and λ_6 is the failure rate in SG sections.

According to (2)-(4), the state function ψ_i for loop i takes $j_{cr}+1$ discrete values $0,\ldots,q_6(j),\ldots,1/m$. The probability that ψ_i is equal to one of these discrete values at an instant $\tau \in [0, T]$ is defined as follows:

$$P_\tau\{\psi_i = q_6(j)\} = \begin{cases} g_j(\tau) \prod_{l=2}^{5} P_l(\tau), & \text{if} \quad \psi_i = q_6(j) > 0; \\ 1 - [\prod_{l=2}^{5} P_l(\tau)] \sum_{j=0}^{j_{cr}-1} g_j(\tau), & \text{if} \quad \psi_i = q_6(j) = 0, \end{cases} \tag{14}$$

where $g_j(\tau)$ is calculated from (12) and (13) correspondingly for strategies C_1 and C_2.

One way of raising the reliability of a unit having sectional SG is to employ backup steam-generating sections. Let the SG in each loop have r backup sections, i.e., $n_S = \hat{n}_S + r$, where $\hat{n}_S$ is the minimum necessary number of working sections in the SG for an individual loop. We assume that the backup sections work in hot backup, and the loop is shut down for repairing the SG when $j_0 = r + 1$ sections fail (we envisage only strategy C_2). Clearly, the SG state function $q_6(j)$ and that for the cooling loop ψ take two discrete values: 1/m and 0.

The probability of realizing these states for loop i is

$$\begin{aligned} P_\tau\left\{\psi_i = \frac{1}{m}\right\} &= \left[\prod_{l=2}^{5} P_l(\tau)\right] \sum_{j=0}^{r} g_j(\tau); \\ P_\tau\{\psi_i = 0\} &= 1 - [\prod_{l=2}^{5} P_l(\tau)] \sum_{j=0}^{r} g_j(\tau), \end{aligned} \tag{15}$$

where $g_j(\tau)$ is calculated as the solution to (13) for

$$j_{cr} = j_0 = r + 1.$$

Formulas (10) and (12)-(15) enable one to calculate the probability of realizing state y:

$$P_\tau(y) = P_1(\tau) P_7(\tau) \prod_{i=1}^{m} P_\tau\{\psi_i = q_6(j_i)\}, \tag{16}$$

where j_i is the number of failed SG sections in loop i, and the probability $P_\tau\{\psi_i = q_6(j_i)\}$ is defined by (14).

The mean available unit power is

$$\overline{N_a}(\tau) = \sum_{y \in E} N_a(y) P_\tau(y), \tag{17}$$

where E is the set of unit states for which $N_a(y) > 0$.

Dependence of φ on Various Factors. The effect of using a sectional SG to improve unit reliability is dependent on various factors: the number of the sections and the reliability characteristics in the SG elements, the type of repair strategy, and the mode constraints on the available unit power. In what follows we consider the effects of these factors on the power use factor φ for a unit in a nuclear power station containing a fast reactor, having four cooling loops with sectional SG. The calculations are based on the above model, which has been implemented as a computer program. Table 1 gives the equipment reliability parameters used in the calculations. The values have been taken on the basis of operating experience with the corresponding equipment or data on the reliability of similar equipment (these may be considered as the authors' approximate estimates). The failure rates are taken as constant, which is usually correct for the period of normal operation, when the

TABLE 1. Equipment Fault-Free Parameters and Repairability

Equipment	Fault rate, h^{-1}	Recovery rate, h^{-1}
First-circuit pump	$3{,}7\cdot10^{-5}$	—
Second-circuit pump	$2{,}2\cdot10^{-5}$	$5\cdot10^{-3}$
Intermediate heat exchanger	$1{,}4\cdot10^{-5}$	—
Steam generator (n_s=16):		
element 5	$1{,}8\cdot10^{-5}$	$6{,}7\cdot10^{-3}$
element 6 (SG section)	$4{,}5\cdot10^{-5}$	$4{,}2\cdot10^{-3}$

running-in period has ended but the period of rapid aging has not begun. To simplify the calculations, the reliability in the core and turbine generator has been taken as substantially higher than that in the other equipment (Table 1).

We estimated the failure rate for element 5 (Fig. 1), which combines elements in the sectional SG whose failure leads to the entire SG and the corresponding loop being shut down, on the assumption that the main contribution comes from the sodium-handling equipment (failures of leak type). The failure rate for element 5 was estimated from

$$\lambda_5 = n_s \gamma \lambda_a, \tag{18}$$

where γ is the number of sodium-handling items per SG section and λ_a is the rate of failure of leak type for the sodium-handling equipment ($\lambda_a \approx 10^{-7}$ 1/h).

We also considered types of SG with different degrees of sectioning (n_S = 16 and n_S = 4), where we incorporated the dimensional effect, which is that the fault-free level of a section decreases as the power increases, which is due to variations in various factors (heat-transfer surface, number of tubes, and number of welded joints), all of which influence the fault experience in an SG section [3]. We assumed that this scale effect may be approximated by a power function of the form

$$\tilde{\lambda}_6 = \lambda_6 \left(\frac{n_s}{\tilde{n}_s}\right)^R, \tag{19}$$

where λ_6 and $\tilde{\lambda}_6$ are the failure rates in an individual section for an SG with the numbers of sections (per loop) n_S and $\tilde{n}_S$, correspondingly, while R = const is the parameter of the scale effect. The calculations were performed for R= 1 and R = 0.5.

The recovery rate μ for the SG with repair strategy C_2 was determined from data on the repairability of SG sections (Table 1) and the mean times involved in the preparatory operations, which was taken as about 70 h.

Table 2 gives calculations on φ for a system containing a fast reactor in the interval between reloading operations (planned preventative repair) $t \approx 3000$ h with the proportion of planned shutdown time $\delta \approx 0.127$. The values of φ in Table 2 have been derived for $d_0 = n_S$ and $\Delta_0 = 1$, i.e., on the assumption that there are no mode constraints on the available power due to possible temperature differences. It is evident that strategy C_1 provides higher values of φ than does C_2, which occurs because it most fully uses the advantages of the sectional SG structure. The advantage thereby gained is largely determined by the degree of SG sectioning, as well as the scale effect, and the maximum values occur for an SG with a small number of sections (n_S = 4) when reliability is low (R = 1). The calculations also showed that when the section reliability is high ($1/\lambda_6 \geq 7\cdot 10^4$ h), the type of SG repair strategy has virtually no effect on φ.

It should be noted that implementing strategy C_1 involves technical difficulties of the shutoff equipment, which has to enable one to repair a failed section while the other sections of the SG in the loop are operating. Therefore, one usually employs strategy C_2 in practice. We considered two particular cases: j_{cr} = 1 and $j_{cr} = n_S$. In the first case, failure in any section leads to the corresponding loop being shut down for SG repair, while in the second case the loop is not shut down when sections fail (one merely shuts down the failed sections) and the repair is combined with the next reactor reloading. Table 2 shows that the latter strategy ($j_{cr} = n_S$) is preferable for an SG with a large number of sections (n_S = 16) since it provides a substantial increase (about 10%) in the equipment reliability parameter. We note that this repair strategy, with failed sections shut down, is possible if a certain specification for the level of repairability in the SG sections is met: The mean section repair (replacement) time should not exceed the reactor reloading time.

TABLE 2. Values of φ in Relation to Repair Strategy and Degree of SG Sectioning

Steam generator form	C_1 strategy	C_2 strategy			
		$j_{cr}=1$	$j_{cr}=2$	$j_{cr}=3$	$j_{cr}=n_s$
$n_s=16$	0,795	0,659	0,728	0,744	0,751
$n_s=4$ $R=0,5$	0,789	0,728	0,724	0,710	0,706
$R=1$	0,774	0,660	0,675	0,644	0,626

TABLE 3. Values of φ in Relation to Mode Constraints

Steam generator form	$d_0=1$	$d_0=2$	$d_0=3$	$d_0=n_s$ ($\Delta_0=1$)
$n_s=16$	0,734	0,746	0,750	0,751
$n_s=4$ $R=0,5$	0,681	0,704	0,706	0,706
$R=1$	0,585	0,620	0,626	0,626

Two factors determine the effects of SG sectioning on φ: the scale effect for the reliability parameters of a section, which is due to the change in unit power, and the scheme effect, which is related to the change in the number of SG sections in the loop. Also, according to (18) any change in the number of SG sections leads to a change in the amount of shutdown equipment in the loop and to a corresponding change in the reliability characteristics of the enlarged element 5 in the SG (Fig. 1). The calculations showed (Table 2) that enlarging the SG sections reduces φ for both repair strategies. As would be expected, the reduction in φ is more substantial for strategy C_2 when there is a substantial scale effect (R = 1). Also, when the number of SG sections is small (n_S = 4) and the section reliability is low (R = 1), there is a pronounced optimum for φ, which is attained if one switches out a loop for SG repair when two sections fail (j_{cr} = 2), Clearly, this optimum is dependent on the degree of SG sectioning, the fault experience level, and the repairability, as well as on the value of the interval [0, t] between reactor reloads (planned preventative repair), and the value in each particular case can be determined from a more detailed analysis.

We now consider the dependence of φ on the available-power constraints due to the possibility of the above temperature differences. The calculations were performed for wide ranges in d_0 and Δ_0, which determine these constraints. The limiting value $d_0 = n_S$ (Δ_0 = 1) corresponds to the case where there are no constraints of this type, while d_0 = 1 corresponds to the case where the latter are considerable. The effects of the constraints on φ are slight for strategy C_1. Table 3 gives calculations for these forms of SG with strategy C_2 ($j_{cr} = n_S$) for $t = 3 \cdot 10^3$ h and $\delta = 0.127$.

Table 3 shows that the constraints may reduce φ if the SG has a small number of sections because these constraints begin to make themselves felt as shutdown states with small numbers of failed SG sections as the unit power of an SG section increases. Because of the scale effect, the probability of such states is fairly high, and therefore the effects of the constraints (or of d_0 and Δ_0) on φ are most pronounced.

This model was also used in analyzing the scope for increasing the reliability of a system containing a fast reactor by using r backup sections in each cooling loop. It was assumed that the backup sections operate in hot backup, while a loop is shut down for repair of the corresponding SG when r + 1 sections fail. For the SG with n_S = 16 working sections, we obtained the following values of φ ($t = 3 \cdot 10^3$ h, δ = 0.127):

$$\varphi = \begin{cases} 0.659, & \text{if } r=0; \\ 0.742, & \text{if } r=1; \\ 0.773, & \text{if } r=2, \end{cases}$$

where the case r = 0 corresponds to strategy C_2 (j_{cr} = 1).

These results showed that backup sections in the SG provide an effective means of raising the system reliability parameters. The largest φ is attained when the number of backup sections is small (r = 1 or 2). A real SG design always has some spare power margin, which can be considered as hot backup in relation to the

nominal SG power. Therefore, the above advantages due to section backup can be realized in practice for example as follows: When one SG section fails, the loop continues to operate at its nominal power because the power levels in the fault-free sections are raised.

LITERATURE CITED

1. O. L. Kazachkovskii et al., At. Energ., 43, No. 5, 343 (1977).
2. R. A. Peskov and É. V. Frolov, Aspects of Nuclear Science and Engineering: Series Nuclear Reactor Physics and Engineering [in Russian], Issue 1 (10) (1980), p. 29.
3. H. Procaccia, Reliability of Nuclear Power Plants, IAEA, Vienna (1975), p. 351.

STATISTICAL ANALYSIS OF REACTOR THERMAL POWER BY THE USE OF THERMAL AND RADIATION METHODS IN THE FIRST UNIT AT THE ARMENIAN NUCLEAR POWER STATION

F. D. Barzali, L. N. Bogachek, V. V. Lysenko, A. M. Muradyan, A. I. Musorin, A. I. Rymarenko, I. V. Sokolova, and S. G. Tsypin

UDC 621.039.564

A very important factor in providing safe operation in a nuclear power station unit is to determine the thermal power of the reactor W with an error of 1-2% [1-4]. Operational methods have been proposed [1, 2, 4] for measuring the thermal power by statistical computer calculation methods; in [3, 5], operational correlation dispersion methods were considered for determining the thermal power by means of radiation meters (with an error of 1-2% at the nominal power), these meters operating with the neutrons leaking from the reactor containment [power meters (PM)] or on the γ radiation from ^{16}N in the coolant [loop detector (LD)]. The data entering these meters are used in determining discrete quantities of statistical nature, and this enables one to obtain given errors in the readings of the PM (N_{PM}) and LD (N_{LD}). Also, a major feature of a radiation meter is that N_{PM} and N_{LD} are strictly proportional to W, as has been confirmed by experiment [3].

In view of these advantages, it is of interest to perform a combined statistical analysis of the data obtained by these methods and those provided by the standard thermal detectors (TD) in order to define the reactor thermal power more accurately and to determine the errors.

Table 1 gives data for one-factor variance analysis, which have been obtained with the first unit at the Armenian nuclear power station (the ratio of the thermal reactor power measured by the TD and expressed as a percentage of the nominal power to the readings of the PM in count/sec). This approach supplements traditional analysis of measurement methods in enabling one to analyze results corresponding to several levels of thermal power (which may differ substantially). The dots in $\bar{W}_{\cdot j}$ and $\bar{W}_{i\cdot}$ indicate averaging correspondingly with respect to the subscripts i and j.

The thermal power was determined by the following thermal methods:

1) i = 1, from the sum of the products of the differences of the enthalpies for the hot and cold parts of the loop by the coolant flow rates in the corresponding main circulation loops;

2) i = 2, from the product of the mean difference in enthalpies of the hot and cold parts of the loop by the total coolant flow through the reactor;

3) i = 3, from the thermophysical coolant parameters in the second circuit beyond the feed pumps;

4) i = 4, from the steam in the steam generators;

5) i = 5, from the feedwater in the steam generators;

Translated from Atomnaya Énergiya, Vol. 57, No. 6, pp. 393-397, December, 1984. Original article submitted September 5, 1983.

0038-531X/84/5706-0821$08.50

TABLE 1. Initial Data for One-Factor Variance Analysis of the Ratio $W_{ij}/N_{PM\,j}$ of the Thermal Detector Readings on the Reactor Power to the PM Readings*

Number of measurement method and statistical-characteristic estimator for thermal power level j	$N_{PM\,j}$, count/sec; W_j, %				Mean thermal power for method of measurement i $\overline{W}_{i\cdot}=\frac{1}{J}\sum_{j=1}^{J}\frac{W_{ij}}{N_{PM\,j}}$	Variance estimator for measurement method j $S_i^2\cdot10^3$
	51,93 / 45,67	70,90 / 68,79	89,55 / 86,72	93,13 / 92,72		
1	0,8230	0,9317	0,9485	0,9787	0,9205	4,6011
2	0,8639	0,9647	0,9749	1,0037	0,9518	3,7075
3	0,8951	1,0333	1,0172	1,0336	0,9948	4,4796
4	0,8190	0,9234	0,9174	0,9685	0,9071	3,9700
5	0,7849	0,9306	0,9358	0,9417	0,8982	5,8304
6	0,9561	0,9942	0,9903	1,0254	0,9915	$8,0496\cdot10^{-1}$
7	1,0137	1,0127	0,9949	1,0171	1,0096	$9,8724\cdot10^{-2}$
$\overline{W}_{\cdot j}=\frac{1}{IN_{PM\,j}}\sum_{i=1}^{J}W_{ij}$	0,8794	0,9701	0,9685	0,9955	—	—
Estimate of the variance $S_j^2\cdot10^3$	6,6924	1,9381	1,2776	1,1306	—	—
Weight of mean $g_j=\frac{1}{S_j^2}$	149,4232	515,9692	782,7176	884,4861	—	—

*Here i is the number of the method of measuring the thermal power, $1\le i\le I$–7 while j is the thermal power level $1\le j\le J=4$.

6) i = 6, from the coolant parameters in the second circuit in the turbine control-stage chambers; and

7) i = 7, from the coolant parameters in the second circuit after the high-pressure heaters.

The variance analysis is performed with the method of measuring the thermal power as the factor. The Bartlett test [6] and the Cochran test [7] enable one to determine whether there is equality in the variances in the data groups.

The Bartlett test is based on comparing the calculated value of χ^2 with the χ^2_{tab} distribution having $I-1$ degrees of freedom. In that case, with probability $1-\alpha = 0.95$, $\chi^2_{tab}(I-1=6) = 12.592 > \chi^2 = 9.338$, so the variance series is homogeneous.

The Cochran test is based on considering the quantity

$$G_i=\frac{S_i^2}{\sum_{i=1}^{I}S_i^2}.$$

The value found $G_{max}=\max\{G_i\}=0.245$ is less than the tabulated one $G_{tab}(I=7, J-1=3)=0.48$ for $1-\alpha=0.95$, i.e., the series of variances S_i^2 is homogeneous.

We test the hypothesis $H_0: \overline{W}_{1\cdot}=\overline{W}_{2\cdot}=\overline{W}_{3\cdot}=\ldots=\overline{W}_{7\cdot}$. Adopting the hypothesis corresponds to the method of measuring the thermal power not being significant as a factor. The quantities needed to test the hypothesis are given in Table 2.

We also used the Fisher test [8], whose statistic is the ratio $F=S_B^2/S_R^2$. If $F<F_{tab}$, the hypothesis is accepted with probability $1-\alpha$, where F_{tab} is the value of the F distribution with ν_B and ν_R degrees of freedom.

Table 2 shows that $F<F_{tab}$, i.e., hypothesis H_0 is true with probability $1-\alpha=0.95$.

As the method of measuring the thermal power is not significant as a factor, the overall mean, which is an estimator for the true value of a ratio, is [6] given by

$$\overline{W}=\frac{\sum_{i=1}^{I}\overline{W}_{i\cdot}}{I}. \qquad (1)$$

The estimator for the variance of the overall mean is given by [6]

TABLE 2. Quantities Needed to Test the Hypothesis H_0: $\overline{W}_{1.} = \overline{W}_{2.} = \ldots = \overline{W}_{7.}$

Variance source	Sum of the squares of the difference	Degree of freedom	Mean square, × 10^3	F ratio (Fisher test)
Between levels	$J\sum_{i=1}^{I}(\overline{W}_{i.}-\overline{W})^2=0{,}0503$	$\nu_B=I-1=6$	$S_B^2=\frac{J\sum_{i=1}^{I}(\overline{W}_{i.}-\overline{W})^2}{\nu_B}=8{,}3858$	$F=\frac{S_B^2}{S_R^2}=2{,}507$
Within levels	$\sum_{i=1}^{I}\sum_{j=1}^{J}(W_{ij}-\overline{W}_{i.})^2=0{,}0702$	$\nu_R=IJ-I=21$	$S_R^2=\frac{\sum_{i=1}^{I}\sum_{j=1}^{J}(W_{ij}-\overline{W}_{i.})^2}{\nu_R}=3{,}3446$	$F_{tab}\ (6,21)=2{,}57$
Total	$\sum_{i=1}^{I}\sum_{j=1}^{J}(W_{ij}-\overline{W})^2$	$\nu_T=IJ-1=27$		

*For simplicity, the symbol W_{ij}/N_{PMj} is replaced by W_{ij}.

$$S_{\overline{W}}^2=\frac{1}{IJ\,(IJ-1)}\left[(J-1)\sum_{i=1}^{I}S_i^2+J\sum_{i=1}^{I}(\overline{W}_i-\overline{W})^2\right], \tag{2}$$

where $S_i^2=\frac{1}{J-1}\sum_{j=1}^{J}(W_{ij}-\overline{W}_{i.})^2$; $S_{\overline{W}}^2=7.38\cdot10^{-5}$.

Further, we use the same data in a one-factor variance analysis now assuming that the PM reading is the factor, or, which is the same, the reactor thermal power level.

We checked the variances for equality on the Bartlett and Cochran tests, which showed that with $1-\alpha=0.95$, $\chi^2=6.3<\chi^2_{tab}\ (J-1=3)=7.18$, but $G_{max}=0.6>G_{tab}\ (J=4,\ I-1=6)=0.6$.

In the case of the more searching Cochran test, we assume that the variance series is inhomogeneous.

On the Fisher test, the hypothesis H_0: $\overline{W}_{.1}=\overline{W}_{.2}=\overline{W}_{.3}=\overline{W}_{.4}$ is rejected, i.e., the thermal power level factor is significant:

$$S_B^2=0.01811,\quad S_R^2=0.00276,$$
$$F=6.56;\ F_{tab}\ (\nu_B=3;\ \nu_R=24)=3.01\ \text{and}\ F>F_{tab}.$$

One also has to consider whether there is a monotone trend (bias). The check was made via the Abbé test [6], which showed that there was no systematic bias.

Therefore, as the variance series is inhomogeneous here, the overall mean is calculated from the following formula [6]:

$$\overline{W}_v=\frac{\sum_{j=1}^{J}g_j\overline{W}_{.j}}{\sum_{j=1}^{J}g_j}=0.97337 \tag{3}$$

with variance

$$S_{\overline{W}_v}^2=\frac{1}{(IJ-1)\sum_{j=1}^{J}g_j}\left[\frac{I-1}{I}\sum_{j=1}^{J}g_jS_j^2+\sum_{j=1}^{J}g_j(\overline{W}_{.j}-\overline{W}_v)^2\right]=8.2696\cdot10^{-5}. \tag{4}$$

Table 1 shows that the data group corresponding to the 45.7% thermal power level has a variance deviating from homogeneity. In fact, if we exclude this level, we find that the Bartlett and Cochran tests are obeyed: $\chi^2=0.462<\chi^2_{tab}\ (J-1=2)=5.991$; $G_{max}=0.45<G_{tab}\ (J=3;\ I-1=6)=0.68$, and the hypothesis H_0: $\overline{W}_{.1}=\overline{W}_{.2}=\overline{W}_{.3}$ is adopted, since $F=0.12<F_{tab}\ (\nu_B=2;\ \nu_R=18)=3.55$.

As the overall mean we take $\overline{W}=0.97802$ as calculated from (1) with the variance $S^2_{\overline{W}}=6.9787\cdot10^{-5}$ derived from (2).

There is agreement between $\overline{W}_v$ (for four levels) and $\overline{W}$ (for three levels) within limits of 0.5%, which means that any of the methods can be used to determine the overall mean to represent the data.

TABLE 3. Initial Data for One-Factor Variance Analysis of the Ratio ($N_{LD\,j}/N_{PM\,j}$) of the Readings of the LD and PM*

LD number and statistical characteristics at thermal power level j	Thermal power level, %			
	45,67	68,79	86,72	92,72
1	18,98513	21,02179	21,26456	21,35204
2	16,90206	18,41803	18,76677	19,3974
3	19,67568	21,51271	21,90422	21,73452
4	18,10867	19,30894	19,32148	19,70669
5	18,4738	19,0873	18,79937	19,4788
6	16,86181	17,13507	17,02104	17,62577
7	21,64438	22,43573	22,79485	22,57515
8	18,96502	19,80766	20,02392	20,73347
Arithmetic mean	18,702053	19,840896	19,987026	20,32548
$\bar{N}_{\cdot j} = \frac{1}{I}\sum_{i=1}^{I}\frac{N_{LD\,ij}}{N_{PM\,ij}}$				
Variance estimator on S_j^2	2,3978927	3,0172178	3,6189341	2,5023178

*Here $1 \le i \le 8$ is the LD number and $1 \le j \le 4$ is the reactor thermal power level.

The thermal power level factor is significant in analyzing four levels but is not significant for three, which indicates considerable error in measuring low thermal power either with TD or by radiation methods since the data set is represented by the ratio $W_{ij}/N_{PM\,j}$.

To elucidate what influences the error in measuring the relative thermal power, we checked the readings of the PM and LD against one another when they were working simultaneously in the first unit at the Armenian nuclear power station, i.e., we performed a one-factor variance analysis of the data given in Table 3.

On testing the hypothesis $H_0: \bar{N}_{\cdot 1} = \bar{N}_{\cdot 2} = \bar{N}_{\cdot 3} = \bar{N}_{\cdot 4}$, we found that the thermal power level factor is not significant. In fact $S_B^2 = 3.9696$, $S_R^2 = 2.8841$, while $F = 1.38 < F_{tab}^2$ ($\nu_B = 3$; $\nu_R = 28$) = 2.95. Hypothesis H_0 is adopted with probability $1 - \alpha = 0.95$, so the significance of this factor for the previous set of data with four power levels is due to the larger error in measurement by means of the TD at power levels below the nominal value.

This was confirmed by regression analysis in deriving the dependence of $\hat{W}_i$ on the readings $\hat{N}_{PM\,i}$ [3]. According to this evaluation, the confidence limit with probability $1 - \alpha/2 = 0.975$ is 5% for a thermal power of about 50% nominal, while the limit is 2.5% for the thermal power determined from the dependence of $N_{LD\,i}$ on $N_{PM\,i}$.

Therefore, combined statistical analysis of the thermal power determined by the standard thermal detectors and by radiation methods firstly enables one to calculate the means and the errors of these independently of the thermal power level and secondly enables one to check radiation meters against one another during operation.

LITERATURE CITED

1. V. A. Voznesenskii, "Some results from operating nuclear power stations containing VVÉR-440 reactors," At. Energ., 44, No. 4, 294 (1976).
2. F. Ya. Ovchinnikov, L. I. Golubev, V. D. Dobrynin, et al., Working Conditions in Pressurized-Water Power Reactors [in Russian], Atomizdat, Moscow (1979).
3. L. N. Bogachek, K. A. Gazaryan, and V. V. Lysenko, "A correlation-variance method of measuring VVÉR power," At. Energ., 50, No. 6, 420-422 (1981).
4. E. I. Ignatenko, V. V. Zverkov, and V. N. Dement'ev, "Computer use in calculating reactor thermal power," Elektricheskie Stantsii, No. 2, 9-12 (1982).
5. L. N. Bogachek, A. L. Egorov, V. V. Lysenko, et al., "Measuring coolant flow rate and power by radiation methods in the first unit at the Armenian nuclear power station," At. Energ., 46, No. 6, 390-393 (1979).
6. K. P. Shirokov (ed.), Methods of Processing Observational Results from Measurments, Trudy Metrologicheskikh Institutakh SSSR, Issue 134(194), Standartov, Moscow–Leningrad (1972).

7. A. S. Zazhigaev, A. A. Kish'yan, and Yu. I. Romanikov, Methods of Planning Physics Experiments and of Processing the Results [in Russian], Atomizdat, Moscow (1978).
8. A. Afifi and S. Eisen, Statistical Analysis: a Computer Approach [Russian translation], Mir, Moscow (1982).

TEST STAND FOR RESEARCH ON THE PHYSICS OF HIGH-TEMPERATURE GAS-COOLED REACTORS

A. M. Bogomolov, V. A. Zavorokhin,
A. S. Kaminskii, S. V. Loboda,
A. D. Molodtsov, V. V. Paramonov,
V. M. Talyzin, and A. V. Cherepanov

UDC 621.039.519.4

During the development of new reactors their physical characteristics are investigated on critical assemblies. High-temperature gas-cooled reactors (HTGR), under development in our country and abroad, have many new aspects. The I. V. Kurchatov Institute of Atomic Energy has built a critical stand GROG which is used to study the physics of HTGR, i.e., the physics that is common to all modifications and the specific physics tha takes into account the features of different versions of HTGR, primarily the VG-400 [1].

The breadth of the studies of the HTGR physics on the GROG stand as well as economic and time considerations have made it necessary to employ modeling principles, making it possible to create a simple and flexible design that provides a capability for forming critical assemblies with different parameters quickly and at low cost and performing a large number of experiments on them. Experiments on one-zone and two-zone assemblies can be carried out on the stand. In the two-zone assemblies the zone under study is formed of full-scale reactor elements and the seed zone is formed of model elements and as a result the criticality of the assembly of the whole is produced. This ensures wide variation of the neutron-physical characteristics of the seed zone and their similarity to the system of full-scale elements as far as properties are concerned. This similarity eliminates boundary effects and this makes the test zone more representative. The capability for wide variation of the neutron-physical parameters in the critical assemblies using model elements and the similarity of such assemblies to the reactors under study make it possible to solve many problems on model systems. Therefore, in the initial stage, when the full-scale elements are absent, the physics of HTGR are studied on critical assemblies formed of model elements. Since products of the reaction of the fuel with neutrons are difficult to use in assemblies, problems pertaining to the burn-up of fuel are also considered on systems containing model elements.

The necessary zones can be built from a combination of elements that are simple and convenient to use: fuel elements (FE) of two types —with enrichment to 10% ^{235}U (at a uranium dioxide density of 0.5 g/cm^3 or with the dioxide of natural density at a density of 0.5 and 1 g/cm^3), dummy moderating elements (DE) (graphite blocks and inserts into them), and absorbing elements (AE).

The full-scale HTGR fuel elements use microfuel dispersed in a graphite matrix. The model fuel elements of the stand GROG, universal physical imitators of HTGR fuel elements, are made in the form of a homogeneous mixture of uranium dioxide and Teflon [2]. This composition of the fuel-element imitators allows them to be prepared by means of a substantially simplified technology and at comparatively low cost.

The fuel-element imitators and graphite inserts are cylinders of diameter 50 mm and height 10, 25, or 50 mm. Graphite sleeves are also used to produce the necessary porosity. Continuous variation of the amount of neutron-absorbing material in the assemblies is effected with the aid of a set of absorbers of diameter 50 mm, made of boron-containing water or aluminum—boron alloy, as well as boron carbide rods of diameter 12 mm. The necessary combination of cylindrical elements is placed in the channels of graphite blocks with a 250 × 250 mm cross section. The graphite blocks have nine 55-mm holes, located at the lattice points of a square lattice with a pitch of 83.5 mm.

Translated from Atomnaya Énergiya, Vol. 57, No. 6, pp. 397-400, December, 1984. Original article submitted February 21, 1984.

0038-531X/84/5706- 0825$08.50

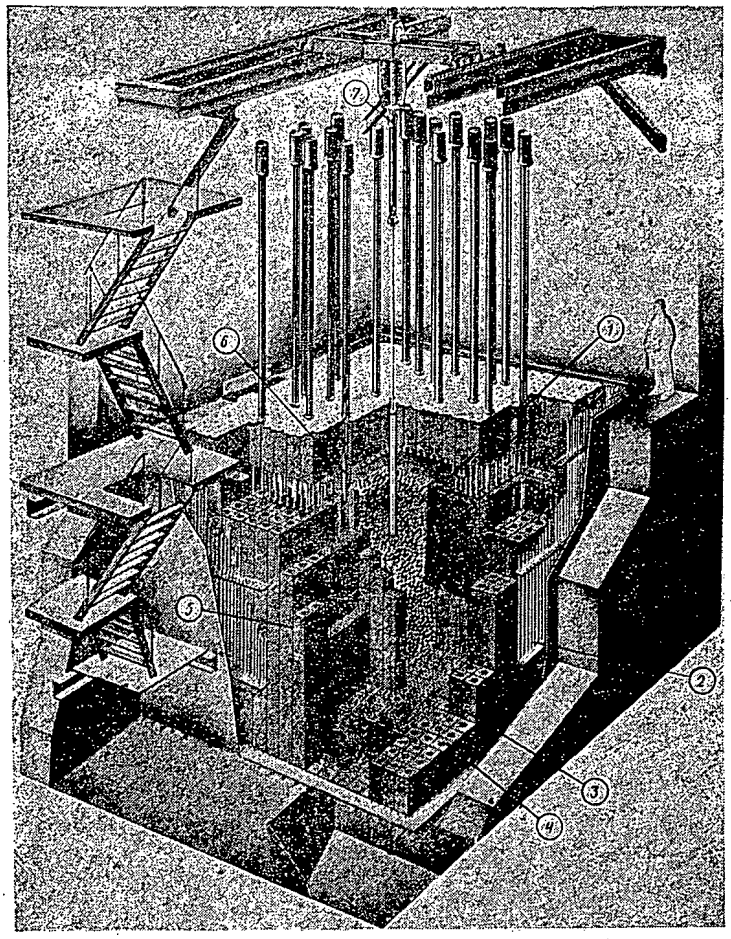

Fig. 1. Critical stand GROG for research on the physics of HTGR: 1) spherical fuel elements of the zone under study; 2) fuel-assembly storage; 3, 4) graphite blocks of the seed zone and reflector; respectively; 5) experimental channel; 6) rod of control and safety system; 7) oscillator.

The neutron-physical characteristics of fresh fuel elements are modeled on the critical assemblies of the stand under the following conditions:

the model system has the same principal isotopes and the same ratios of their nuclear concentration as does the full-scale system;

the model and full-scale systems approximate a homogeneous system for nonresonance neutrons (the blocking in the fuel is less than 10%);

the resonance effects in the model and full-scale systems are the same. The necessary ratio of the nuclear concentrations of the isotopes and the required resonance effects are attained by means of an appropriate set and combination of fuel elements and graphite inserts.

The considered set of elements makes it possible also to simulate burn-up on the assemblies of the stand. The products of the reaction of the fuel with neutrons are simulated by using ^{235}U, ^{238}U, and boron. The combination of fuel elements and absorbing elements (fuel-assembly module) required for this purpose is selected from the condition that the fission and absorption integrals be preserved for the full-scale and model systems and that the macroscopic cross sections coincide in the energy range of the neutrons.

Computational studies showed that the necessary neutron-physical properties of an HTGR over the entire range of parameters considered are ensured in the critical assemblies of the stand. In particular, the stand provides a good simulation of the field of energy release and spectral characteristics, even in a highly inhomogeneous system with the principle of OPAZ in the equilibrium state.

Structurally, the critical assembly of the stand GROG has been built as follows. A set of graphite blocks forms a cubic stack with a 450-cm face. Different geometrical and physical parameters of the core and reflec-

TABLE 1. Main Characteristics of Methodological Assemblies

Parameter	Assembly							
	1-01	2-01	2-02		2-03		3-01	4-01
			A	B	A	B		
Size of core, mm								
x	75	75	75	25	75	25	75	75
y	92	75	75	25	75	25	75	75
z	80	110	110	110	110	110	170	120
Ratio of carbon and uranium nuclear concentrations	250	500	500	500	500	500	250	250
Structure of fuel-assembly module	FE-50	FE-50	FE-50	FE-30	FE-50	FE-10	FE-25	FE-25
	FE-50	DE-50	DE-50	FE-30	DE-50	DE-10	AE-0.5/5	AE-0.5/10
	FE-50	FE-50	FE-50	FE-30	FE-50	FE-10	FE-25	FE-25

Composition of the elements of the module: FE-50 (30, 10, 25) – a universal physical imitator of height 50 (30, 10, 25) mm with 10% uranium enrichment; DE-50 (30, 10) – a graphite insert of height 50 (30, 10) mm; AE-0.5/5 (0.5/10) – a disk of boron-containing paper of thickness 0.5 mm and boron content 5 and 10 mg.

tor are provided by placing different combinations of cylindrical elements into the channels of the graphite stack. Control rods can be placed in the central channels of the columns of the graphite stack. Cylindrical channels of diameter 15 mm in the corners of the graphite columns can hold boron carbide absorbing elements, of diameter 12 mm for simulating perturbations, as well as sensors of the measuring system. When some of the graphite blocks are removed their place can be taken by a fragment, or a mockup of a fragment, of the reactor under study. In particular, mockups of spherical fuel elements, absorbing elements, and dummy elements of the VG-400 reactor are used in the stand.

Figure 1 shows the makeup of the critical assembly of the stand GROG, including a central zone of spherical elements that is under study, a seed zone, and a graphite moderator surrounding them. As in high-temperature gas-cooled reactors, there is a space between the active zone (core) and the upper end reflector.

The design of the stand allows sensors of the measuring system to be arranged in any way desired. Besides in-line acquisition and processing of experimental results, the multichannel automatic system of data acquisition, storage, and processing, including a computer and terminals, makes it possible substantially to extend the application of techniques directed at fuller and higher-quality research.

The main parameters of the stand GROG are:

No. of graphite columns	324
Maximum linear size of core, mm	4000
Maximum number of channels	2304
Uranium enrichment, %	0.7-10
Maximum ^{235}U charge, kg	250
Volume porosity of core, %	5-40
Ratio of carbon and uranium nuclear concentrations	200-2000
Simulated regimes of HTGR operation	initial, transient, equilibrium
Number of randomly arranged rods of control and safety system	up to 24

The experiments on GROG were carried out in a certain sequence determined by the aims and logic of the development of the investigations as well as by the methodological and technical preparedness for each stage. The experiments started with a study of small, methodological critical assemblies that were simple in composition and configuration; in the first place this decreases the number of indeterminacies upon comparison with the results of calculations and, second, makes it possible for experiments with a large number of versions to be carried out rapidly and simply. Subsequent experiments were aimed at verifying the simulation of the required neutron-physical properties and studying the distinctive features of the HTGR studied, primarily the VG-400.

The scope of the investigations on the methodological assemblies encompassed the development of experimental methods and the technique of work on the stand, verification of the initial (specification) data on the ma-

TABLE 2. Composition of Measurements on Methodological Assemblies

Parameter studied	Assembly					
	1-01	2-01	2-02	2-03	3-01	4-01
K_{eff}	+	+	+	+	+	+
Reactivity effect	+	+	+	+	+	+
Eff. of control and safety rod system	+	+	+	+	+	+
Reaction rate						
^{164}Dy (n, γ)	+					
^{63}Cu (n, γ)	+	+	+	+	+	+
Thermal-neutron activation:						
^{164}Dy	+					
^{63}Cu	+	+	+	+	+	+
Abs. density of neutron flux	+					
Flux distribution:						
resonance neutrons	+	+				
fast neutrons	+					
Spectral index S (Lu, Dy)	+	+	+	+	+	
R_{Cd}^{164Dy}	+					
R_{Cd}^{63Cu}	+	+	+	+	+	
R_{Cd}^{197Au}	+	+				
Rate of $^{238}U(n, \gamma)$ reaction:						
along radius of physical imitator	+	+	+	+	+	+
along height of physical imitator		+	+	+		
Plutonium coefficient f	+	+	+	+	+	+
$\langle\sigma_c^8\rangle/\langle\sigma_f^5\rangle$	+	+	+	+	+	+
ρ_{28}	+	+	+	+	+	+
Reaction rate measured with fission and boron chambers	+	+	+	+	+	+

+ experiment.

TABLE 3. Effective Neutron-Multiplication Factor in Assemblies

Method	Assembly			
	1-01	2-01	3-01	4-01
Experiment	1,0066± 0,0002	1,0046± 0,0002	1,055± 0,003	1,0105± 0,0005
Calculation	0,997	1,006	1,046	1,015

terial composition of the assemblies, and approval of some methods and programs for the physical design of HTGR and methodological assemblies (Tables 1 and 2). Most of the measuring methods are used in experiments on different critical assemblies. Two original features of GROG are scanning of the neutron flux over the volume of the core with the aid of small fission and boron chambers [3] and measurement of appreciable variations of reactivity in physically large breeding systems.

The neutron-physical design of the assemblies was carried out in two stages. First we calculated unit cells to obtain homogenized macroscopic constants, which were then used to determine the neutron-physical parameters of the assemblies. With allowance for the distinctive features of the assemblies of the stand GROG the group constants were calculated with the aid of the programs WIMS [4, 5], MONR1 [6], and PIT [7]. The neutron-multiplication factor K_{eff} and the space–energy distribution of neutrons in the assemblies were determined from the three-dimensional program QUM-3-HER [8]. Some distributions of the reaction rate and estimates of the effects were found from the two-dimensional program PENAP [9].

The specification data for the elements of the assembly were checked, analyzed, and statistically processed beforehand. Computational and experimental studies [10] indicated the homogeneity of the properties of the graphite stack in different directions. The agreement, within the limits of the error of measurement (2%) between the measured neutron diffusion length in a continuous graphite medium and the corresponding calculated value, obtained by using the specification data for graphite elements, gives confidence as to the correct-

ness of the latter. The calculations showed that the technological deviations of the parameters of the assembly elements have a weak influence on the principal characteristics of the assembly: no more than 0.1% on K_{eff} and no more than 1% on the relative deviation of the neutron fluxes [11].

As follows from Table 3, the calculated values of the effective neutron-multiplication factor in the assemblies are in satisfactory agreement with the experimental data (the difference does not exceed 1%).

The experimental and calculated values of the spectral parameters agree to within 7% while the difference between the experimental and calculated values in the distribution of the reaction rate may reach 10%.

A transition to experiments on more complex assemblies, close in geometry and composition to the cores of HTGR, will help improve the methods and programs for the design of such reactors.

LITERATURE CITED

1. E. V. Komarov, F. V. Laptev, V. G. Lyubivyi, F. M. Mitenkov, et al., "The VG-400 atomic-power engineering facility. Possible reactor core designs," At. Energ., 47, No. 2, 79 (1972).
2. A. M. Bogomolov, A. S. Kaminskii, A. D. Molodtsov, et al., "Fuel element of the critical assembly of a reactor," Inventor's Certificate No. 915628, Byull. Izobret., No. 30, 300 (1982).
3. A. B. Dmitriev and E. K. Malyshev, Neutron Ionization Chambers for Reactor Engineering [in Russian], Atomizdat, Moscow (1975).
4. J. Ackew et al., "A general description of the lattice code WIMS," J. BNES, 5, No. 4, 564 (1966).
5. N. I. Laletin and V. A. Lyul'ka, "On resonance absorption of neutrons in ^{238}U," in: Neutron Physics [in Russian], Part 4, Atomizdat, Moscow (1980), pp. 35-37.
6. A. G. Sboev, "Program for the calculation of resonance absorption of neutrons in reactor cells by the Monte Carlo method MONR1," Vopr. At. Nauki Tekh., Ser. Fiz. Tekh. Yad. Reakt., No. 5(18), 91 (1981).
7. A. S. Kaminskii and L. V. Maiorov, "The PIT program for the calculation of fluxes of slow neutrons by the Monte Carlo method with allowance for thermalization," Vopr. At. Nauki Tekh., Ser. Fiz. Tekh. Yad. Reakt., No. 8(21), 76 (1981).
8. S. S. Gorodkov, M. I. Gurevich, and N. L. Pozdnyakov, "Instruction for the use of the QUM-3-HER program for the calculation of a three-dimensional or two-dimensional heterogeneous reactor," Preprint IAÉ-2794, Kurchatov Institute of Atomic Energy, Moscow (1977).
9. P. N. Alekseev, S. M. Zaritskii, L. N. Usachev, and L. K. Shishkov, "The TVK-2D complex of programs," Vopr. At. Nauki Tekh., Ser. Fiz. Tekh. Yad. Reakt., No. 4(33), 32 (1983).
10. L. A. Anikina, A. S. Kaminskii, and E. S. Subbotin, "Measurement of the diffusion length of a graphite stack by an improved prism method," Vopr. At. Nauki Tekh., Ser. Yad. Konstanty, No. 4(53), 44 (1983).
11. L. A. Anikina, A. M. Bogomolov, and A. S. Kaminskii, "Influence of spreads of parameters of elements of critical assemblies of the stand GROG on their neutron-physical characteristics," in: Experimentation in Reactor Physics [in Russian], Moscow (1983), pp. 237-241.

STUDY OF MODEL COILS MADE OF SUPERCONDUCTOR INTENDED FOR THE WINDING OF THE T-15 TOKAMAK

I. O. Anashkin, E. Yu. Klimenko,
S. A. Lelekhov, N. N. Martovetskii,
S. I. Novikov, A. A. Pekhterev,
and I. A. Posadskii

UDC 539.312.62

The preparation for outfitting the Tokamak-15 has included several stages of tests on a superconducting current-carrying element (SCCE): study of the current-carrying capability of short specimens, and tests of model coils, full-scale test coils, and regular windings of the facility. Much attention to the behavior of SCCE in a winding has been paid since the decision to use niobium–tin multifilamentary conductor as the basis of the current-carrying element of the superconducting toroidal-field winding (STFW) for the T-15. Since 1978 tests on windings made of niobium–tin conductors similar in construction to the current-carrying element of the STFW have been under way at the I. V. Kurchatov Institute of Atomic Energy. Some of the results have been published [1-3]. The testing of the model coils was preceded by the construction of special stand equipment and was carried out on a stand designed for tests of niobium–tin windings with a diameter of ~ 1 m [4]. This, on the one hand, gave reason to hope that the tests could be performed fairly rapidly but, on the other hand, led to a risk of damage to the niobium–tin filaments of the SCCE, designed for use in a construction with a bending radius three times that of the model coil. This program came into being in connection with the almost formal necessity of making certain that the behavior of the SCCE, mockup specimens of which were successfully tested in 1977, would be predictable in the model winding. The first experiments, however, gave some unsettling results: The model windings went into the normal state at a current that was only half that used for short specimens of the current-carrying element (Fig. 1). As is seen, the results did not confirm the hopes for ensuring the operating characteristics of the T-15. The main objective of the second series of tests of model coils, which are described in this paper, was to ascertain the causes of the current degradation, to demonstrate the possibility of obtaining in the windings currents close to the current in a short specimen, and provisionally to verify that the design of the winding adopted for the T-15 facility is appropriate for its purpose.

The following assumptions about the causes of current degradation in model coils could be made a priori:

1. The existence of macroinhomogeneities of the conductor (weak spots). It could be assumed that in 1979 since the tests were conducted on a limited number of specimens such weak spots were not detected and in tests of the model coil it was those weak spots that determined the critical current. (Now that 100 short specimens have been tested and their total length is several times the length of the model winding and not a single test in a strong magnetic field gave a result below the theoretical requirements, this cause need not be considered.)

2. Damage to the current-carrying element during transportation or winding.

3. Deformation of the winding under the action of ponderomotive forces, leading to heat release exceeding the stability threshold of the current-carrying element.

In order to ascertain which of the last two causes was responsible for the observed degradation, a careful study was made of the last model of the first series of tests [3], henceforth called model A; its parameters are given in Table 1. The arrangement for the tests did not differ from that described earlier [3] (Fig. 2). A segment of the model winding was placed in the gap of a superconducting niobium–tin solenoid of diameter 240 mm. This solenoid produced a magnetic field of up to 8 T in part of the winding and its interaction with the model winding resulted in a force of up to $1.2 \cdot 10^5$ N that bent the model winding. The solenoid was cooled by immersion in liquid helium and the model winding was cooled by a flow of helium along the hollow current-carry-

Translated from Atomnaya Énergiya, Vol. 57, No. 6, pp. 401-404, December, 1984. Original article submitted March 6, 1984.

0038-531X/84/5706-0830$08.50

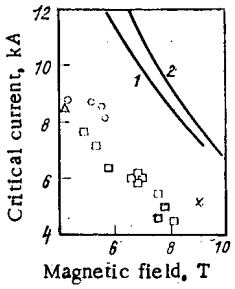

Fig. 1. Results of first series of tests of model windings: Δ) double pancake coils of diameter 560 mm; ○) glued pancake coil of diameter 560 mm; □) imitation of STFW; model A; ×) operating point of glued pancake coil; 1, 2) characteristics of SCCE of glued pancake coil and model A, respectively.

TABLE 1. Parameters of Models Tested in the Second Series

Parameter	Model A	Model B	Model C
Material of winding	STENO-2K-9-7225*	STENO-2K-11-7225	STENO-2K-11 14641
Type of winding	Double pancake	Single pancake	Double pancake
No. of turns	11	4	8
Winding dimensions, mm:			
inner diameter	780	760	770
outer diameter	860	835	850
height	38	18	38
Presence of pulsed toroidal winding	Yes	No	Yes
Coupling factor, T/kA:			
between field and current of model winding	0,15	0,04	0,073
between field and current of external solenoid	0,95	1,04	0,865
between field and current of toroidal winding	0,8	—	2,4

*Superconducting current-carrying element with two cooling channels and nine niobium–tin cores, each containing 7225 filaments.

ing element [1]. The model winding was insulated from the liquid helium in the cryostat by fiberglass textolite tape, reducing the heat exchange with the helium in comparison with internal cooling enough so that it could be neglected. Wound around the model winding was an auxiliary toroidal winding, imitating the field of the plasma column, directed parallel to the axis of the current-carrying element. The model and solenoid windings received their power supply in series from a 10-kA generator and an auxiliary 3-kA generator made it possible to add current to or subtract current from the model winding. This arrangement made it possible to study the dependence of the critical current of the model on the magnetic field.

In the second series of tests we used an additional compensator winding that increased the sensitivity of the bridge circuit for the detection of the normal phase so that the reverse part of the current–voltage (I–V) characteristics of the model would be observed. Tensometric displacement gauges were also set up to record changes in the shape of the winding and any possible displacements of the winding relative to the solenoid.

In tests of model A no abrupt deformations of the model were recorded up to the level of current attained. Recording of the I–V characteristics allowed an unambiguous conclusion to be made about the cause of the degradation. The smearing of the I–V characteristic of the transition of the model was several times the smearing of the I–V characteristic of the SCCE specimen (the parameter of the growth of the electric field with the current was 1050 A for the model and 360 A for the short specimen, Fig. 3). This allows the lowering of the current-carrying capability of the winding to be attributed to local damage to it during winding, transportation, or previous tests.

Identification of the causes of the failure of model A led to the preparation of a new model in which the probability of damage to the SCCE would be reduced to a minimum. The second problem in the preparation of

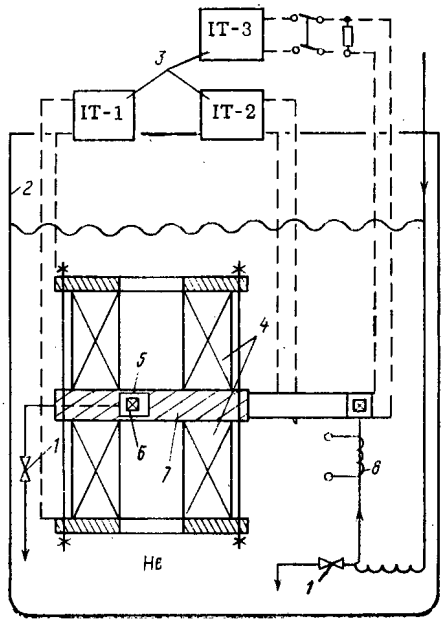

Fig. 2. Arrangement for tests of model windings: 1) control valves; 2) cryostat; 3) power supplies; 4) solenoid setting up field in segment of winding; 5) pulsed toroidal winding; 6) model winding; 7) bearing flange; 8) heater.

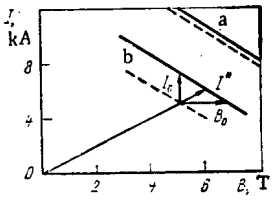

Fig. 3

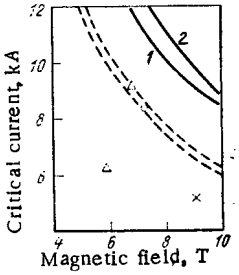

Fig. 4

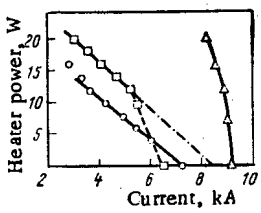

Fig. 5

Fig. 3. Comparison of the parameters of the growth of the electric field with the current for the model (a) and the short specimen of SCCE from which the model was made (b).

Fig. 4. Results of second series of tests of model windings: ○) model B; △) model C; ×) operating point of T-15 STFW; 1, 2) characteristics of SCCE of models B and C.

Fig. 5. Results of tests of models by the method of "extrapolation to zero heater" (the squares correspond to the case when the critical current was limited by mechanical perturbations in the winding): ○, △, □) models B, C, and C'; –·–·–) expected behavior of model C' in the absence of mechanical perturbations.

model B was that of demonstrating the possibility of producing a winding in which not only degradation but also conditioning of the SCCE would be eliminated. The latter is essential since at the design current of 5.2 kA the T-15 winding (STFW) is not stabilized in a stationary state and the beginning of conditioning of such a large magnet system can be tantamount to a limitation of its working capacity. Model B (see Table 1) was a one-layer pancake coil, glued on either side to 0.8-mm stainless steel sheet. To diminish the risk of breakage of the niobium–tin filaments, immediately after the application of a stabilizing layer of electrolytic copper [5] the current-carrying element was wound on a receiving cassette with an inner diameter of 0.8 m. It was not subsequently rewound. Before the gluing the tension in the SCCE was reduced and this permitted fiberglass textolite insulating insert to be placed between the windings. Because of the bandaging scheme adopted model B has an

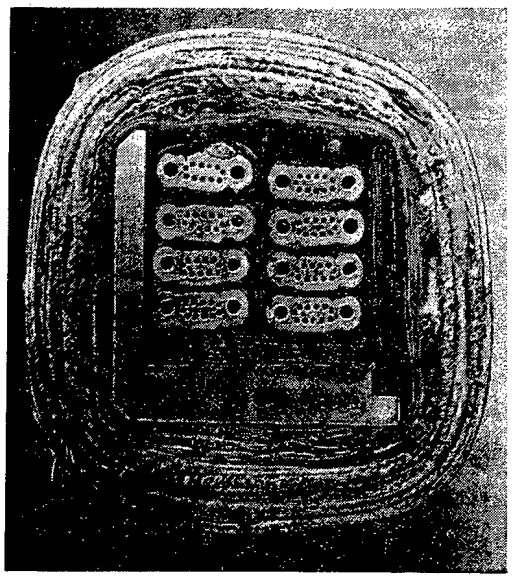

Fig. 6. Cross section of winding of model C.

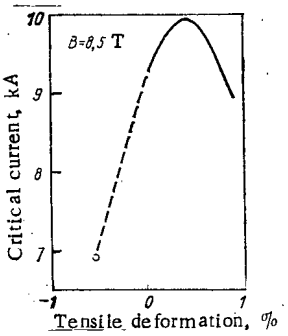

Fig. 7.

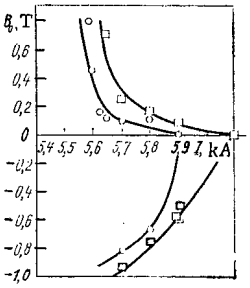

Fig. 8.

Fig. 7. Dependence of critical current of the SCCE on the tensile–compressive deformation: O) extrapolated critical current of model B.

Fig. 8. Dependence of the stability of the SCCE on the amplitude of the pulsed magnetic field, the relative orientation of I and B_0 during cooling with two-phase helium at a pressure of 0.13-0.15 MPa (□) and supercritical helium at a pressure of 0.4-0.5 MPa (O).

extremely great rigidity with respect to bending in the plane of the winding. The tests were carried out according to the scheme indicated above. Without any conditioning a reversible transition to the normal state was attained at a current substantially above the critical current of model A (Fig. 4). Further on we discuss why the current of the short specimen is not attained in small-diameter models. In any case the slope of the I–V curves, which coincides with the slope of the I–V curve of the short specimen, indicates that the SCCE in model B was not damaged. This is also indicated by the results of tests using the so-called method of "extrapolation to zero heater" (Fig. 5): the current at which a resistive zone appears in the winding is studied as a function of the power of a local heater arranged on it or as a function of the readings of a thermometer placed together with the heater. In the absence of damage in the SCCE and perturbations in the winding, this dependence is plotted as a smooth, almost straight line and the point corresponding to the transition of the winding when the heater is switched on lies on this line (models B and C).

If the SCCE has been damaged and the heater turned out not to be at the site of the damage, it is unlikely that characteristic kinks would appear on this line. If the transition is caused by perturbations, e.g., of a mechanical origin, then starting from a certain value of current at which the acting forces reach an appreciable value the critical current ceases to depend on the power of the heater and the transition takes place abruptly, without a recorded resistive segment of the I–V curve (model C').

The fact that a current satisfying the requirements of the STFW for the T-15 tokamak was attained in model B with rigidly fastened winding without any conditioning stimulated the construction of model C, whose design imitated the design of the T-15 STFW. The current-carrying element was wound on a rigid stainless steel ring with an L-shaped cross section (Fig. 6). In this winding, too, we managed to approach the current of a short specimen, but only after a single conditioning. This is a cause of some concern since the forces acting in the STFW of the T-15 will be several orders of magnitude greater than in the model and the number of conditionings may increase sharply.

The fact that in models B and C the critical current is somewhat below the level of current in the short specimen can be explained if the dependence of the current-carrying capacity of the SCCE on the deformation is taken into account (Fig. 7). During winding of a heat-treated SCCE of radius 0.4 m the inner layer of the transported cores turns out to be compressed 0.5% and their current-carrying capacity should diminish. This decrease cannot be compensated by an increase in the current-carrying capacity of the stretched cores of the outer layer since the cross resistance of the conductor is too high for the current to be redistributed between the stretched and compressed cores over the transposition length (80 mm) on which the cores change places. The critical current of the bent SCCE practically coincides with the critical current of the compressed current-carrying element.

The earlier hypothesis that the sensitivity of the SCCE to perturbations by a pulsed magnetic field depends on the relative direction of transposition, the current in the winding, and the pulsed field has been checked on models A and B. Since the transposed cores of the SCCE form helices about the axis of the conductor, a change in the longitudinal magnetic field can induce in them a current in the same direction as the transport current or in the opposite direction. At the same time eddy currents in the stabilizing copper warm up the superconductor slightly. Depending on the resultant current that flows in the superconductor, this warming up either causes the transition of the superconductor to the normal state or is insufficient to do so.

Figure 8 gives the results of a study of this effect on model A. A current slightly below the critical value (6 kA) was introduced into the model winding. Then a current of 0 to 1200 A was introduced into the toroidal winding wound around the model winding, up to a certain value, starting from 50 A. After this the current was removed from the winding approximately exponentially with a time constant of 7-10 msec; this imitated the nature, amplitude, and rate of change of the magnetic field of the plasma during tearing of the plasma in the T-15 facility. If with such removal of current the model winding remained in the superconducting state, the current in the toroidal winding was increased by 50 A and if it went into the normal state the corresponding value of the longitudinal field was recorded as the maximum attainable for the given value of current in the model winding. The experiments were conducted in three SCCE cooling regimes, corresponding to two-phase and one-phase supercritical helium in the channels. It was shown that cooling with two-phase helium slightly increases the stability of the winding.

Thus, after a second series of tests of model windings of the current-carrying element intended for the STFW of the T-15 tokamak it has been established that the material of the winding is suitable for use and has a considerable reserve of stability in stationary regimes and in pulsed perturbations by a longitudinal magnetic field. The current-carrying element can be used in the STFW of the T-15 tokamak, but the requirements as to ensuring the rigidity of the winding are much more stringent.

LITERATURE CITED

1. N. Chernoplekov, "Status and trends of superconducting magnets for thermonuclear research in the USSR," IEEE Trans., MAG-17, No. 5, 2158 (1981).
2. D. P. Ivanov et al., "Study of the properties and stability of a superconducting current-carrying element for the Tokamak-15 facility with respect to pulsed poloidal fields," in: Proceedings of the All-Union Conference on the Engineering Problems of Fusion Reactors [in Russian], Vol. 8, A. D. Efremov Scientific-Research Institute of Electrophysical Apparatus, Leningrad (1982), pp. 94-103.
3. D. P. Ivanov et al., "Study of model coils of the superconducting current-carrying element of the Tokamak-15 facility," Preprint IAE-3715/7, Institute of Atomic Energy, Moscow (1983).
4. I. L. Zotov et al., "Test stand for large superconducting magnet systems," Prib. Tekh. Eksp., No. 6, 176 (1974).
5. V. Agureev et al., "Electroplated stabilized multifilament superconductor," IEEE Trans., MAG-11, No. 2, 303 (1975).

OSCILLATIONS IN THE CONCENTRATION OF ARTIFICIAL RADIONUCLIDES IN THE WATERS OF THE BALTIC AND NORTH SEAS IN 1977-1982

D. B. Styro, G. I. Kadzhene,
I. V. Kleiza, and M. V. Lukinskene

UDC 551.464.679

As a result of extended atmospheric tests of nuclear and thermonuclear weaponry a certain "background" of artificial radionuclides has been formed in the environment [1]. Up to the present time this background has decreased significantly in the waters of the Pacific Ocean. Oscillations of it have turned out to be primarily associated with discharges of radioactive wastes by undertakings of the nuclear industry [2, 3] or with the effects of individual atmospheric nuclear explosions carried out up to the present by the People's Republic of China [4, 5].

The Baltic and North Seas are contaminated with various radionuclides, of which the most radioactively dangerous are ^{137}Cs, ^{90}Sr, and to a lesser degree, ^{144}Ce. If contamination of the waters of the Baltic Sea is caused mainly by global fallout, the waters of the North Sea are contaminated predominantly by the wastes of undertakings of nuclear industry [2, 3, 6].

Regular observations of the radioactive contamination of the water areas of these seas have been made by us since 1973 [7-10]. The natural data obtained have permitted estimating the possible values of the concentration of various radionuclides, investigating with the help of a mathematical method (the so-called objective analysis) the structure of the radionuclide concentration fields [10-12], and revealing the possible source of the contamination [13].

The isolation of radionuclides from seawater was performed by the radiochemical methods described in [14, 15] and with the help of a very rapid sorption procedure for ^{137}Cs [16]. We have determined the maximum possible error of a test from the results of numerous measurements of the concentration of the radionuclides of one and the same sample of water. In the determination of the concentration of ^{137}Cs and ^{144}Ce it amounted to 25% and for ^{90}Sr – 15%. The results of measurements obtained on the basis of the sorption procedure under natural conditions were selectively monitored by radiochemical analyses during each series of observations. The average values of the concentration of the radionuclides investigated are not constant in the waters of the Baltic Sea, and especially large variations in the concentration of ^{90}Sr are characteristic (Fig. 1). The concentrations of the other radionuclides are subject to oscillations to a lesser extent.

It has been established in the analysis of the published data [4, 5, 17-20] that the variations in the concentration of radionuclides in the surface waters of the Baltic Sea are caused by changes in the global fallout due to atmospheric nuclear tests conducted by the People's Republic of China. The time of the nuclear tests correlates well with the time of increase in the average concentration of radionuclides in the waters of the Baltic Sea (mainly ^{90}Sr). A more noticeable increase in the average concentration of ^{137}Cs and ^{144}Ce has been noted in the fall of 1980 after thermonuclear tests in the People's Republic of China [5] (see Fig. 1). One should emphasize that the increase in the intensity of global fallout in recent years has been accompanied mainly by an increase in the concentration of ^{90}Sr in the Baltic Sea; it has reached its own "natural" background values in a more extended period of time than has ^{137}Cs.

The contamination of the North Sea waters is caused mainly by discharges of wastes by undertakings of the nuclear industry [2, 3]. Therefore the variations in the global fallout do not cause noticeable variations in the ^{137}Cs concentration, as has been observed in the Baltic Sea. The average concentration of ^{137}Cs in the surface waters of the North Sea has increased especially strongly since 1976: thus from 1975 through 1976 it increased from 36 to 60 Bq/m^3, in 1977 it increased to 108 Bq/m^3, and it maintained approximately the same value up to 1981 (106 Bq/m^3). A decrease to 84 Bq/m^3 was detected only in the fall of 1982.

Translated from Atomnaya Énergiya, Vol. 57, No. 6, pp. 405-407, December, 1984. Original article submitted April 4, 1984.

0038-531X/84/5706-0835$08.50

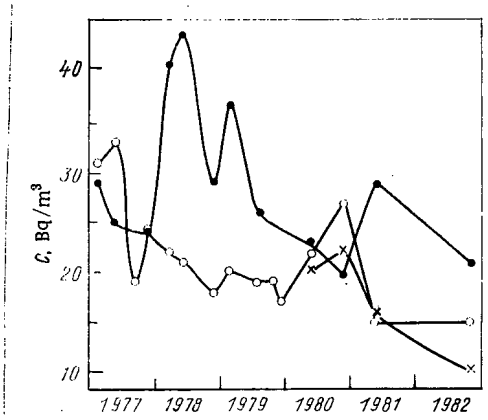

Fig. 1

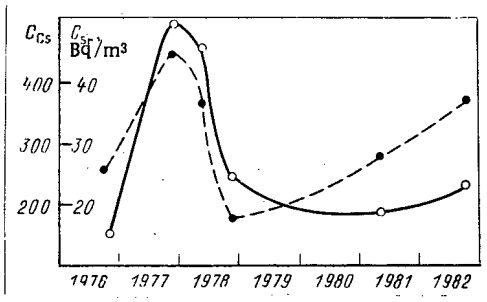

Fig. 2

Fig. 1. Average values of the ^{137}Cs (○), ^{90}Sr (●), and ^{144}Ce (×) concentrations in the surface waters of the Baltic Sea.

Fig. 2. Variation of the ^{137}Cs (○), and ^{90}Sr (●) concentrations in the surface waters of the North Sea near the bay of the Firth of Forth.

TABLE 1. Concentration of Radionuclides in September-October 1982 in the Surface Waters of Seas, Bq/m^3*

Sea	^{137}Cs	^{90}Sr	^{144}Ce
Baltic	25/7	34/8	16/5
North	233/32	37/9	48/6
Norwegian (southern part)	8/4	9/3	33/5

*The numerator denotes the maximum concentration, and the denominator denotes the minimum concentration.

The most contaminated waters evidently enter the North Sea from the bay of the Firth of Forth, which is connected by systems of canals with the Irish Sea. Many years of observations have permitted detecting a constantly increased ^{137}Cs concentration in this region of the sea [2, 10, 13]. One should note that here the increases or decreases in the ^{137}Cs and ^{90}Sr concentrations correlates well, although the absolute values of the ^{90}Sr content are lower by an order of magnitude (Fig. 2). In this region the concentration of both radionuclides have their largest values as a rule. Consequently, the waters of the North Sea are contaminated by both radionuclides due to discharges of wastes by undertakings of the nuclear industry.

We shall dwell in more detail on the results of measurements of the concentration of radionuclides in the surface waters of the Baltic and North seas in the fall of 1982, since they have been published first. The total content of the radionuclides under discussion in the surface waters of the Baltic Sea decreased significantly in comparison with 1981 (see Fig. 1) except for ^{137}Cs, whose average concentration remained the same (15 Bq/m^3) [10]. However, the absolute values of the concentration of these radionuclides in the surface waters measured at different points of the Baltic Sea vary within rather wide limits (see Table 1).

Figure 3 illustrates the nonuniformity of the distribution of radionuclide concentrations in the surface waters of the Baltic Sea. The greatest nonuniformity in concentration is characteristic of ^{90}Sr (Fig. 3b). Here an interesting regularity is revealed: the ^{137}Cs concentration decreases mainly at the points where the ^{90}Sr and ^{144}Ce concentrations increase. Natural oscillations of the radionuclide concentrations in the waters of the Baltic Sea significantly exceed the errors of the measurement results. The cited method – objective analysis using the experimental information obtained – was applied to the investigation of the structure of the concentration fields of radionuclides in the reservoirs under investigation.

The structure of the ^{137}Cs concentration field in the surface waters of the Baltic Sea in the fall of 1982 is given in Fig. 4a. This structure has changed noticeably in comparison with the spring of 1981 [10], although

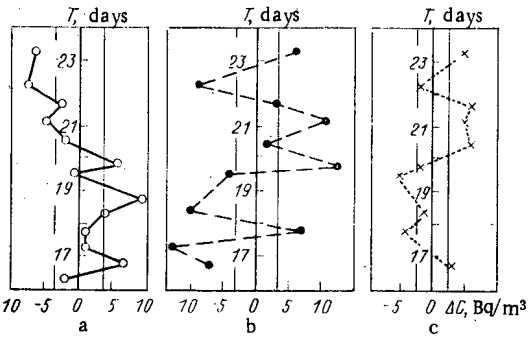

Fig. 3. Variations of the (a) ^{137}Cs, (b) ^{90}Sr, and (c) ^{144}Ce concentrations in the surface waters of the Baltic Sea in the fall of 1982 (vertical solid lines denote the maximum experimental errors).

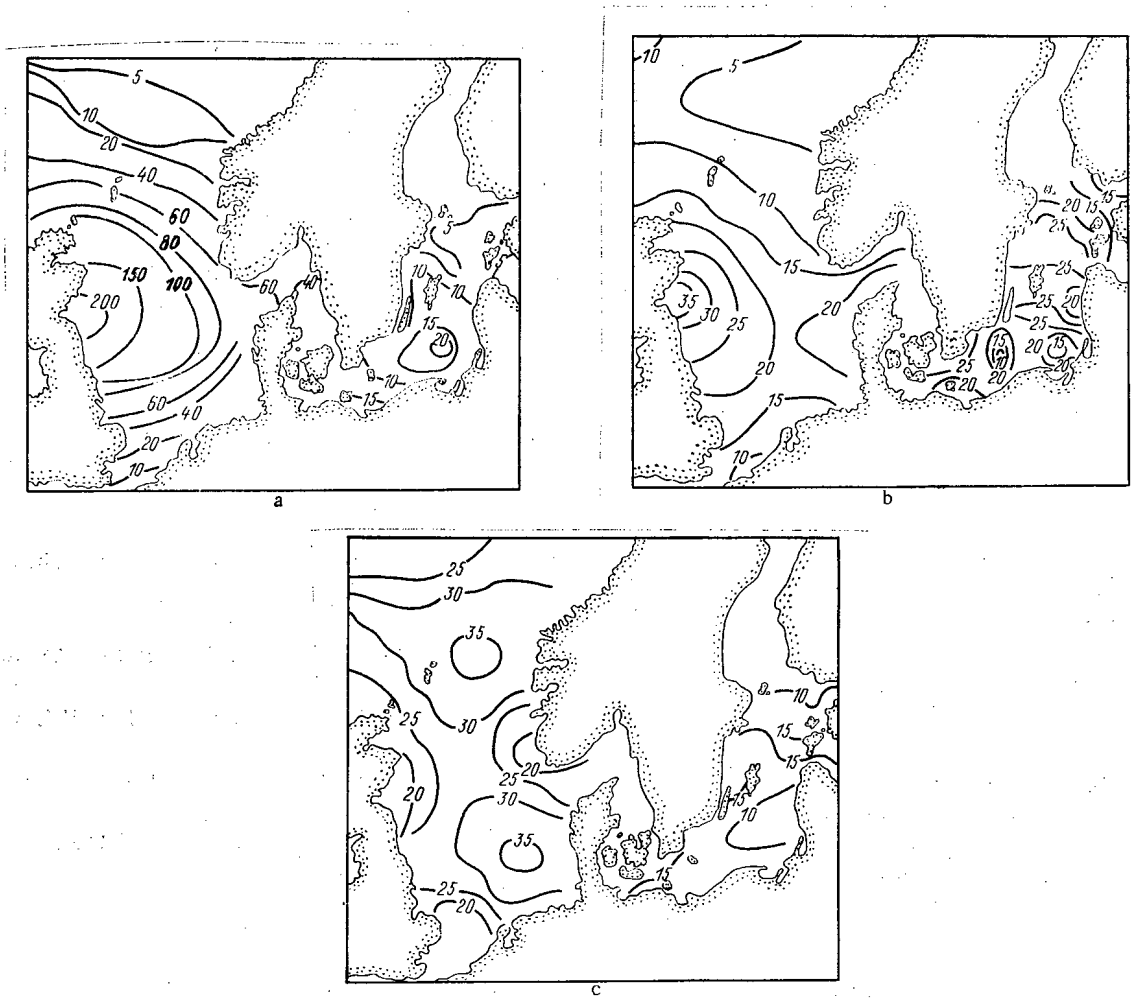

Fig. 4. Concentration field of (a) ^{137}Cs, (b) ^{90}Sr, and (c) ^{144}Ce in the surface waters of the Baltic, North, and Norwegian (southern part) Seas in the fall of 1982 in Bq/m^3.

the average value of the concentration remained the same: the absolute values of the ^{137}Cs concentration decreased in the northern part and then increased in the central part. The absolute values of the ^{90}Sr concentration decreased significantly, and the structure of its field changed completely (Fig. 4b). In this case the greatest values of the concentration were exhibited in the central part of the sea. The ^{144}Ce concentration field in the Baltic Sea appears comparatively uniform (Fig. 4c), and the average concentration of this radionuclide in the surface waters decreased from 16 to 10 Bq/m^3 from the spring of 1981 [10] to the fall of 1982.

The structure of the ^{137}Cs and ^{90}Sr concentration fields was noticeably altered in the waters of the North Sea (Figs. 4a and b) in comparison with the spring situation of 1981. A gradual decrease in the concentration of these radionuclides has been noted as one moves away in all directions from the bay of the Firth of Forth. The average value of the ^{90}Sr concentration in the surface waters decreased somewhat in comparison with the spring of 1981 [10] and reached 20 Bq/m^3, but ^{144}Ce increased by approximately a factor of two (21 Bq/m^3).

A gradual decrease in the ^{137}Cs and ^{90}Sr concentrations in the northern direction is observed in the southern part of the Norwegian Sea (see Figs. 4a and b). However, the structure of the ^{144}Ce concentration field turned out to be completely different – two regions of enhanced values in the southern parts of the North and Norwegian Seas (see Fig. 4c).

One should note that the structure of the ^{137}Cs and ^{90}Sr concentration fields in the waters of the North Sea and its oscillations are explained on the one hand by a variation in the action of contamination sources and on the other hand by the specific properties of hydrometeorological factors. The structure of the ^{144}Ce concentration field in this case is evidently associated with the peculiarity of global fallout. The structure of the concentration fields of the radionuclides under investigation and its variation in the waters of the Baltic Sea are related mainly to oscillations of the atmospheric fallout and hydrometeorological conditions.

LITERATURE CITED

1. B. A. Nelepo, Nuclear Hydrophysics [in Russian], Atomizdat, Moscow (1970).
2. H. Kautsky, Dtsch. Hydrogr., Z., No. 6, 241 (1973).
3. H. Kautsky, Dtsch. Hydrogr., Z., No. 7, 217 (1977).
4. E. Reiter, Atmospheric Transport Processes, Part 4: Radioactive Tracers, Technical Information Center, U.S. Department of Energy, Washington (1978).
5. S. Sadasivan and U. Mishra, J. Geophys. Res., C87, No. 9, 7343 (1982).
6. G. I. Kadzhene et al., in: Radioactivity of the Atmosphere and Hydrosphere. Radioactive Tracers [in Russian], Mokslas, Vilnius (1977), p. 207.
7. D. B. Styro et al., At. Energ., 45, No. 3, 201 (1978).
8. D. B. Styro et al., At. Energ., 49, No. 1, 43 (1980).
9. D. B. Styro et al., At. Energ., 51, No. 2, 116 (1981).
10. D. B. Styro et al., At. Energ., 55, No. 4, 238 (1983).
11. D. B. Styro and I. V. Kleiza, in: Propagation of Impurities in the Environment [in Russian], Mokslas, Vilnius (1980), p. 148.
12. D. B. Styro and I. V. Kleiza, Okeanologiya, 21, No. 3, 464 (1981).
13. D. B. Styro and I. V. Kleiza, in: Problems of Investigations of Atmospheric Contamination [in Russian], Mokslas, Vilnius (1981), p. 119.
14. L. M. Ivanova, Radiokhimiya, 9, No. 5, 622 (1967).
15. Yu. Ya. Mikhailov, "A procedure for determination of strontium-90, cesium-137, cerium-144, and lead-210 in samples of plant origin," Inst. Exptl. Vetern., Moscow (1980).
16. D. B. Styro, in: The Propagation of Impurities in the Environment [in Russian], Mokslas, Vilnius (1980), p. 121.
17. A. Yamato, Radioisotopes, 30, No. 2, 104 (1981).
18. J. Roy et al., Health Phys., 41, No. 3, 449 (1981).
19. R. Reiter and K. Munzert, Arch. Meteorol. Geophys. and Bioclimatol., B31, No. 3, 191 (1982).
20. L. Burchfield et al., J. Geophys. Res., C87, No. 9, 7273 (1982).

ENHANCEMENT OF HEAT TRANSFER IN THE RBMK AND RBMKP

A. I. Emel'yanov, F. T. Kamen'shchikov, Yu. M. Nikitin, V. P. Smirnov, and V. N. Smolin

UDC 621.039.553.34

The increase of unit power of nuclear reactors and the related increase in heat removal is one of the pressing problems of the development of nuclear power [1]. An effective way of solving this problem is the enhancement of heat transfer in fuel-element assemblies (FEA).

Heat-removal enhancement is a complicated problem, related not only to an increase in heat removal while maintaining the accepted criteria of the working capacity of the fuel elements, but also to the solution of such concomitant problems as the decrease of the energy expended to pump through the coolant, the guarantee of the necessary technological effectiveness of the proposed enhancement devices, the account of the possible effect of these devices on the physical parameters of the core, etc.

The approaches to the increase of heat removal in FEA with two-phase and single-phase coolants are quite different. This is a result of the different nature of the heat and mass transfer processes which determine the maximum thermal stress of the fuel-element cladding, which in turn is the main barrier to the release of radioactive fission products. For a FEA with a boiling coolant we take as an implicit parameter of the maximum thermal stress of the fuel-element cladding the critical heat flux density characterizing the overall growth or local spikes of the fuel-element temperature.

The onset of a heat-transfer crisis in the disperse annular flow of the coolant, realized in channels with a boiling coolant, is related to the overall or local (stable or periodic) disappearance of the liquid film from the heated surface as a result of the imbalance of the removal processes, evaporation and deposition in the presence of an appreciable amount of moisture in the flow core [2-4]. The cooling conditions of fuel elements are generally not identical over a cross section of a FEA because of possible thermohydraulic inequalities of individual elementary hydraulic cells (both as a whole and over the azimuth of each fuel element). Such a heat-transfer mechanism in disperse annular flow also predetermines possible methods of increasing heat removal in a FEA: the deposition of moisture from the flow core on heated surfaces and the equalization of the thermohydraulic parameters of the coolant over the cross section of a FEA. In doing this it must be kept in mind that this separation of enhancement methods is somewhat arbitrary, since they may accompany and be produced by common enhancement devices.

An effective heat-transfer enhancement method is the rotation of the coolant stream. This produces a centrifugal acceleration field which separates the moisture from the flow core on the heated surface. In most of the articles on the study of this method of heat-transfer enhancement, as noted earlier [5, 6], a favorable effect is observed which increases with increasing stream content [7]. As applied to a FEA with fuel rods, heat-transfer enhancement is accomplished by using vortex generators which produce a rotation of the flow in each elementary hydraulic cell of a straight-through cross section of the assembly.

Research performed at the All-Union Institute of Heat Engineering (VTI) [8] on the heat-transfer crisis in assemblies with twisted tapes over the whole length showed the possibility of achieving crisis-free operating conditions up to steam contents of 80, 70, and 60%, specific heat loads of 0.58, 0.93, and 1.16 MW/m^2, mass velocities of 800-1000 kg/m^2 · sec, and a pressure of 6.9 MPa. It was shown in [9, 10] that the steam content at a channel exit when twisted tapes extended along the whole length could be increased from 10.5 to 25-35%. When the tapes extended along the whole length of the assembly, technological difficulties arose, particularly in long channels, and also the amount of absorbing material in the reactor core is appreciably increased. To decrease the core absorption and the hydraulic resistance, it is more expedient to use short twisted tapes, but this decreases the effectiveness of the heat-transfer enhancement [9].

Local heat-transfer enhancers in the form of short twisted tapes were tested experimentally at NIKIÉTe in an RBMK FEA consisting of a 19-rod bundle of fuel elements 7 m long [11, 12]. The structural parameters

Translated from Atomnaya Énergiya, Vol. 57, No. 6, pp. 408-413, December, 1984. Original article submitted March 2, 1984.

0038-531X/84/5706-0839$08.50

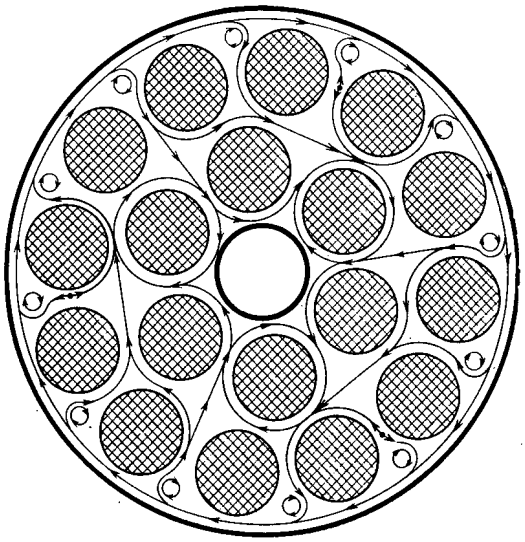

Fig. 1. Schematic diagram of circulation of single-phase flow in a transverse straight-through section of a 19-rod FEA following an axial twist enhancer.

and the positions of the short twisted tape enhancers along the height of the assembly were optimized. Tests to estimate the effectiveness of such enhancers were performed on electrically heated assemblies with seven rods 2.2 m long and three rods 7 m long.

The experiments were performed for the following range of parameters: pressure 7.4 and 9.8 MPa, mass velocities from 600 to 2000 kg/m^2 · sec, and heat fluxes from 0.3 to 1.6 MW/m^2 with underheated water entering the assembly at the saturation temperature.

The results showed that for the same heat flux density the absolute growth of the critical mass steam content was 20-30%, and this growth increases with an increase in the mass velocity and pressure. Calculation of the maximum power of a FEA from these data showed the possibility of increasing the RBMK power by 50%. Further development of the heat-transfer enhancers was directed toward producing more technological types of heat-transfer enhancers based on the RBMK-1000 FEA spacer lattices.

It should be noted that because of the mixing of the flow and the redistribution of phases, practically all types of spacer lattices permit an increase in the critical heat flux density. The heat flux density increases appreciably immediately after the spacer elements, and gradually decreases with increasing distance from them. Therefore, experiments were first performed on assemblies with the regular RBMK spacer lattices for a decrease in their spacing along the height of the assembly. Shortening the distance between them from 350 to 175 mm increased the critical heat flux density by 10-20%, and the hydraulic resistance by 50-60%. Various kinds of enhancement elements were placed on the rims and mesh of the spacer lattices to increase their effectiveness. A similar approach to heat-transfer enhancement was discussed in [13, 14].

In placing the enhancement elements, consideration was given to their effect on the heat-transfer crisis and its place of origin in the assembly. Tests on the electrically heated model of a RBMK FEA showed that the heat-transfer crisis arises in the hottest triangular hydraulic cell between the inner and outer sets of rods, and also on those parts of the perimeter of the fuel element tubes of the outer row of the assembly, which are separated from an unheated channel by a narrow gap. This can be accounted for qualitatively by the fact that the elementary cells are not thermally or hydraulically equivalent, and by the effect of an unheated (cold) wall along which an appreciable part of the moisture flows, which lowers its flow rate on the surface of the fuel elements in this region.

The variants of lattice-enhancers developed are mainly of two types. One type is based on the idea of rotating the flow in each elementary hydraulic cell of a FEA by using straight vane-deflectors to produce centrifugal acceleration fields. These are substantially more effective than vortex generators in the form of twisted tapes [15]. The other type uses structural elements between the outer set of rods and the channel, and also in the least-filled parts of the straight-through cross section between the inner and outer sets of rods. These greatly assist the mixing of the coolant in a FEA cross section.

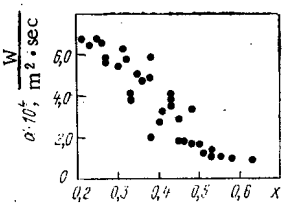

Fig. 2. Dependence of heat-transfer coefficients on mass steam content for an assembly with axial twist enhancers in an experiment with p = 7.5 MPa, $\rho w = 1000-2000$ kg/m^2 · sec, and q = 0.9 MW/m^2.

The experiments were performed in several stages. First, the study of the spacer lattices of the heat-transfer enhancers was completed on a stand at the ÉNIS branch of the VNIIAÉS [16]. The experiments on crisis heat transfer and hydraulic resistance were performed on the RBMK FEA thermohydraulic model, consisting of a 19-rod bundle with a full-scale straight-through cross section and a heated length of 1.1 m. This model permitted the study of full-scale enhancers, and since it was more mobile than the full-scale model, it speeded up the completion of the experimental study of the enhancers, and broadened the possibilities of diagnosing the heat-transfer crisis. The use of thin-walled electrically heated tubes on a shortened assembly (δ = 0.2 mm) made it possible to place thermocouples in the center of a tube to measure the average temperature, and other thermocouples on the inner surface of a tube (up to five in one of its cross sections) to fix the location of the onset and development of a heat-transfer crisis from the local wall temperature. Based on the possibilities of the stand, tests were performed for p = 7.5 MPa, ρw = 1000-2000 kg/m^2 · sec, and q up to 1 MW/m^2 for a steam–water mixture supplied at the entrance.

This approach to the study of a heat-transfer crisis in rod assemblies with heat-transfer enhancers is justified experimentally by the agreement of results obtained on shortened and full-scale FEA models [17].

A comparison of the results of experiments performed on shortened FEA models with developed types of heat-transfer lattice enhancers [18] permitted the determination of the most effective type of axial twist enhancers [19]. The subsequent stages of the experimental research on these heat-transfer enhancers, performed on full-scale electrically heated models on a stand at the Institute of Atomic Energy [20], and also in in-pile tests [21], showed the possibility of using such enhancers in RBMK-1500 FEA.

For a broader understanding of the kinematics of flow beyond axial twist enhancers, the velocity field was measured on the aerodynamic model of an RBMK-1500 assembly on a scale of 2:1. The results gave a qualitative picture of the circulation of flow in a section of the assembly (Fig. 1), explaining the probable mechanism of the effect of enhancers on vapor–liquid flow: the equalization of the parameters as a result of axial rotation between assembly and channel, the equalization of the liquid film around the periphery of a fuel element as a result of the circulation around the rods, and the separation of moisture from the flow core on the fuel elements as a result of the formation of secondary vortex flows.

In considering the effect of axial twist enhancers on the heat-transfer crisis, it should also be noted that in addition to the increase in critical parameters, the character of supercritical heat transfer is also changed, and consequently also the supercritical thermal conditions of the fuel-element cladding. The graph of the supercritical heat-transfer coefficient $\alpha = f(x)$ in Fig. 2 shows a smooth decrease of the heat-transfer coefficients from values characteristic for the development of boiling, to values characteristic of heat transfer after the accumulation of a sufficient number of experimental data clearly permits raising the question of the possibility of operating FEA (if only temporarily) in the supercritical region up to the maximum admissible temperature for the fuel-element cladding, and the incorrect use of such a criterion as the critical heat flux density as controlling.

The production of more effective heat-transfer enhancers will, in our opinion, be determined largely by the development of research on mass transfer processes in disperse-annular flows and supercritical heat-transfer processes which takes account of the possible effect of the structural elements of the lattices [22]. This requires improving the diagnostics and methodology of local crisis phenomena. Such work should culminate in programs for calculating the thermohydraulic parameters in a FEA. The development of these programs is still in the initial stage.

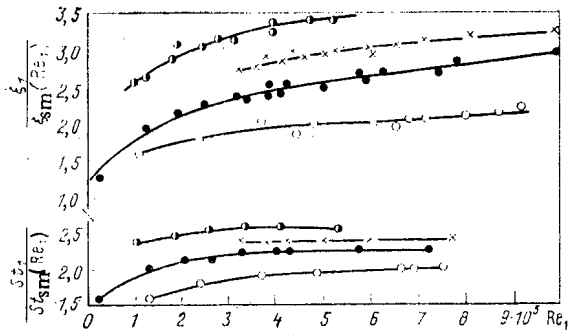

Fig. 3 Dependence of heat-transfer coefficient and coefficient of friction on Re and height h of roughness protrusions or s/h = 10; ◑) h = 0.1; ×) 0.075; ●) 0.05; ○) 0.03 mm.

Questions of heat-transfer enhancement for gas (vapor)-cooled nuclear reactor cores such as the BGR-300 [23] and the RBMKP [1] are very important. Heat transfer in the FEA of such reactors is characterized by greater heating of the coolant in the core and larger thermal heads between the fuel-element surface and the coolant. The magnitude of the thermal stresses in the structural materials of the fuel-element cladding is the basic criterion of the effectiveness of heat-transfer enhancement. It is known that the thermal heads for heat transfer with a gaseous coolant are determined by the thermal resistance of a thin boundary layer. Practically the only effective way to improve heat transfer from the heat-transfer surface to the flow core is to create detachment zones and other vortex structures in the boundary layer. Such vortex zones as a rule are produced by regular protrusions (turbulators, artificial roughness) of various heights and shapes.

Many papers have been devoted to the study of heat-transfer enhancement by regular roughness. The most complete summary of these papers is given in [24, 25]. Most of the experiments were performed with turbulators which practically could not be mass produced because of the great difficulty and complexity of ensuring stable geometry of protrusions with a height of ~0.1 mm. Therefore, the first step in solving the problem of heat-transfer enhancement in FEA of gas-cooled reactors was the selection of a method of forming regular turbulators on the surface of the fuel-element cladding. Research abroad [26] showed that the most promising methods of forming artificial roughness of fuel-element cladding are mechanical and electrochemical. Removal of metal in electrochemical roughening occurs mainly as a result of electrochemical processes. The shape of the fins is determined by the shape of the abrasive disk.

An experimental-industrial unit, the TÉV-1, was built at the Tula Polytechnic Institute (TPI) under the direction of E. I. Pupkov to produce artificial roughness of the outer surface of fuel-element cladding by an electrochemical treatment (ECT) with a rotating cathode. The working surface of the cathode was shaped in the form of the hollow between the protrusions of the artificial roughness for a spiral relative motion of the cathode and the billet [27]. The ECT method ensures that the height of the roughness profile is accurate to within 0.005 mm in the absence of cold working and corrosion along the grain boundaries of the metal, and can easily be realized on a large scale.

The thermohydraulic characteristics of the artificial roughness formed by the ECT were obtained by making a batch of samples of roughened tubes ~10 mm in diameter with a wall thickness of 1 mm. Most of the studies were on symmetrical trapezoidal shaped roughness with a relative pitch s/h in the range 7-35 and a height of 0.03-0.1 mm. The experiments were performed at the VTI on an electrically heated annular channel with a flow of air [27]. Roughened tubes were inserted into a tube with an inside diameter of 19.46 mm. The Reynolds number was varied from 25×10^3 to 650×10^3, air was heated 30-40°K from entrance to exit, the thermal head varied from 60 to 100°K, the temperature factor was 1.2-1.3, and the Mach number did not exceed 0.5.

Figure 3 shows how the ratios of the coefficients of hydraulic resistance ξ_1/ξ_{sm} and the Stanton numbers St_1/St_{sm} depend on the relative pitch s/h for the region of the annulus adjacent to the inner roughened tube. The experimental data for this region were scaled by the Wilki method [28]. The relations shown in Fig. 3 confirm the earlier conclusions [24] for roughness of the nontechnological type that the maximum increase in the Stanton number St_1 over St_{sm} for a smooth tube at the same values of the Reynolds number Re_1 occurs for s/h = 10-12. The dependences of ξ_1/ξ_{sm} and St_1/St_{sm} on Re_1 (Fig. 3) show that artificial roughening of the fuel-element cladding by ECT can increase the heat-transfer coefficient by a factor of 2-2.5 while increasing the hydraulic resistance by a factor of 2.7-4.

While ECT produces highly accurate roughness, it is a slow process (5 mm/min), but it can be speeded up by using a multifilament cathode to produce roughness in the form of multiturn helical grooves while maintaining between protrusions a distance equal to the pitch of single-turn roughness. Experiments on the VTI stand using samples of tubes with four-turn artificial roughness made at the TPI showed that such tubes have approximately the same thermohydraulic characteristics as tubes with single-turn roughness [27]. However, the ECT speeded up the process by a factor of 3.5. A further increase in the number of cathode filaments should show how much the ECT can speed up the process while maintaining the thermohydraulic characteristics of the roughness.

The problem of heat-transfer enhancement in an overheated RBMKP FEA is related to the problem of the buildup of artificial roughness by the precipitation of salts. According to recommendations in [24], for Reynolds numbers of $(5-8)\cdot 10^5$, which are characteristic for an overheated assembly, the optimum height of roughness protrusions is ~ 0.03 mm, which can be commensurate with the thickness of a layer of precipitated salts. In addition, the flow around protrusion type roughness is accompanied by the formation of stagnation zones near the protrusions. More intense precipitation of salts may occur in these zones, which leads to a leveling off of the protrusions and a decrease of the heat-transfer enhancement effect. In our opinion these unfavorable effects can be avoided by using wave-type roughness.

Experiments [29] on the VTI stand with tubes having artificial wave-type roughness which were made at the TPI by ECT showed that for $Re = 7\cdot 10^5$ the height of this type of roughness could be increased by a factor of five to six, while preserving the values of St_1 and ξ_1, as also for roughness of the rectangular protrusions type. By increasing the height of the roughness to 0.15-0.2 mm and removing the stagnation zones, wave-type roughness offered better resistance to the precipitation of salts on the fuel-element cladding in the steam flow.

The high sensitivity of the thermohydraulic characteristics of gas (vapor)-cooled FEA with rod fuel elements, depending on the characteristics of their construction and on the distribution of fuel elements over the cross section, introduces increased requirements in the calculation of the thermal state of the fuel elements. As also for evaporative assemblies, further experimental research with careful diagnostics and the introduction of the results into programs for calculating the thermohydraulic parameters of the assemblies is proposed. In addition it should be noted that for single-phase coolants great success has been achieved in producing such computational programs [30], although there are some complications. For example, the use of the ordinary cellular methods [31] for FEA with few rods, and also for the peripheral cells of multirod FEA may lead to inaccuracies in the calculation of the temperature of the fuel-element cladding of up to 20-30°C.

In our opinion cellular methods can be refined by solving the thermohydraulic problem for a number of FEA cross sections while maintaining the average values of the thermohydraulic parameters in the cells found by the cellular method of calculation. In such methods of analysis of multirod FEA, the cross section is assumed uniform in each elementary cell (although mixing factors are also taken into account). In addition, for cells of complex shape, which are typical for peripheral cells, and very full bundles, the azimuthal nonuniformities of the tangential stresses and the velocity fields, which in turn affect the coefficient of friction and the heat-transfer coefficient in a given cross section, must be very important.

Therefore, after calculations of the average parameters in the cells, it is expedient to perform additional thermohydraulic calculations in the chosen cross sections of the FEA under the assumption of stabilization of the flow, as for a channel of complex shape, using, for example, methods of the type proposed in [32]. In doing this, iterative return to cellular methods is possible to correct the coefficient of friction and heat-transfer coefficient, if this is necessary. The realization of this method is logical for FEA of evaporative channels also. But once again it should be emphasized that the development of any cellular methods, including refined methods, requires careful experimental research with accurate diagnostics, which also may serve at the present stage of development as the only means of producing high-stress FEA.

LITERATURE CITED

1. N. A. Dollezhal', "Nuclear power and the scientific–technical problems in its development," At. Energ. 44, No. 3, 203 (1978).
2. V. E. Doroshchuk, Heat Transfer Crises during Boiling in Tubes [in Russian], Énergiya, Moscow (1970).
3. V. N. Smolin, "Model of the heat-transfer crisis mechanism during the motion of a steam–water mixture and methods of calculating crisis conditions in tubular fuel elements," in: Seminar TF-74 [in Russian], IAE, Moscow (1974), pp. 209-224.

4. P. L. Kirillov, "Contemporary ways of developing theories of heat-transfer crisis during boiling in channels," in: Proc. Physics and Power Institute [in Russian], Atomizdat, Moscow (1974), p. 242.
5. A. V. Zhukovskii, V. B. Khabenskii, and G. S. Shvertsman, "Enhancement of heat transfer in two-phase flows," Sudostr. Rubezhom, No. 2, 68 (1969).
6. N. I. Perepilitsa and A. P. Sapankevich, "Methods of increasing parameters during a heat-transfer crisis," (Analytic review). Preprint FÉI [in Russian], Obninsk (1976).
7. L. S. Tong, Boiling Heat Transfer and Two-Phase Flow, Krieger (1975).
8. Yu. D. Barulin, A. S. Kon'kov, and A. I. Leont'ev, "Study of heat-transfer enhancement and hydraulic resistance in a model of a fuel element assembly of a boiling reactor," [3], pp. 323-334.
9. I. Vollradt, "Boiling water reactor with twisted tapes between the fuel rods," Atomwirtschaft, 12, 595 (1967).
10. A. Rosuel and X. Rouvillois, "Use of twisted tapes for increasing the power density of boiling-water reactors," Energ. Nucl., 9, 496 (1967).
11. V. N. Smolin and V. K. Polyakov, "Heat-transfer enhancement in a rod bundle using local vortex generators," [3], pp. 307-312.
12. V. N. Smolin, V. K. Polyakov, R. E. Polyakova, and L. I. Ezhova, "Study of heat-transfer enhancement in rod bundles with local vortex generators," Vopr. At. Nauki Tekh., Ser. Reaktorostr., No. 1 (12), 15 (1976).
13. J. O. Cermak, R. F. Farman, L. S. Tong, et al., "The departure from nucleate boiling in rod bundles during pressure blowdown," Trans. ASME, J. Heat Transfer, 92, 621 (1970).
14. E. Rosal et al., "High-pressure rod bundle DNB data with axially nonuniform heat flux," Nucl. Eng. Design, 31, 1 (1974).
15. F. T. Kamen'shchikov, V. A. Reshetov, A. I. Emel'yanov, and T. A. Pikuleva, "Optimization of vortex generators in centrifugal heat-transfer enhancers and centrifugal steam separators," Vopr. At. Nauki Tekh., Ser. Fiz. Tekh. Yad. Reaktorov, 3 (16), 15 (1981).
16. A. N. Ryabov, F. T. Kamen'shchikov, V. N. Filippov, et al., "Experimental study of heat-transfer crisis, temperature behavior, and hydraulic resistance in rod bundles with heat-transfer enhancers," Vopr. At. Nauki Tekh., Ser. Reaktorstr., 1 (12), 36 (1976).
17. A. I. Emel'yanov, F. T. Kamen'shchikov, Yu. M. Nikitin, et al., "Experimental evidence of the possibility of investigating heat-transfer crisis on shortened models of fuel element assemblies," Vopr. At. Nauki Tekh., Ser. Fiz. Tekh. Yad. Reaktorov, 4 (26), 14 (1982).
18. A. N. Ryabov, F. T. Kamen'shchikov, V. N. Filippov, et al., "Investigation of heat-transfer crisis and hydraulic resistance in rod bundles with heat-transfer enhancers," in: Fifth Minsk Conference on Heat and Mass Transfer, Vol. 3, Part 2 [in Russian] (1976), pp. 28-39.
19. V. G. Aden and V. N. Filippov, "Fuel element assemblies of RBMK type reactors," Vopr. At. Nauki Tekh., Ser. Fiz. Tekh. Yad. Reaktorov. 1 (21), Part 1, 28 (1978).
20. V. Aden, V. Asmolov, T. Blagovestova, et al., "The study of heat exchange enhancement in models of fuel element bundles with boiling coolant," in: Proc. Sixth Int. Heat Trans. Conf., Vol. 5, Hemisphere Pub. Co., Toronto (1978), pp. 41-46.
21. V. G. Aden, I. A. Varovin, B. A. Vorontsov, et al., "Testing of RBMK-1500 cassettes in the reactor at the Leningrad power station," At. Énerg., 51, No. 3, 150 (1981).
22. A. I. Emel'yanov, F. T. Kamen'shchikov, E. V. Stolyarov, et al., "Effect of heat-transfer spacer lattice enhancers on heat-transfer crisis in steam generator channels," Vopr. At. Nauki Tekh., Ser. Fiz. Tekh. Yad. Reaktorov, 2 (31), 49 (1983).
23. V. V. Gur'ev, "High-temperature gas-cooled nuclear reactors," Vopr. At. Nauki Tekh., Ser. Fiz. Tekh. Yad. Reaktorov, 1 (21), 117 (1978).
24. É. K. Kalinin, G. A. Dreitser, and S. A. Yarkho, Heat Transfer Enhancement in Channels [in Russian], Mashinostroenie, Moscow (1981).
25. A. A. Zhukauskas, Convective Transport in Heat Exchangers [in Russian], Nauka, Moscow (1982).
26. M. Peehs, J. Lindgren, and P. Moser, "Gas-cooled fast breeder core element fabrication technology," Nucl. Eng. Design, 40, 101 (1977).
27. V. L. Lel'chuk, Yu. M. Nikitin, E. I. Pupkov, et al., "Enhancement of convective heat transfer," Teploenergetika, 2, 57 (1980).
28. D. Wilki, "Calculation of heat transfer and flow resistance at rough and smooth surfaces in a single passage," in: Proc. Third Int. Heat Trans. Conf., Paper No. 2, Chicago (1966), pp. 20-31.
29. Y. Barulin, A. Konjkov, A. Leontiev, et al., "Enhancement of heat transfer in core models of water-moderated, water-cooled, and gas-cooled reactors," XX JAHR Congress Proc. Subjects, Vol. 4, Moscow (1983), pp. 580-589.

30. L. V. Zhukov et al., Methods and Programs of In-Channel Thermohydraulic Calculation of Fuel Element Assemblies, Taking Account of Interchannel Interaction of Coolant (Analytic Review) [in Russian], FÉI, Obninsk (1980).
31. G. S. Mingaleeva and Yu. V. Mironov, "Thermohydraulic calculations of multirod heat-liberation piles cooled by single-phase heat carrier," At. Énerg., 48, No. 5, 303 (1980).
32. M. Kh. Ibragimov, I. A. Isupov, L. L. Kobzar', and V. I. Subbotin, "Calculation of tangential stresses at the wall of a channel and the velocity distribution in a turbulent flow of liquid," At. Energ., 21, No.2, 101 (1966).

STRESSES IN SPHERICAL FUEL ELEMENTS OF A HIGH-TEMPERATURE GAS-COOLED REACTOR (VTGR) AS A RESULT OF THE HEAT LOAD AND RADIATION SHRINKAGE OF GRAPHITE

V. S. Egorov, V. S. Eremeev, and E. A. Ivanova

UDC 621.039.546

The core of high-temperature gas-cooled reactors (VTGR) developed in the USSR contains spherical dispersion type fuel elements with graphite cladding and a core of matrix graphite [1]. The fuel is UO_2. The fuel elements fall through special locks into the upper part of a spherical charge, and move downward. The fast neutron fluence up to the end of the reactor operating life is $\sim 1.5 \times 10^{21}$ cm^{-2}. The variations of the temperature T_c at the center of a fuel element, the temperature drop ΔT, and the integrated flux F of fast neutrons as functions of the displacement of a fuel element along the axis of the reactor are described by the data in Table 1 [1].

Stresses arise mainly from the nonuniform variation of the volume over the cross section of a fuel element, which is determined by the temperature distribution and the graphite shrinkage caused by neutron bombardment. The computational model for the analysis of thermal stresses in an elastic isotropic body is based on the familiar linear relation between the components σ_{ik} of the stress tensor and u_{ik} of the strain tensor [2]

$$\sigma_{ik} = -K\alpha(T - T_0)\delta_{ik} + Ku_{ll}\delta_{ik} + 2\mu\left(u_{ik} - \frac{1}{3}\delta_{ik}u_{ll}\right), \quad (1)$$

where $K = E/3(1-2\nu)$ is the bulk modulus; E, Young's modulus; ν, Poisson's ratio; μ, shear modulus; α, volume coefficient of thermal expansion in the absence of stresses; T, temperature; and δ_{ik}, Kronecker symbol.

It can be shown that the form of Eq. (1) is preserved in the description of stresses resulting from arbitrary nonuniform variations of volume [3-5]. Without considering the specific cause of the nonuniform variation of volume $\omega(r, t)$, which in general is a function of the spatial coordinate r and the time t, we rewrite Eq. (1) in the form

$$\sigma_{ik} = K(u_{ll} - \omega)\delta_{ik} + 2\mu\left(u_{ik} - \frac{1}{3}\delta_{ik}u_{ll}\right). \quad (2)$$

Equation (2) was used in [6] to analyze the stresses in graphite-based spherical fuel elements.

We assume that a fuel element is displaced in a core characterized by the parameters listed in Table 1. Stresses are caused by thermal expansion and the nonuniform shrinkage of graphite under neutron bombardment. The dependence of the relative change of the linear dimensions of graphite on the neutron fluence and the temperature is shown in Fig. 1 [6].

The problem was solved by using the viscoelastic Maxwell model for a radially symmetric temperature field. In view of the small concentration of fuel, it was assumed that the physical and mechanical properties of the fuel-element core and cladding are those of graphite. The tangential stress σ_φ is the most dangerous, acting in a direction perpendicular to the radius. The general solution of the problem for a nonuniformly heated sphere for constant values of Young's modulus, Poisson's ratio, and the viscosity has the form [2]:

$$\sigma_\varphi(r, t) = \sigma_\varphi^{el}(r, t) - e^{-st}\int_0^t se^{st'}\sigma_\varphi^{el}(r, t')\,dt', \quad (3)$$

where $\sigma_\varphi^{el}(r, t)$ is the solution of the corresponding problem for an elastic medium, $s = E/6(1-\nu)\eta$, and η is the viscosity. The stress $\sigma_\varphi^{el}(r, t)$ was calculated from a well-known formula [2] in which, following recommendations in the discussion of Eq. (2), the temperature variation of volume was replaced by $\omega(r, t)$:

Translated from Atomnaya Énergiya, Vol. 57, No. 6, pp. 415-417, December, 1984. Original article submitted April 15, 1983.

0038-531X/84/5706-0846$08.50

TABLE 1. Calculated Variations of T_c, ΔT, and F for a Fuel Element as Functions of its Displacement Along the Axis of the Reactor [1]

Distance from level of upper charge, m	T_c, °C	ΔT, °C	$F \cdot 10^{-21}$, cm^{-2}
0,1	790	210	0,06
0,3	960	260	0,18
0,5	1090	290	0,30
0,9	1220	270	0,60
1,3	1240	200	0,90
1,7	1230	130	1,10
2,1	1230	80	1,30
2,7	1220	45	1,50
3,3	1220	25	1,55
3,95	1210	15	1,60

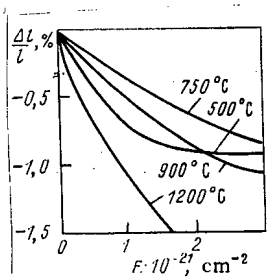

Fig. 1

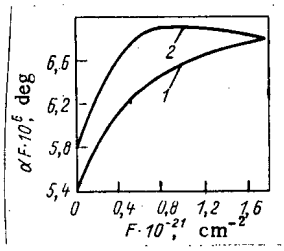

Fig. 2

Fig. 1. Relative variation of linear dimensions of Mark A3 graphite under neutron bombardment [6].

Fig. 2. Variation of the linear coefficient of thermal expansion 1) on the surface and 2) at the center of a fuel element [6].

$$\sigma_{\varphi}^{el}(r, t) = \frac{E}{3(1-\nu)}\left[\frac{2}{R_0^3}\int_0^R \omega(r, t)\, r^2\, dr + \frac{1}{r^3}\int_0^r \omega(r, t)\, r^2\, dr - \omega(r, t)\right], \quad (4)$$

where r is the running radius, and R is the outside radius of the fuel element.

The variation of volume $\omega(r, t)$ in this case is made up of the thermal expansion and the nonuniform graphite shrinkage. The rate of viscous flow $\dot{u}_{11}$ of the material under a uniaxial load under irradiation is

$$\dot{u}_{11} = (B_T + K_p n)\,\sigma_{11}, \quad (5)$$

where B_T is the creep constant in the absence of neutron bombardment, K_p is the radiation creep constant, and n is the neutron flux.

The viscosity is determined [7] in terms of B_T and K_p by the formula

$$\eta = [3(B_T + K_p n)]^{-1}. \quad (6)$$

At a temperature ≥ 1300-1500°C graphite shows practically no thermal creep ($B_T = 0$) [8]. Therefore, taking account of Eq. (6) and $B_T = 0$, the integration with respect to time in Eq. (3) can be transformed to an integration with respect to the fluence F:

$$\sigma_{ij}(r, t) = \sigma_{\varphi}^{el}(r, F) - e^{-pF}\int_0^F p e^{pF'} \sigma_{\varphi}^{el}(r, F')\, dF', \quad (7)$$

where $p = EK_p/2(1-\nu)$.

Strictly speaking, Eq. (7) was derived by assuming that the parameters E, ν, and η are constant in the absence of stresses at time t = 0. Calculations similar to those in [2] show that the expression under consideration retains its form also when there are stresses at t = 0, if they satisfy the equations of thermoelasticity.

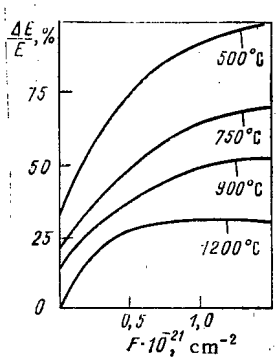

Fig. 3

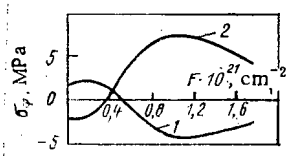

Fig. 4

Fig. 3. Dependence of relative change of the elastic modulus of A3 graphite on the fast neutron fluence for a constant irradiation temperature [6].

Fig. 4. Variation of stresses 1) on the surface and 2) at the center for motion of a spherical fuel element along the reactor axis.

This permits a step-by-step calculation by dividing the total fluence into several intervals. The computational procedure was reduced to the following. Suppose the stress distribution at the k-th step is known. Then the problem is reduced to the determination of the stresses at the end of the k + 1-th interval, with the physical and mechanical properties changed in accordance with the data of Table 1 and Figs. 1-3 [6]. All the parameters were assumed independent of the fluence within the limits of the chosen interval, which corresponds to approximating the time dependence of the parameters by a step function. To ensure the continuity of the stresses, at each new step the initial conditions were taken as the stresses accumulated at the end of the preceding step, multiplying them by the ratio of the elastic modulus in the k + 1-th interval to that in the k-th interval.

Poisson's ratio and the radiation creep constant were assumed constant: $\nu = 0.2$, $K_p = 5 \times 10^{-25}$ (neutrons/$cm^2 \cdot MPa]^{-1}$: the radius of the fuel element R = 3 cm, and the initial value of Young's modulus E= 5 GPa. In spite of the fact that E varies strongly with the fluence, its variation with the radius was small, and in the most unfavorable case for a neutron fluence of $\sim 10^{21}$ cm^{-2} it did not exceed 20%, which lies within the limits of experimental errors in the measurement of the mechanical properties of graphite. Thus, the maximum error of the calculation made with the simple formula (7), which is valid when Young's modulus is independent of the spatial coordinate, does not exceed 20%.

The temperature distribution over a cross section of a fuel element was described by a formula corresponding to the solution of the steady-state heat-conduction equation with the thermal characteristics of the fuel element in the interval under consideration assumed approximately constant:

$$T(r) = T_c - \Delta T \frac{r^2}{R^2}. \tag{8}$$

The values of T_c and ΔT were taken from Table 1. Certain difficulties arose in estimating Young's modulus because of its strong dependence on irradiation. The data in Fig. 3 [6] were obtained for a constant temperature. In order to take account of the simultaneous variation of the temperature and fluence, we consider a very simple model of the effect of radiation on mechanical properties.

The time dependence of Young's modulus is determined by the rate of radiation damage and the rate of annealing of defects

$$\frac{dE}{dt} + \frac{E}{\tau(T)} = A(T)\, n, \tag{9}$$

where $\tau(T)$ is the relaxation time of the defects, A(T) is a parameter numerically equal to the change of Young's modulus per incident neutron, and n is the neutron flux.

The solution of Eq. (9) has the form

$$E = E_{in} + e^{-\int_0^t \frac{dt'}{\tau}} \int_0^t A n e^{\int_0^{t'} \frac{dt''}{\tau}} dt'', \tag{10}$$

where $A = a\gamma$.

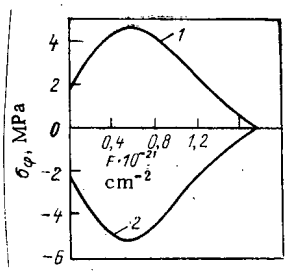

Fig. 5

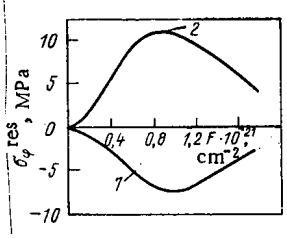

Fig. 6

Fig. 5. Variation of thermoelastic stresses 1) on the surface and 2) at the center of a spherical fuel element.

Fig. 6. Residual stresses 1) on the surface and 2) at the center of a spherical fuel element as a function of the fast neutron fluence.

The integral in (10) contains two temperature-dependent constants τ and A, which were found by processing the experimental results for isothermal conditions (Fig. 3). Then, using the known values of τ and A, Young's modulus was calculated from Eq. (10) as applied to the trajectory of a fuel element as given by the data in Table 1. The change in volume was determined as the sum of the thermal expansion (Fig. 2) and the graphite shrinkage under neutron bombardment (Fig. 1). The calculated values of the tangential stresses acting on the surface and at the center of a fuel element are shown in Figs. 4-6.

The calculated variation of the stresses under the experimental conditions is illustrated by the data of Fig. 4. For a neutron fluence of $\sim 5 \times 10^{20}$ cm^{-2} there is a tensile stress of ~2.0-2.5 MPa on the surface, due mainly to the heat load. Later, as shrinkage phenomena develop, which occur at a higher rate in a hot zone, the outer surface becomes compressed, and the central part of the fuel element is expanded, with the maximum value of σ_φ = 7.5 MPa.

Additional thermal stresses appear at reactor shutdown. As a result the residual stresses will be

$$\sigma_\varphi^{res} = \sigma_\varphi - \sigma_\varphi^{el}. \qquad (11)$$

The values of σ_φ^{el} calculated with Eq. (4) are shown in Fig. 5, and the residual stresses in Fig. 6. The most dangerous situation arises after the neutron fluence reaches 9×10^{20} cm^{-2}. In this case (Fig. 6) the central part of the fuel element is under uniform tension with σ_φ = 11 MPa. If E = 7 MPa initially, the maximum value of σ_φ at the center of a fuel element reaches 16 MPa.

The main error in the calculations arises from the choice of the radiation creep constant and the values of the graphite shrinkage under irradiation. Shrinkage phenomena depend strongly on the technology of the fuel element manufacture. The data in Fig. 2 refer to foreign Mark A3 graphite. Nevertheless, analysis of the stress-strain state by the method described is of definite engineering interest during the stage of design and development of the technology of spherical fuel-element manufacture.

Calculations with various values of K_p gave the following results. For an increase in K_p by a factor of 2-3 above the nominal value, the maximum stresses in Fig. 6 are shifted to the left to fluences of $(3-4) \times 10^{20}$ cm^{-2}. The stresses themselves are only slightly changed. If K_p is decreased by a factor of 2-3, the maximum values in Fig. 6 are shifted to the right into the region of higher neutron fluence, while the character of the variation of σ_φ with F remains unchanged.

The maximum value of σ_φ at the center of a fuel element, equal to 11 MPa (Fig. 6), is smaller than the flexural strength, which is 30-33 MPa [9]. Consequently, one should expect that a fuel element will be sufficiently stable against stresses arising from temperature distributions and shrinkage phenomena. In-pile tests of fuel elements of the construction being considered confirmed their suitability under operating conditions in the VG-400 reactor [9].

Thus, we have developed an algorithm for calculating stresses in graphite-base spherical fuel elements, taking account of the temperature distribution, the nonuniformity of the shrinkage of the material, and radiation creep. We have determined that the maximum tensile stresses, as applied to the VG-400 reactor, develop in the central part of the fuel element after core shutdown, and, according to the calculations, lie within admissible limits.

LITERATURE CITED

1. A. N. Protsenko, and I. G. Belousov, "Basic requirements on nuclear power sources for technological factories and high-temperature gas-cooled reactors," in: Atomic-Hydrogen Power and Technology [in Russian], No. 2, Atomizdat, Moscow (1980), pp. 5-57.
2. B. Boley and J. Weiner, Theory of Thermal Stresses, Wiley, New York (1960).
3. B. Ya. Lyubov and N. S. Fastov, "Effect of concentration pressures on diffusion processes in solid solutions," Dokl. Akad. Nauk SSSR 84, 939 (1952).
4. Ya. S. Podstrigach, "Diffusion theory of the anelasticity of metals," Zh. Prikl. Mekh. Tekh. Fiz., 62, 67 (1965).
5. V. S. Eremeev, "Phenomenological analysis of diffusion in metal alloys," Fiz. Met. Metalloved., 42, 231 (1976).
6. Elers, "Stress in spherical fuel elements of a high-temperature reactor," in: Physical and Mechanical Research and Structural Design of Atomic Industry Plants, No. 1 [in Russian], NIIINFORMTYaZhMASh (1975).
7. V. S. Eremeev and A. I. Gudkov, "On the relation of the rheological and microscopic models of sintering," Poroshk. Metall., No. 3, 31 (1978).
8. Properties of Carbon-Base Structural Materials [in Russian], Metallurgiya, Moscow (1975).
9. A. S. Chernikov, V. S. Kolesov, L. N. Permyakov, et al., "Design and basic characteristics of VTGR fuel elements," Vesti Akad. Nauk BSSR, Ser. Fiz.-Energ. Nauk, No. 3, 77 (1982).

DEVELOPMENT OF AN OIL-FREE FOREVACUUM UNIT FOR AN OPERATING PRESSURE OF 150-300 Pa FOR THE TOKAMAK-15

I. A. Raizman, V. A. Pirogov, L. G. Reitsman, E. A. Maslennikov, and V. V. Martynenko

UDC 621.52

A vacuum is one of the necessary conditions for the operation of many physics facilities. Multistage vacuum units, in which forevacuum pumps produce a pressure of 1-100 Pa, are necessary for attaining the required rarefaction and Roots twin-rotor, turbomolecular, booster, sorption, and other types of pumps are used for further rarefaction. These pumps cannot operate at a pressure appreciably above 100 Pa.

The forepumps used at present operate with vacuum oil. The entry of oil vapor into the spaces undergoing evacuation lead to undesirable consequences. To prevent oil vapor from seeping in, traps of various types are installed in these units ahead of the forevacuum pumps but these traps are not sufficiently reliable. The development of oil-free forevacuum units thus is an important task for vacuum engineering.

Multistage steam ejector pumps are oil-free, but they cannot always be used; water-ring pumps are also oil-free. The maximum vacuum that these pumps can produce, however, is 2.5-5 kPa. If they are to be used as forevacuum pumps, this limit must be lowered by a factor of roughly 50-100. This can be done by connecting a steam–air ejector pump to a water-ring pump (Fig. 1). The ejector is connected to the intake fitting of the pump, in which pressure is maintained at 10 kPa. Air enters into the active nozzle AN directly from the atmosphere. The passive nozzle PN is connected to the space being evacuated. The two streams enter the mixing chamber MC, in which the velocity fields are equalized. The gas then goes to the diffuser D. The ratio of the pressure of the working gas to the pressure of the gas at the ejector exit is $p_1^*/p_4^* \geq 10$, which ensures normal operation of the ejector.

Figure 2 presents the characteristics of steam–air ejectors of some foreign firms. Their capacity is 50-70% of that of a water-ring pump. The capacity of the second stage of a two-stage ejector can also be 50-70% of that of the first stage. As a result, the total capacity of the system is 25-50% of the capacity of the initial pump. It is evidently because of this that multistage ejectors are not made in other countries.

Translated from Atomnaya Énergiya, Vol. 57, No. 6, pp. 417-419, December, 1984. Original article submitted December 12, 1983.

0038-531X/84/5706-0850$08.50

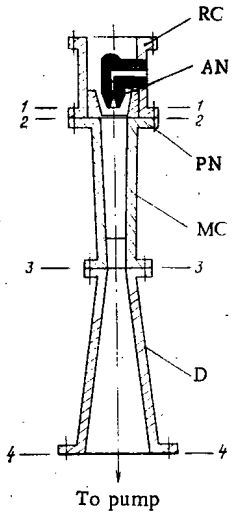

Fig. 1. Diagram of steam–air ejector: RC) receiving chamber; AN) active (operating) nozzle; PN) passive nozzle; MC) mixing chamber; D) diffuser; 1, 2, 3, 4) cross section of the ejector.

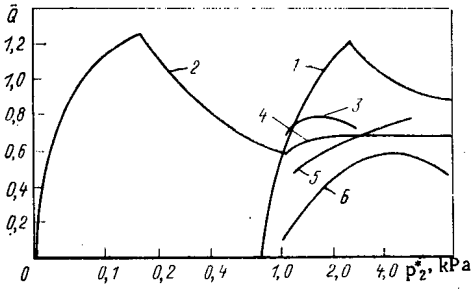

Fig. 2

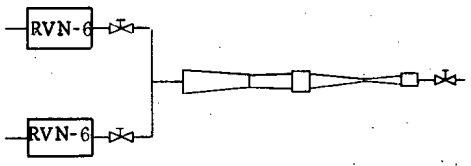

Fig. 3

Fig. 2. Characteristics of ejectors: 1) VVN2-12 with a one-stage ejector; 2) VVN2-12 with a two-stage ejector; 3) LHG14 WEDAG; 4) 2BA 322 Siemens; 5) L6624 SIHI; 6) CL703 NASH; $\bar{Q}$ is the ratio of the ejector capacity to the capacity of the water-ring pump at 10 kPa; here and in Fig. 4 p_2^* is the suction pressure.

Fig. 3. Diagram of T-15 forevacuum unit with two ejectors.

It is our hypothesis that the low capacity of these pumps is due to the fact that their theory has not been developed sufficiently. The complexity and inadequate accuracy of the calculations for the design of ejectors with conical mixing chambers have been pointed out in [1]. Under the conditions under consideration the ratio of the total pressure of the working gas and the gas being pumped off reaches a value of 1000 or more. Without ejector design calculations of an acceptable degree of accuracy and also without optimization of the ejector parameters, therefore, a high ejector capacity cannot be attained. We give a system of equations that describes the operation of an ejector with a conical mixing chamber;

$$p_3^* = p_1^* \sqrt{(n+1)(n\theta+1)}\,\frac{q(\lambda_1)}{q(\lambda_3)}\,\frac{F_1}{F_3}\,; \qquad T_3^* = T_1^*\,\frac{n\theta+1}{n+1}\,;$$

$$\sqrt{(n+1)(n\theta+1)}\left[z(\lambda_3)+\frac{1}{2}\chi\lambda_3\right] = z(\lambda_1)+n\theta z(\lambda_2)+\frac{\tilde{k}(k+1)(k-1)^{-1}}{2}\,\frac{(p_2+p_3)(F_3-F_1-F_2)}{p_1^* F_1^* q(\lambda_1)}\,;$$

$$\frac{1}{q(\lambda_2)} = 1+\frac{z(\lambda_2)-1}{z(\lambda_1')-z(\lambda_1)}\,\frac{1}{\Pi_0}\left[\frac{1}{q(\lambda_1')}-\frac{1}{q(\lambda_1)}\right];$$

$$n = \frac{1}{\Pi_0\alpha\sqrt{\theta}}\,\frac{q(\lambda_2)}{q(\lambda_1)}\,,$$

where p is the pressure, T is the temperature, F is the cross-sectional area, Q is the pump capacity, k is the isoentropic exponent, n is the ejection coefficient, $\theta = T_2^*/T_1^*$, $\alpha = F_1/F_2$, $\Pi_0 = p_1^*/p_2^*$, λ is the reduced velocity, $z(\lambda)$ and $q(\lambda)$ are gasdynamic functions, χ is the reduced length of the mixing chamber, and $\tilde{k}$ is a correction factor which, according to experimental results, is equal to 0.9-1.0 (the subscripts 1, 2, 3, 4 correspond to the cross sections of the ejector; see Fig.1); the prime denotes the choking cross section and the asterisk denotes drag parameters.

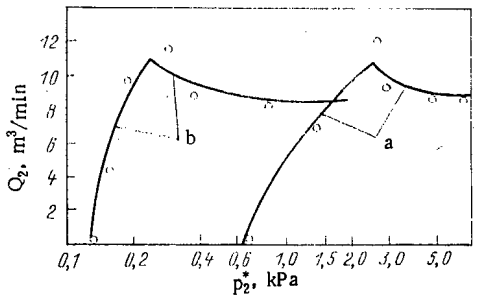

Fig. 4. Design (——) and experimental (○) characteristics of the two-stage steam–air ejector of the Tokamak-15 forevacuum unit: a, b) first and second stages of the ejector (Q_2 is the flow rate of the pumped-off gas).

For the operating conditions under consideration we have formulated a problem of an optimum ejector that is different from the traditional problem. An optimum ejector is one which, for the specific pump characteristic $Q_4 = f(p_1)$ at a specified suction pressure, ensures the maximum volumetric capacity for the gas being pumped off. In carrying out the mathematical optimization of the ejector, we took into account the fact that its operation is characterized by 12 independent parameters: five parameters (pressure and temperature of the working gas and the gas being pumped off as well as the gas flow rate through the pump) are prescribed and we have four independent equations. Thus, three parameters are free and determine the optimality of the ejector. These could be the ratio of the areas of the characteristic cross sections of the ejector and the reduced velocities α, λ_1, and λ_3. The optimization determines the geometrical dimensions of the nozzles for the working gas and the gas to be pumped off as well as the size of the mixing chamber.

A procedure has also been developed for the calculation of the characteristics of the stages of an ejector. Besides the parameters indicated above, also known are the cross-sectional areas F_1, F_2, F_3, and F_4 which makes the problem uniquely definable.

Both calculations and experiments have shown that the characteristic consists of two branches. If the suction pressure is lower than the calculated value, the velocity of the pumped-off gas in the choking cross section is critical and if this pressure is higher than the calculated value, the gas velocity is subcritical. Therefore, the characteristic has a peak at the calculated point. The second (from the pump) stage of the ejector is calculated with the aid of the same procedure, taking the characteristic of the first stage is assumed to be the initial characteristic.

A two-stage ejector makes it possible, using a water-ring pump, to obtain a pressure of ~200-300 Pa in the operating regime and 70 Pa in the limiting regime. Instead of a water-ring pump, any other forevacuum pump that ensures a pressure of ~10 kPa can be used.

A forevacuum unit consisting of two RVN-6 vane-type rotary pumps and a two stage steam–air ejector (Fig. 3) has been developed for the Tokamak-15. The casings of the ejectors were made of D-16 Dural and the ejector nozzles were made of Kh18N10T steel. The characteristic of the unit is given in Fig. 4. Its ultimate vacuum is ~100 Pa, and the pumping rate at ~300 Pa is above 100 liters/sec, which is commensurate with the pumping rate of the NVZ-150 pump at this pressure. The unit can pump off any gas, including corrosive gases. The ejector does not require cooling and the electrical consumption is determined in practice by the RVN-6 pumps.

It is proposed that the forevacuum unit with a two-stage steam–air ejector be used for pumping down the T-15 cryostat with an effective volume of ~350 m^3, from atmospheric pressure to about 100 Pa. The unit has been pretested on a cryostat designed for testing superconducting magnetic coils of the longitudinal field of the T-15, which has an effective volume of ~90 m^3. A pressure of ~100 Pa was obtained in the test cryostat in ~5 h.

The experience gained from prolonged operation of water-ring pumps with steam–air ejectors has been positive [2]. The water-ring pumps manufactured at this time enable units with a capacity of 5-5000 liters/sec to be built.

LITERATURE CITED

1. G. N. Abramovich, Applied Gas Dynamics [in Russian], Nauka, Moscow (1969), p. 457.
2. Yu. M. Prilutskikh, I. A. Raizman, A. D. Chuchuryukin, and M. V. Demchenko, "Introduction of a vacuum system based on water-ring pumps into the production of titanium ingots," Tekhnol. Legkikh Splavov, No. 11-12, 37-40 (1982).

SURFACE TENSION OF MOLTEN MIXTURES OF FLUORIDES OF LITHIUM, BERYLLIUM, AND THORIUM

A. A. Klimenkov, N. N. Kurbatov, S. P. Raspopin, and Yu. F. Chervinskii

UDC 532.61:546.161-143

Melts of mixtures of fluorides of lithium, beryllium, thorium, and uranium satisfy most completely the many requirements imposed on fuel composites and breeder-zone materials in a liquid-salt nuclear reactor [1], and therefore there is a need for information on the physicochemical properties of such melts.

The surface tension of three-component melts containing fluorides of thorium, beryllium, and lithium were measured by the maximum-pressure method in a gas bubble. The salts investigated were placed in glass-carbon crucibles. The material used for the capillaries was nickel, which is resistant to the action of fluoride melts. As the working gas, we used argon from which the traces of moisture and oxygen had first been removed.

In determining the surface tension, we used data on the density of melts taken from [2]. The surface tension was calculated according to the Cantor–Schrödinger formula [3]. In our investigations, we paid close attention to the preparation of the appropriate anhydrous salts. The anhydrous lithium fluoride was obtained by air-drying the initial chemically pure salt by successive gradual heating in a vacuum to the melting point and slow crystallization in an argon medium. The thorium tetrafluoride was obtained by the method described earlier in [4]. The technically pure beryllium fluoride was subjected to vacuum distillation at 1400°K. The melting points of the resulting salts, determined by the method of differential-thermal analysis, are in good agreement (±2 °K) with the most reliable published data [5].

The surface tension of the melted mixtures of the three-component system $LiF-BeF_2-ThF_4$ was studied by the method of polythermal sections made from the beryllium-fluoride vertex of the concentration triangle to the opposite side. In the system we investigated seven such sections in each of which the ratio of the lithium-fluoride concentration to the thorium-fluoride concentration remained constant. The results of the measurements were processed by the method of least squares. The temperature dependence of the surface tension of each melt in the temperature intervals investigated is described fairly satisfactorily by linear equations whose coefficients are shown in Table 1. The table also gives the mean-square deviations S of the experimental values from those calculated by using the equations, and the temperature intervals of the measurements are indicated.

The surface tension of the molten mixtures within the limits of each polythermal section decreases substantially as the beryllium-fluoride concentration increases, and this suggests that it is surface-active with respect to the other components of the mixture. After the minimum values have been reached (the mole fraction of the BeF_2 is 60%), the surface tension begins to increase, which is apparently due to the process of polymerization and the formation of vitreous structures in the melts with a high percentage of beryllium fluoride, characterized by its polymer nature [6]. Figure 1 shows the curves of equal surface tension of the melts of the investigated system in the plane of the concentration triangle. As the concentration of thorium tetrafluoride decreases, the surface tension in the melts of the system decreases as well, and the slowest rate of decrease is observed in the regions with a high concentration of lithium fluoride. The nature of the variation of surface

Translated from Atomnaya Énergiya, Vol. 57, No. 6, pp. 419-420, December, 1984. Original article submitted January 1, 1984.

0038-531X/84/5706-0853$08.50

TABLE 1. Surface Tension of Molten Mixtures of the $LiF-BeF_2-ThF_4$ System

Mole fraction, %			$\sigma = A - B \cdot T$, mJ/m^2		S	Temp. interval, °K	Mole fraction, %			$\sigma = A - B \cdot T$, mJ/m^2		S	Temp. interval, °K
BeF_2	ThF_4	LiF	A	B			BeF_2	ThF_4	LiF	A	B		
10	9	81	333,0	0,1084	0,6	970—1170	40	24	36	329,4	0,1323	0,9	1070—1220
20	8	72	322,0	0,1095	0,8	870—1170	50	20	30	323,6	0,1321	0,8	1020—1170
30	7	63	322,5	0,1212	0,9	870—1170	60	16	24	328,8	0,1412	1,0	1020—1170
40	6	54	313,0	0,1254	0,8	870—1170	10	45	45	398,2	0,1544	0,6	1170—1220
50	5	45	283,4	0,1108	0,8	870—1120	20	40	40	393,4	0,1622	0,7	1170—1220
60	4	36	312,7	0,1392	1,0	870—1120	30	35	35	378,0	0,1602	0,8	1170—1220
70	3	27	340,9	0,1618	1,4	870—1120	40	30	30	356,7	0,1514	1,0	1170—1220
10	18	72	358,0	0,1284	0,8	970—1170	50	25	25	339,5	0,1435	0,9	1090—1170
20	16	64	352,0	0,1345	0,8	970—1170	60	20	20	353,8	0,1593	1,2	1070—1170
30	14	56	353,7	0,1451	1,0	970—1170	10	54	36	397,6	0,1512	0,8	1170—1270
40	12	48	364,9	0,1682	0,9	970—1120	20	48	32	374,1	0,1427	1,0	1170—1270
50	10	40	336,1	0,1527	0,8	920—1120	30	42	28	361,0	0,1412	0,8	1120—1220
60	8	32	351,8	0,1693	1,0	920—1170	40	36	24	353,0	0,1445	1,0	1120—1220
10	27	63	390,7	0,1561	0,6	1020—1220	50	30	20	335,4	0,1358	1,1	1120—1220
20	24	56	378,9	0,1554	0,8	1020—1170	60	24	16	351,5	0,1526	1,0	1120—1220
30	21	49	363,8	0,1538	0,7	920—1170	10	67,5	22,5	409,1	0,1564	0,8	1220—1320
40	18	42	345,9	0,1490	0,8	920—1170	20	60	20	396,0	0,1575	0,9	1220—1300
50	15	35	326,0	0,1384	1,0	970—1120	30	52,5	17,5	376,9	0,1524	1,0	1170—1270
60	12	28	338,8	0,1532	1,1	970—1120	40	45	15	353,5	0,1412	0,8	1150—1270
10	36	54	383,5	0,1445	1,1	1020—1220	50	37,5	12,5	338,9	0,1324	1,0	1120—1220
20	32	48	362,6	0,1378	0,8	1070—1220	60	30	10	338,8	0,1358	1,1	1120—1220
30	28	42	345,3	0,1344	1,0	1070—1220	70	22,5	7,5	358,5	0,1513	1,0	1070—1220

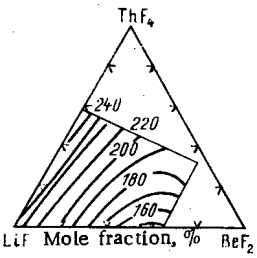

Fig. 1. Curves of equal surface tension (σ, mJ/m^2) of melts of the $LiF-BeF_2-ThF_4$ system at 1130°K.

tension as a function of the concentration indicates that in relation to the thorium tetrafluoride, the beryllium fluoride has a higher surface activity than the lithium fluoride.

LITERATURE CITED

1. V. L. Blinkin and V. N. Novikov, Liquid-Salt Reactors [in Russian], Atomizdat, Moscow (1978).
2. A. A. Klimenkov, N. N. Kurbatov, S. P. Raspopin, and Yu. F. Chervinskii, Density of Molten Three-Component Mixtures of Fluorides of Lithium, Beryllium, and Thorium [in Russian]. Submitted article No. 578KhP-82. Cherkassy: Division of the Scientific-Research Institute of Technical and Economic Investigations of the Ministry of the Chemical Industry, May 17, 1982.
3. V. K. Semenchenko, Surface Phenomena in Metals and Melts [in Russian], Gostekhteorizdat, Moscow (1957).
4. V. N. Desyatnik, A. A. Klimenkov, N. N. Kurbatov, et al., "Density and kinematic viscosity of the melts $NaF-ThF_4$ and $KF-ThF_4$," At. Energ., 51, No. 6, 390-392 (1981).
5. Handbook of Molten Salts [Russian translation], Vol. 1, Khimiya, Leningrad (1972).
6. A. Rahman, R. Fower, and A. Norten, J. Chem. Phys. 52, No. 7, 3010-3012 (1972).

EXPERIMENTAL STUDY OF THE INTERACTION OF PULSATIONS OF THE NEUTRON FLUX AND THE COOLANT FLOW IN A BOILING-WATER REACTOR

P. A. Leppik

UDC 621.039.564.2

In [1], based on calculations utilizing a refined model of the dynamics of a boiling-water reactor [2, 3], it is concluded that the interaction of the neutron flux and the coolant flow plays an important role in the mechanism of high-frequency (HF) resonant instability of the VK-50 boiling-water reactor. In order to confirm this conclusion and to check the working model, signals from probes measuring the flow rate of the coolant and the neutron flux were recorded simultaneously (with the help of a magnetograph) in experiments performed in 1981 on driving the VK-50 reactor into the HF resonant instability regimes. Estimates were then obtained for the statistical characteristics of the pulsations of the flow rate and of the neutron flux, including the cross-correlation functions and coherence functions. The basic results of these studies are reported in this paper.

The reactor was driven into the HF resonant instability regime by gradually increasing its head load while maintaining the pressure in the range p = 1.0-3.0 MPa. As the so-called extrapolated linear boundary of instability was approached [4], the amplitude of the pulsations of the neutron flux reached 20-30%. Two-blade flowmeters (TF), based on the work performed at the G. M. Krzhizhanovskii Power-Engineering Scientific-Research Institute [5], were used as probes for measuring the flow rate of the coolant. The signal from the TF is excited with the help of a permanent magnet, fastened on the axis of the rotor, and an induction coil with a magnetic core. We positioned the flowmeters at the inlet to several fuel assemblies at different distances from the axis of the active zone. The rate of rotation of the rotors of the TF varied from 15 to 30 Hz under the experimental conditions.

To convert the primary signal from the TF into a flow-rate signal, we used a fast frequency-to-voltage converter developed at the I. V. Kurchatov Institute of Atomic Energy, whose principle of operation is based on the measurement of each half-period of the input signal. The converter contains an internal digital computing setup and analog setups at the input and output. The neutron-flux signals were obtained simultaneously from an ionization chamber (IC), positioned outside the reactor, and from a direct-charging probe (DCP), positioned at the center of the active zone.

We performed the sampling estimates of the main statistical characteristics of the pulsations of the flow rate and of the neutron flux with the help of apparatus manufactured by the Honeywell Company (SAI-43A correlation meter with a SAI-470 Fourier transformer). We estimated the coherence functions using the technique described in [6]. The duration of the realizations processed varied from 7 to 20 min and the sampling time was 0.05 sec. At the input to the correlation meter, all signals were passed through identical low-frequency and high-frequency filters with a transmission band of 0.1-4 Hz.

Figures 1 and 2 show typical examples of the estimates of the spectral power densities (spd) and the coherence functions of the flow rate and of neutron flux for a state close to the linear stability boundary.* It is evident that the spd of the flow rate, just as for the neutron flux, has a resonant peak at the frequency $f_r \approx 0.85$ Hz, but does not decrease as rapidly away from the resonant peak. The flow rate and the neutron flux have a significant coherence at a frequency close to the resonant frequency. At f = 0.75-0.95 Hz, the coherence function reaches a value of 0.8-0.95, but away from the resonant frequency the coherence of the pulsations of the flow rate and of the neutron flux decreases markedly. This, in all probability, is associated with the presence of components in the flow-rate signal measured which are not correlated with the neutron flux (turbulent pulsations of the flow velocity of the coolant in the fuel assembly, noise in the measuring channel, etc.)

*The form of the autocorrelation function (ACF) of the neutron flux is close to $\sigma_N^2 e^{-\alpha|\tau|}\cos\omega_0\tau$ (for the state under study $\sigma_N^2 = (15\%)^2$, $\alpha = 0.22$ sec^{-1}; $\omega_0 = 5.6$ sec^{-1}). The ACF of the flow rate and the cross-correlation function of the flow rate and neutron flux differ in form in that the first has a sharp peak near the point $\tau = 0$, whereas the peak in the second is shifted to the right by 0.25 sec.

Translated from Atomnaya Énergiya, Vol. 57, No. 6, pp. 420-422, December, 1984. Original article submitted March 14, 1984.

0038-531X/84/5706-0855$08.50

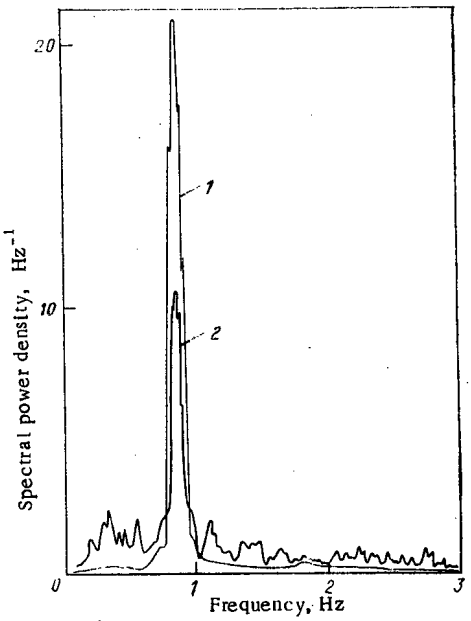

Fig. 1

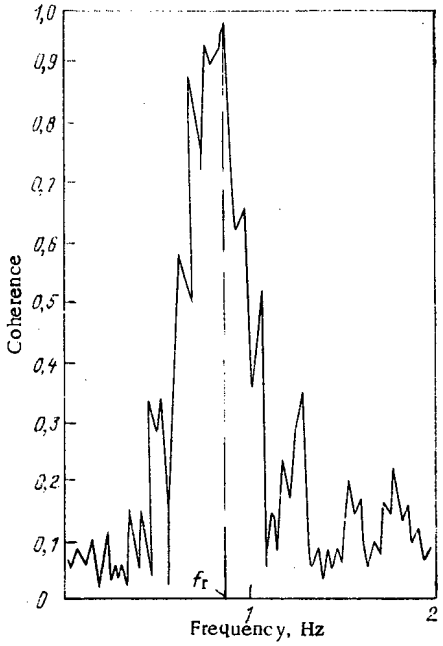

Fig. 2

Fig. 1. Normalized estimates of the spectral power densities of the neutron flux (1) and coolant flow rate in the fuel assembly (2) (obtained using the signals from the TF in the third row of fuel assemblies and from the IC for a state with a pressure of 2.5 MPa and a heat load of 137 MW).

Fig. 2. Estimate of the flow-rate – neutron-flux coherence function.

An analysis of the estimation obtained for the statistical characteristics of the pulsations of the flow rate and of the neutron flux made it possible to check the working model of the reactor dynamics [2, 3] used in [1]. For this, with the help of the working model, we checked the ratio of the amplitudes and phases of periodic oscillations of the flow rate of the coolant and neutron flux in states at the boundary of linear stability (the pressure and heat load were given in accordance with the linear boundary of stability of the reactor determined from the experiment using the procedure described in [4]; exact coincidence of the computed stability boundary with the experimental boundary was achieved by adjusting the thermal resistance of the gaseous gap in the fuel elements). The computed ratio was compared with the measured ratio of the amplitudes and phases of the components of the pulsations of the flow rate and neutron flux with frequency f_r for a number of states close to the stability boundary. The latter was estimated from the equations:

$$K_{NG}=\frac{A_N}{A_G}\approx\frac{|\tilde{S}_{GN}(j\tilde{f}_r)|}{\tilde{S}_{GG}(\tilde{f}_r)}\approx\frac{\tilde{S}_{NN}(\tilde{f}_r)}{|\tilde{S}_{NG}(jf_r)|};$$

$$\Delta\varphi_{NG}=\varphi_N-\varphi_G=\Delta\tilde{\varphi}^*_{NG}-\delta\tilde{\varphi}_{NG},$$

where

$$\Delta\tilde{\varphi}^*_{NG}=\arg\tilde{S}_{GN}(jf_r)\approx-2\pi\Delta\tilde{\tau}\tilde{f}_r;$$

$$\delta\tilde{\varphi}_{NG}=\delta\tilde{\varphi}_N-\delta\tilde{\varphi}_G;$$

A_N and A_G are the amplitudes while φ_N and φ_G are the phases of the oscillations of the neutron flux and flow rate; S_{GN} is the cross spectral power density of the flow rate and of the neutron flux; S_{NN} and S_{GG} are the spd of the neutron flux and of the flow rate; $\Delta\tau$ is the time shift, corresponding to the peak in the cross-correlation function of the flow rate and the neutron flux; $\delta\varphi_N$ and $\delta\varphi_G$ are the phase shifts in the measuring channels for the neutron flux and flow rate*; and, the symbol ~ denotes estimated quantities.

*For the channel from the IC $\delta\tilde{\varphi}_N \leq 5°$; for the channel from the TF $\delta\tilde{\varphi}_G \leq 5°$; and, for the channel from the DCP $\tilde{\delta\varphi}_N \approx 20$–$25°$. The large phase shift in the signal in the channel from the DCP is a result of the uncertain selection of the parameters of the correction (phase-lead) feedback device at the output of the channel (we estimated $\delta\varphi_N$ after the experiment by a test method on a stand using a sinusoidal signal generator). The dynamic attenuation of the signal amplitudes at the frequency f_r for all measuring channels was insignificant (<5%).

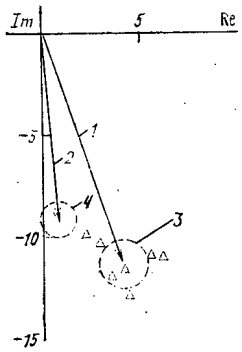

Fig. 3. Comparison of the experimental and computed values of K_{NG} and $\Delta\varphi_{NG}$; 1) experimental ($K_{NG}^{meas} e^{j\Delta\varphi ND}$); 2) calculation ($K_{NG}\, e^{j\Delta\varphi NG}$); 3) 95% confidence region; 4) region of computed estimates; Δ separate samples of experimental estimates.

An analysis of the computed estimates showed that along the boundary of linear stability and away from it, within the limits of the region of reactor parameters studied the deviations of K_{NG} and $\Delta\varphi_{NG}$ from their average values are much smaller (8-12% and 5-8°, respectively) than the spread in the experimental estimates. In this connection, we checked the working model by comparing the averaged (over an ensemble of states) computed and experimental estimates.

The results of the comparison of the data obtained from the calculation and experiment on K_{NG} and $\Delta\varphi_{NG}$ are shown in Fig. 3. Here, the averaged data from the calculation (K_{NG}^{comp}, $\Delta\varphi_{NG}^{comp}$) and experiment ($K_{NG}^{meas}$, $\Delta\varphi_{NG}^{meas}$) are illustrated in the form of vectors in the complex plane. The lengths of the vectors (K_{NG}^{comp}, and K_{NG}^{meas}) correspond to the ratio of dimensionless (taken in fractions of the average value) amplitudes of pulsations of the neutron flux and the flow rate. The phases are equal to $\Delta\varphi_{NG}^{comp}$ and $\Delta\varphi_{NG}^{meas}$. The dashed curves show the 95% confidence region for the experimental estimate of the vector. It is evident that the disagreements between the calculation and experiment are not very large and have a quite systematic character; for $K_{NG}^{meas} \approx 9$ and $\Delta\varphi_{NG}^{comp} \approx -85°$, $K_{NG}^{meas}/K_{NG}^{comp} \approx 1.1\text{-}1.5$ and $\Delta\varphi_{NG}^{meas} - \Delta\varphi_{NG}^{comp} \approx 10\text{-}25°$.

The indicated disagreements are apparently attributable to the approximate nature of the working model used (inaccurate description of the dynamics of the thrust section, neglect of nonlinear effects, and the characteristics of the sources of noise).

On the whole, the results of the study performed demonstrate the validity of the working model [2, 3] and confirm the basic results of [1].

LITERATURE CITED

1. P. A. Leppik, S. P. Pavlov, and V. I. Plyutinskii, "The problem of the mechanism of HF-resonant instability of the VK-50 reactor," At. Energ., 52, No. 6, 379-382 (1982).
2. P. A. Leppik et al., Preprint IAÉ-3576/5, Moscow (1982).
3. P. A. Leppik et al., Preprint IAÉ-3667/5, Moscow (1982).
4. B. V. Kebadze, V. I. Plyutinskii, and L. A. Adamovskii, "Statistical characteristics of a boiling-water reactor near the stability boundary," At. Energ., 32, No. 5, 407-408 (1972).
5. I. S. Dubrovskii and I. I. Kalmykov, Teploenergetika, No. 9, 91 (1967).
6. J. S. Bendat and A. G. Piersol, Random Data: Analysis and Measurement Procedures, Wiley (1971).

CONTROL EXPERIMENT ON CRITICAL HEAT TRANSFER DURING WATER FLOW IN PIPES

P. L. Kirillov, O. L. Peskov, and N. P. Serdun'

UDC 536.2

The control experiments on critical heat transfer during the flow of water in pipes, in which a large number of scientific-research organizations of the USSR participated, were completed in 1982-1983. The necessity of the control experiment was dictated by the following. Many organizations accumulated over the period 1950-1980 extensive factual data on critical heat transfer in pipes. Experimental data, obtained in different organizations under analogous conditions and with similar geometrical parameters, in a number of cases differ quantitatively and, when represented in the form $q_{cr} = f(x, p, \rho w)$, qualitatively also. The reasons for these disagreements were unclear.

The experimental data were obtained on stands with different layouts and designs, using different procedures, and with the help of measuring systems which had different accuracies and capabilities. These factors could have been responsible for some of the indicated disagreements in the experimental data. In particular, there recently appeared data which prove that the quantitative characteristics of the steam–water flow in a dispersed-annular flow state can differ, depending on the layout of the stand. Three types of stands are currently used in thermophysical experiments:

stands with a closed circulating loop and an electrically heated experimental section, in which the water–steam mixture is prepared. Such stands are available at the I. V. Kurchatov Institute of Atomic Energy, Institute of Engineering Thermophysics of the Academy of Sciences of the Ukrainian SSR, the Special Design Office (SDO) "Gidropress," NIKIÉT, FÉI, and Scientific-Production Union (SPU) "Énergiya" and other organizations;

a closed circulation loop, but with a buffer volume at the outlet from the experimental section (Kiev Polytechnical Institute); and,

a single-pass loop with the steam–water mixture prepared in a mixer (steam and water from a boiler) and injection of this mixture into the experimental section (F. É. Dzerzhinskii All-Union Heat Engineering Institute, I. I. Polzunov Central Boiler-Pipe Institute).

In some organizations, for example, at the Institute of Engineering Thermophysics of the Academy of Sciences of the Ukrainian SSR, the flow rate of the water is measured with fast-response turbine flowmeters, which permit fixing the pulsation regimes of the flow of the water–steam mixture and separating out the experimental data for these regimes, while flow-measuring devices with slower response are used in other organizations.

In accordance with the program of the control experiment, the tests were performed on stands available at the organizations using a procedure adopted in each organization; standard pipes from a single batch (fusion and treatment) with a diameter and wall thickness of 12 × 2 mm consisting of Kh18N10T steel were used as the working sections; the experiments were performed at pressures of 7.0, 10.0, 14.0, and 18.0 MPa; the mass velocity was equal to 500, 1000, 2000, and 4000 kg/(m^2·sec); the water temperature at the inlet was 100-(t_s − 10°C); and the pipe lengths were 1, 3, and 6 m. The control experiment performed by ten organizations yielded ~ 2500 experimental values of the critical power.

The primary analysis of the experimental data showed that in the $N_{cr}(t_{in})$ plane, under identical conditions, the data on the critical power of different organizations differ in separate cases by up to 10-12 kW, which comprises 16-32% for a pipe 1 m long and approximately 10% for a pipe 3 m long (Fig. 1). The experimental data $N_{cr}(t_{in})$ of different organizations follow, as a rule, parallel lines. In the $q_{cr}(x)$ plane, the spread in the experimental data was larger (Fig. 2). It follows from data obtained at many organizations that for some com-

Translated from Atomnaya Énergiya, Vol. 57, No. 6, pp. 422- 423, December, 1984. Original article submitted March 29, 1984.

0038-531X/84/5706-0858$08.50

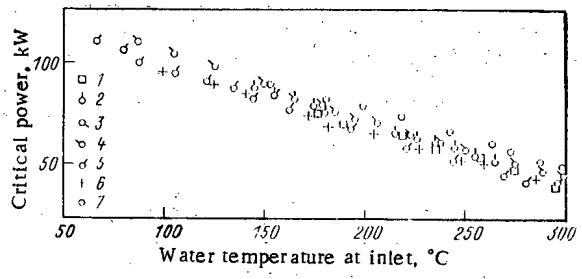

Fig. 1. Dependence of the critical power for a 1-m pipe on the water temperature at the inlet at a pressure of 10.0 MPa and with a mass velocity of 2000 kg/(m^2 · sec). Here and in Fig. 2, 1 denote the SPU data; 2 denote the FÉI data; 3 denote the SDO data; 4 denote the NIKIÉT data; 5 denote the data from the Kiev Polytechnical Institute; 6 denote the data from the Institute of Engineering Thermophysics of the Academy of Sciences of the Ukrainian SSR; and, 7 denote the data from the F. É. Dzerzhinskii All-Union Heat Engineering Institute.

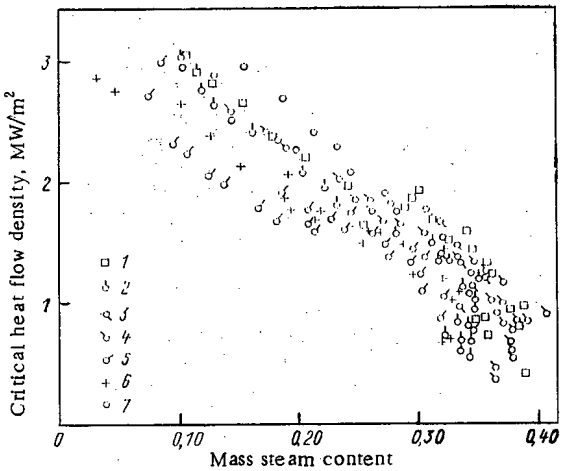

Fig. 2. Dependence of the critical power of a 3-m pipe on the water temperature at the inlet at a pressure of 14.0 MPa and with a mass velocity of 400 kg/(m^2 · sec).

binations of state parameters, one value of the steam content corresponds to two values of the critical heat flow density (though the data were obtained with pipes of different length).

Thus, even the experimental data obtained in the course of the control experiment, which was prepared with special care in channels with the simplest geometry, presented in the coordinates $N_{cr}(t_{in})$ and $q_{cr}(x)$ exhibited a spread. It should be noted that the experimental data obtained by each organization are statistically uniform and their spread falls within the limits of the experimental error. The spread in the experimental data from different organizations exceeds the error of the measurement and therefore cannot be attributed to the latter.

The analysis established that the experimental data from FÉI, NIKIÉT, and SDO, i.e., data obtained on stands with a closed circulating loop (with the exception of the data from SPU and the Institute of Engineering Thermophysics of the Academy of Sciences of the Ukrainian SSR), agree well with one another.

Possible reasons for the disagreements in the experimental data could be the following:

difference in the layouts of the stands (F. É. Dzerzhinskii All-Union Heat Engineering Institute, Kiev Polytechnic Institute);

inaccuracy in maintaining the state parameters while performing the experiments (SPU and Kiev Polytechnic Institute);

inadequate use of modern systems for measuring state parameters;

inadequate care in preparing and performing the experiments (calibration of thermocouples and flow-measuring complexes, determination of heat losses to the surrounding medium, etc.

The processing and analysis of the experimental data obtained are continuing.

INDEX

SOVIET ATOMIC ENERGY

Volumes 56-57, 1984

SOVIET ATOMIC ENERGY
Volumes 56-57, 1984
(A translation of Atomnaya Énergiya)

L

M

N

O

P

R

S

T

U

V

W

Y

Z

SOVIET ATOMIC ENERGY

Volumes 56-57, 1984

(A translation of Atomnaya Énergiya)

Volume 56, Number 1 January, 1984

Volume 56, Number 2 February, 1984

Volume 56, Number 3 March, 1984

Volume 56, Number 4 April, 1984

Engl./Russ.

Volume 56, Number 5 May, 1984

Volume 56, Number 6 June, 1984

Volume 57, Number 1 July, 1984

Volume 57, Number 3 September, 1984

Volume 57, Number 4 October, 1984

Volume 57, Number 4 November, 1984

Volume 57, Number 6 December, 1984

MEASUREMENT TECHNIQUES
Izmeritel'naya Tekhnika
Vol. 27, 1984 (12 issues) $520

MECHANICS OF COMPOSITE MATERIALS
Mekhanika Kompozitnykh Materialov
Vol. 20, 1984 (6 issues) $430

METAL SCIENCE AND HEAT TREATMENT
Metallovedenie i Termicheskaya Obrabotka Metallov
Vol. 26, 1984 (12 issues) $540

METALLURGIST
Metallurg
Vol. 28, 1984 (12 issues) $555

PROBLEMS OF INFORMATION TRANSMISSION
Problemy Peredachi Informatsii
Vol. 20, 1984 (4 issues) $420

PROGRAMMING AND COMPUTER SOFTWARE
Programmirovanie
Vol. 10, 1984 (6 issues) $175

PROTECTION OF METALS
Zashchita Metallov
Vol. 20, 1984 (6 issues) $480

RADIOPHYSICS AND QUANTUM ELECTRONICS
Izvestiya Vysshikh Uchebnykh Zavedenii, Radiofizika
Vol. 27, 1984 (12 issues) $520

REFRACTORIES
Ogneupory
Vol. 25, 1984 (12 issues) $480

SIBERIAN MATHEMATICAL JOURNAL
Sibirskii Matematicheskii Zhurnal
Vol. 25, 1984 (6 issues) $625

SOIL MECHANICS AND FOUNDATION ENGINEERING
Osnovaniya, Fundamenty i Mekhanika Gruntov
Vol. 21, 1984 (6 issues) $500

SOLAR SYSTEM RESEARCH
Astronomicheskii Vestnik
Vol. 18, 1984 (6 issues) $365

SOVIET APPLIED MECHANICS
Prikladnaya Mekhanika
Vol. 20, 1984 (12 issues) $520

SOVIET ATOMIC ENERGY
Atomnaya Énergiya
Vols. 56-57, 1984 (12 issues) $560

SOVIET JOURNAL OF GLASS PHYSICS AND CHEMISTRY
Fizika i Khimiya Stekla
Vol. 10, 1984 (6 issues) $235

SOVIET JOURNAL OF NONDESTRUCTIVE TESTING
Defektoskopiya
Vol. 20, 1984 (12 issues) $615

SOVIET MATERIALS SCIENCE
Fiziko-khimicheskaya Mekhanika Materialov
Vol. 20, 1984 (6 issues) $445

SOVIET MICROELECTRONICS
Mikroèlektronika
Vol. 13, 1984 (6 issues) $255

SOVIET MINING SCIENCE
Fiziko-tekhnicheskie Problemy Razrabotki Poleznykh Iskopaemykh
Vol. 20, 1984 (6 issues) $540

SOVIET PHYSICS JOURNAL
Izvestiya Vysshikh Uchebnykh Zavedenii, Fizika
Vol. 27, 1984 (12 issues) $520

SOVIET POWDER METALLURGY AND METAL CERAMICS
Poroshkovaya Metallurgiya
Vol. 23, 1984 (12 issues) $555

STRENGTH OF MATERIALS
Problemy Prochnosti
Vol. 16, 1984 (12 issues) $625

THEORETICAL AND MATHEMATICAL PHYSICS
Teoreticheskaya i Matematicheskaya Fizika
Vol. 58-61, 1984 (12 issues) $500

UKRAINIAN MATHEMATICAL JOURNAL
Ukrainskii Matematicheskii Zhurnal
Vol. 36, 1984 (6 issues) $500

Send for Your Free Examination Copy

Plenum Publishing Corporation, 233 Spring St., New York, N.Y. 10013
In United Kingdom: 88/90 Middlesex St., London E1 7EZ, England
Prices slightly higher outside the U.S. Prices subject to change without notice.

RUSSIAN JOURNALS IN THE PHYSICAL AND MATHEMATICAL SCIENCES

AVAILABLE IN ENGLISH TRANSLATION

ALGEBRA AND LOGIC
Algebra i Logika
Vol. 23, 1984 (6 issues) $360

ASTROPHYSICS
Astrofizika
Vol. 20, 1984 (4 issues) $420

AUTOMATION AND REMOTE CONTROL
Avtomatika i Telemekhanika
Vol. 45, 1984 (24 issues) $625

COMBUSTION, EXPLOSION, AND SHOCK WAVES
Fizika Goreniya i Vzryva
Vol. 20, 1984 (6 issues) $445

COSMIC RESEARCH
Kosmicheskie Issledovaniya
Vol. 22, 1984 (6 issues) $545

CYBERNETICS
Kibernetika
Vol. 20, 1984 (6 issues) $445

DIFFERENTIAL EQUATIONS
Differentsial'nye Uravneniya
Vol. 20, 1984 (12 issues) $505

DOKLADY BIOPHYSICS
Doklady Akademii Nauk SSSR
Vols. 274-279, 1984 (2 issues) $145

FLUID DYNAMICS
Izvestiya Akademii Nauk SSSR, Mekhanika Zhidkosti i Gaza
Vol. 19, 1984 (6 issues) $500

FUNCTIONAL ANALYSIS AND ITS APPLICATIONS
Funktsional'nyi Analiz i Ego Prilozheniya
Vol. 18, 1984 (4 issues) $410

GLASS AND CERAMICS
Steklo i Keramika
Vol. 41, 1984 (6 issues) $590

HIGH TEMPERATURE
Teplofizika Vysokikh Temperatur
Vol. 22, 1984 (6 issues) $520

HYDROTECHNICAL CONSTRUCTION
Gidrotekhnicheskoe Stroitel'stvo
Vol. 18, 1984 (12 issues) $385

INDUSTRIAL LABORATORY
Zavodskaya Laboratoriya
Vol. 50, 1984 (12 issues) $520

INSTRUMENTS AND EXPERIMENTAL TECHNIQUES
Pribory i Tekhnika Eksperimenta
Vol. 27, 1984 (12 issues) $590

JOURNAL OF APPLIED MECHANICS AND TECHNICAL PHYSICS
Zhurnal Prikladnoi Mekhaniki i Tekhnicheskoi Fiziki
Vol. 25, 1984 (6 issues) $540

JOURNAL OF APPLIED SPECTROSCOPY
Zhurnal Prikladnoi Spektroskopii
Vols. 40-41, 1984 (12 issues) $540

JOURNAL OF ENGINEERING PHYSICS
Inzhenerno-fizicheskii Zhurnal
Vols. 46-47, 1984 (12 issues) $540

JOURNAL OF SOVIET LASER RESEARCH
A translation of articles based on the best Soviet research in the field of lasers
Vol. 5, 1984 (6 issues) $180

JOURNAL OF SOVIET MATHEMATICS
A translation of Itogi Nauki i Tekhniki and *Zapiski Nauchnykh Seminarov Leningradskogo Otdeleniya Matematicheskogo Instituta im. V. A. Steklova AN SSSR*
Vols. 24-27, 1984 (24 issues) $1035

LITHOLOGY AND MINERAL RESOURCES
Litologiya i Poleznye Iskopaemye
Vol. 19, 1984 (6 issues) $540

LITHUANIAN MATHEMATICAL JOURNAL
Litovskii Matematicheskii Sbornik
Vol. 24, 1984 (4 issues) $255

MAGNETOHYDRODYNAMICS
Magnitnaya Gidrodinamika
Vol. 20, 1984 (4 issues) $415

MATHEMATICAL NOTES
Matematicheskie Zametki
Vols. 35-36, 1984 (12 issues) $520

continued on inside back cover

Declassified and Approved For Release 2013/02/22 : CIA-RDP10-02196R000300050006-1